Award Number: W81XWH-12-1-0303

TITLE: Piezoelectric Composite Micromachined Multifrequency Transducers for High-Resolution, High-Contrast Ultrasound Imaging for Improved Prostate Cancer Assessment

PRINCIPAL INVESTIGATOR: Paul A. Dayton

CONTRACTING ORGANIZATION: University of North Carolina at Chapel Hill
Chapel Hill, NC 27599

REPORT DATE: October 2016

TYPE OF REPORT: Final Report

PREPARED FOR: U.S. Army Medical Research and Materiel Command
Fort Detrick, Maryland 21702-5012

REPORT DOCUMENTATION PAGE

Form Approved
OMB No. 0704-0188

1. REPORT DATE	2. REPORT TYPE	3. DATES COVERED
October 2016	Final	1 AUG 2012 - 31 JUL 2016

4. TITLE AND SUBTITLE
Piezoelectric Composite Micromachined Multifrequency Transducers for High-Resolution, High-Contrast Ultrasound Imaging for Improved Prostate Cancer

5a. CONTRACT NUMBER

5b. GRANT NUMBER
W81XWH-12-1-0303

5c. PROGRAM ELEMENT NUMBER

6. AUTHOR(S)
Paul A. Dayton (primary contact) and Xiaoning Jiang, and team members both labs

E-Mail: padayton@email.unc.edu

5d. PROJECT NUMBER

5e. TASK NUMBER

5f. WORK UNIT NUMBER

7. PERFORMING ORGANIZATION NAME(S) AND ADDRESS(ES)

Primary contracting: University of North Carolina at Chapel Hill
Administrative Office Building, Suite 2200
104 Airport Drive, CB#1350
Chapel Hill, NC 27599-1350

Subcontracting:
North Carolina State University
2701 Sullivan Drive, Suite 240
Raleigh, NC 27695

8. PERFORMING ORGANIZATION REPORT NUMBER

9. SPONSORING / MONITORING AGENCY NAME(S) AND ADDRESS(ES)
U.S. Army Medical Research and Materiel Command
Fort Detrick, Maryland 21702-5012

10. SPONSOR/MONITOR'S ACRONYM(S)

11. SPONSOR/MONITOR'S REPORT NUMBER(S)

12. DISTRIBUTION / AVAILABILITY STATEMENT
Approved for Public Release; Distribution Unlimited

13. SUPPLEMENTARY NOTES

14. ABSTRACT

From the original abstract: "The objective of this proposal is to develop new technology for substantially improving the sensitivity of ultrasound to prostate cancer. This technology will be enabled by recent advances in ultrasound transducer fabrication techniques and ultrasound contrast imaging approaches. We hypothesize that a transrectal ultrasound probe utilizing a novel dual-frequency ultra-broadband approach will provide a new highly-sensitive diagnostic technique for prostate cancer imaging."

The attached final report summarizes our progress towards the originally stated aims of the project, our accomplishments, our challenges, as well as a summary of published materials and presented abstracts. We have provided basic details in the attached text. Extensive additional data, discussion, and conclusions are included in the attached published manuscripts.

15. SUBJECT TERMS
Nothing listed

16. SECURITY CLASSIFICATION OF:			17. LIMITATION OF ABSTRACT	18. NUMBER OF PAGES	19a. NAME OF RESPONSIBLE PERSON
a. REPORT	b. ABSTRACT	c. THIS PAGE			USAMRMC
U	U	U	UU	96	19b. TELEPHONE NUMBER *(include area code)*

Table of Contents

Introduction

Prostate cancer is challenging to assess with standard ultrasound. Our team has recently demonstrated a new approach of ultrasound imaging that uses a contrast agent with a dual-frequency transducer to produce high resolution images of microvascular structure. It is hypothesized that microvascular structure and density are related to degree of cancer, and that this new imaging approach may help us assess prostate cancer. However, to date, there are no dual-frequency transducers designed for prostate cancer imaging that can perform this high-resolution imaging approach. The objective of the proposed research is to design and test a dual-frequency transducer specifically for prostate cancer imaging using contrast agents.

Keywords

Ultrasound, acoustic angiography, dual-frequency, transducer, contrast agents, prostate

Acronyms

PC-MUT	Piezo Composite Micromachined Ultrasound Transducer
TRUS	Trans Rectal Ultrasound
KLM	Krimholtz–Leedom–Matthaei
PMN-PT	Lead Magnesium Niobate-Lead Titanate

Accomplishments

The original tasks as proposed are listed in blue, and the following black text details progress towards these tasks.

Aim 1) Develop a new type of dual-frequency PC-MUT co-linear array with broad bandwidth to enable a new dual-frequency imaging technology for high-resolution, high sensitivity nonlinear transrectal contrast imaging.

Task 1 PC-MUT co-linear array design (Months 1-12)
Extensive modeling will be performed to design 1D and 2D dual frequency (5 MHz/20 MHz) co-linear arrays. The pressure field with amplitude > 2 MPa at a few cm depth is expected from a 5 MHz array for effective microbubble excitation. A 20 MHz PC-MUT with -6dB bandwidth > 90% will be developed as the receiver and integrated with the 5 MHz transmitter for TRUS contrast imaging.

Methods and Results for Task 1:

Design of single-element 1D PC-MUT transducers:

A single element dual frequency transducer was developed first to verify the detection of super harmonic responses from microbubbles excited by low frequency ultrasound. The low frequency transmitter for contrast-enhanced super harmonic imaging is required to exhibit not only high negative pressure but also short ringing near the resonant frequency of microbubbles (Ma 2014, Martin 2014). However, due to the spatial and frequency limitation in many interventional ultrasound imaging probes, a conventional transmitter design with a thick and lossy backing layer for a short ringing at a low frequency is not practical. Therefore, a new design concept considering optimal matching, backing, and isolation layers as well as the active layers is required for the dual-frequency ultrasound enabled super harmonic imaging.

The schematic design of the single element dual-frequency transducer is shown in Figure 1**Error! Reference source not found.**. In this research, the low frequency transmitter without backing material was designed to reduce the total thickness. To redeem a narrow bandwidth due to the absence of the backing layer, 1-3 piezoelectric composite was used as an active material of the transmitter. In the aspect of the receiver, wideband performance is also required for the efficient detection of the high-frequency and broadband harmonics scattered from micro-bubbles. Thus, the 1-3 piezo composite was used for a receiver with broad bandwidth. If both transmitter and receiver are made of piezoelectric composites with relatively low acoustic impedance (~19 MRayl), the isolation layer between the low frequency transmitter and the high frequency receiver should be carefully designed for efficient acoustic wave propagation. Due to the low acoustic impedance of the composites, conventional epoxy materials based isolation layer design

cannot make a large enough impedance difference at the boundary between two composites (Kim 2014, Ma 2014). Therefore, a dual-layer design was adopted for the isolation layer.

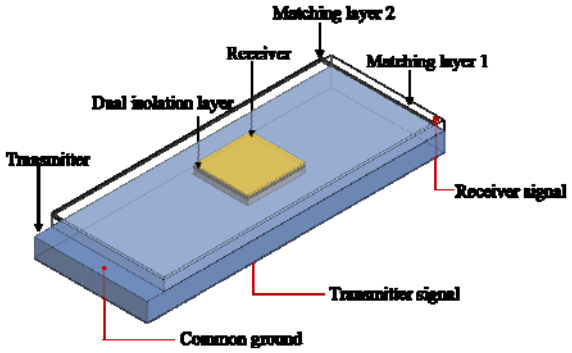

Figure 1. Schematic view of a dual frequency TRUS transducer design (Kim 2014).

Single element design with KLM modeling

The dimensions of each part were designed by using a Krimholtz–Leedom–Matthaei (KLM) model. Although our original proposal involved a 5 MHz transmitter, we have revised our design to utilize a 2 MHz transmitter based on more recent data showing improved signal to noise at this lower frequency. The material properties and dimensions of designed components are listed in **Error! Reference source not found.**. A steel shim was used as a second isolation layer which is next the transmitter due to its high acoustic impedance (~50 MRayl). The large difference between acoustic impedance of isolation layers 1 and 2 can provide a strong reflection of received high frequency waves at the boundary. Although this reflection may slightly reduce the receiving bandwidth, the isolation layers would block the wave transmission to the transmitter and backscattered wave from the backside of the transmitter. The thickness of both isolation layers was selected as a quarter wavelength, and then adjusted by analyzing pulse echo amplitude and bandwidth using the KLM model. The simulation results are shown in **Error! Reference source not found.**. A slight degradation of the transmitting performance can be estimated due to isolation layer in front of the radiation area, but its area is just small portion of the low frequency radiation area (~14 %). Moreover, the thickness of the isolation layer is negligible (less than 1/20 wavelength) of the for the designed low frequency transmission.

Table 1. Parameters of single element dual frequency transducer.

	Material	Density (kg/m^3)	Acoustic impedance (MRayl)	Dimension (mm^3)
Transmitter	1-3 composite	5300	19.1	3.8×8.0×0.71
Receiver	1-3 composite	5450	20.0	2.0×2.0×0.08
Matching layer	Al_2O_3/epoxy	2900	5.80	3.8×8.0×0.30
Isolation layer 1	E-solder 3022	2600	5.50	2.0×2.0×0.05

Isolation layer 2	Steel	8840	51.7	2.0×2.0×0.08

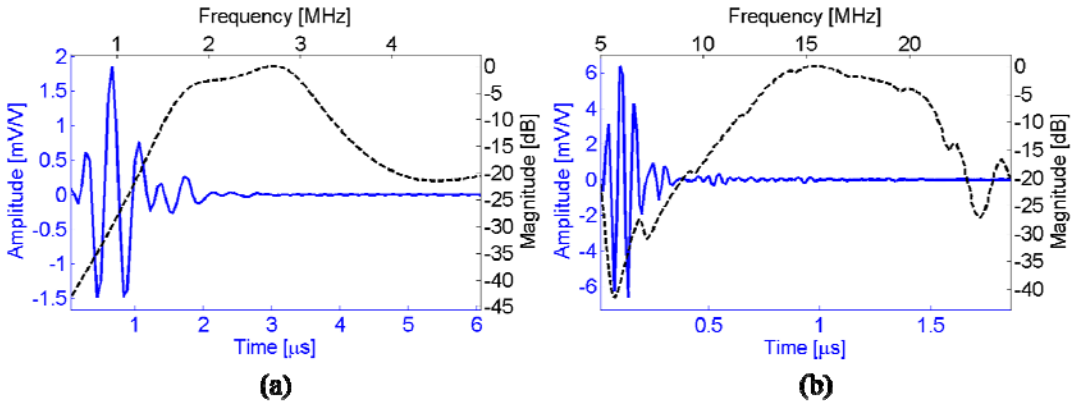

Figure 2. Impulse responses from KLM model for the single element dual frequency TRUS transducer: (a) impulse results for the transmitter (b) impulse results for the receiver.

The peak-to-peak voltage and -6dB bandwidth were for both transmitter and receiver were calculated from the pulse-echo modeling results. The transmit excitation response was calculated using KLM model to estimate the achievable peak negative pressure value. The calculated peak negative pressure was 6.1 kPa with the 2 cycles of 1 V_{pp} sinusoidal excitation, thus about 1.8 MPa negative pressure can be generated with 2 cycles of 300 V_{pp} sinusoidal excitation. The designed transmitter showed the loop sensitivity of 3.4 mV_{pp}/V and the -6dB fractional bandwidth of 61.2 %. The high-frequency receiver exhibited the sensitivity and bandwidth of 12 mV_{pp}/V and 49.3 %, respectively. Based on previous experimental results, it is reasonable to develop a dual frequency linear array with the same configuration utilizing a 2 MHz transmitter and 20 MHz receiver (Kim 2014).

Multi element array design and modeling

In array design, the number of active elements is limited by the imaging system, thus the element pitch and total aperture size was designed by considering imaging system limitations and the maximum acceptable probe dimensions for transrectal ultrasound. Also, the TX and RX elements need to be physically separated while also sharing the same aperture, the array transducer was designed using a stacked configuration (Figure 3). The RX and TX were coupled with isolation layer (E-solder conductive epoxy), which also served as common ground. To improve the transmission sensitivity, air backing was used for the low frequency array (Li 2015).

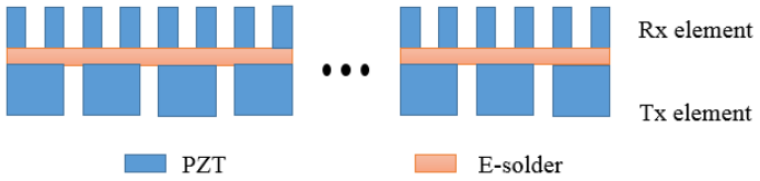

Figure 3 Schematic of array transducer (Li 2015)

The KLM model was used to estimate the performance of elements in the linear array. PZT ceramic (CTS 3203HD, CTS Corporation, Elkhart, Indiana, USA) and 2-2 composites were selected as the active material for TX and RX. The pulse-echo performance of TX at 3 MHz and RX at 15 MHz were modeled considering different element size and materials. Low frequency transmitting (3 MHz) and high frequency receiving (15 MHz) configurations were simulated separately (Figure 4).

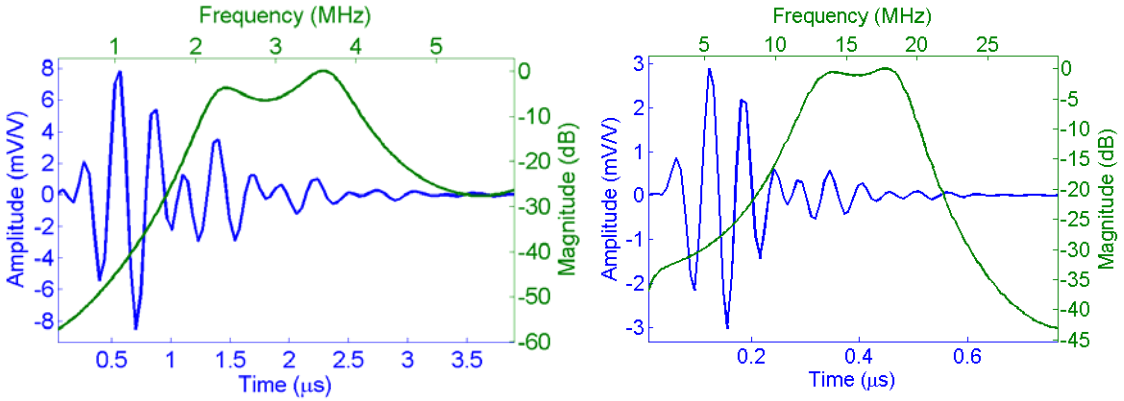

Figure 4 Pulse-echo response of low frequency (3 MHz) element (left) and high frequency (15 MHz) element (right).

An isolation layer of E-solder epoxy was used to improve the performance. Due to the selected element pitch and aperture design, the piezoelectric layers were operated in pure sliver mode for the low frequency (TX) elements and in 2-2 composites sliver mode for the high frequency (RX) elements. To minimize interference between TX and RX elements, a λ/4 layer of E-solder were added. The detailed parameters and corresponding simulation results were summarized in Table 2**Error! Reference source not found.**.

Table 2 Design parameters of co-linear array

Property	Value	
Aperture	8 mm by 18 mm	
Working mode	Transmitting (3 MHz)	Receiving (15 MHz)
Pitch	280 μm (0.5 λ)	140 μm (1 λ)
Element number	64	128
Material	PZT	2-2 composites

The pressure field was then investigated for the array. Field II, a Matlab toolkit, was used for the field simulation to determine the pitch size and group firing scheme. Figure 5 shows the pressure information in 3 MHz transmitting (left) and 15 MHz receiving (right). The focus was set at 35 mm far from the probe. With phased delay set-up, the -6 dB beam width at low frequency reaches 1.4 mm, and 0.5 mm at high frequency receiving (Li 2015).

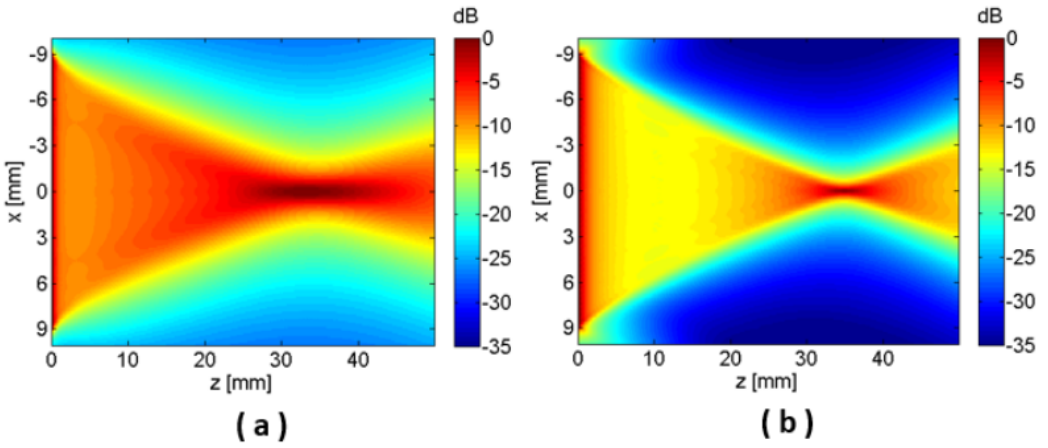

Figure 5 Simulation of beam profile in 3 MHz transmitting (a) and 15 MHz receiving (b), focus at 40 mm.

Task 2 Dual frequency PC-MUT co-linear array fabrication (Months 4-21)

Dual frequency co-linear array fabrication processes will be developed under this task for dual frequency co-linear array prototyping. At the end of this task, a co-linear array with 64-element 5 MHz 1D array and 128-element 20 MHz 1D array will be fabricated for demonstration of dual frequency PC-MUT co-linear array technology.

Subtask 2.1 1-3 piezocomposite fabrication (Months 3-6)

The fabrication of 20 MHz PC-MUT receivers will follow the standard PC-MUT fabrication process. For the 5 MHz PC-MUT transmitter, PIN-PMN-PT 1-3 composite will be fabricated using dice-and-fill process. The electromechanical coupling coefficient of fabricated 1-3 piezo composites are expected to be > 0.75.

Subtask 2.2 Multilayering process (Months 6-12)

Conductive through-wafer-vias (TWV) process will be developed for multilayer transducer demonstration. Bonding process for single layer and multilayer dual frequency co-linear array fabrication will be developed under this subtask.

Subtask 2.3 Dual frequency co-linear array prototyping (Months 12-21)

The 5 MHz composite layer will be fabricated first, followed by attachment of the 20 MHz receiver and matching layers. The bonded co-linear array acoustic stack will then be wired and tested.

Methods and Results for Task 2:

Prototype dual-frequency piezoelectric composite (PC-MUT) single element fabrication

Based on the design parameters, the prototypes of dual frequency transducer were fabricated. At first, the dual isolation layers were fabricated using E-solder and a steel shim. The E-solder (Von Roll Isola, Inc., New Haven, CT) was pasted on the one side of the steel shim which has a designed thickness of 80 μm and cured for 10 hours at 45°C, and then, shaped to 2.0 × 2.0 mm^2 which is similar to the size of the receiver aperture. The E-solder side was lapped down to the designed thickness of 50 μm. The steel side was attached to the low frequency transmitter and E-solder side was attached to the high frequency receiver using Epo-tek 301 (Epoxy Technology Inc., Billerica, MA). For the transmitter, PMN-PT/epoxy 1-3 composites with the volume fraction of 65 % and a pitch of 430 μm was used. Another 1-3 composite (volume fraction of 75 % and a pitch of 60 μm) was used as a receiver material. The matching layer material (Epo-tek 301 mixed with 0.3 micron Al_2O_3 powders) was poured on the front side of the transmitter submerging the receiving part. The cured matching layer part was then lapped until the high frequency composite part was exposed. The gold electrode was next deposited on the lapped surface to form a common ground. The matching layer of the receiver was fabricated using the similar process of transmitter's matching layer fabrication. The back side of the low frequency composite was attached to the tip of a syringe which is used as a support fixture. As a final step, the wires were connected and both high and low frequency composites were re-poled. Figure 5 shows the fabricated prototypes. The difference between prototype 1 and 2 is the aperture size of the receiver. The receiving aperture of prototype 1 was modified to 3.8×2.0 mm^2 from the designed dimension in Table 1 to validate the appropriate size of the receiver in a stacked dual-frequency transducer structure, whereas the receiving aperture of prototype 2 was 2.0×2.0 mm^2 (Kim 2015)

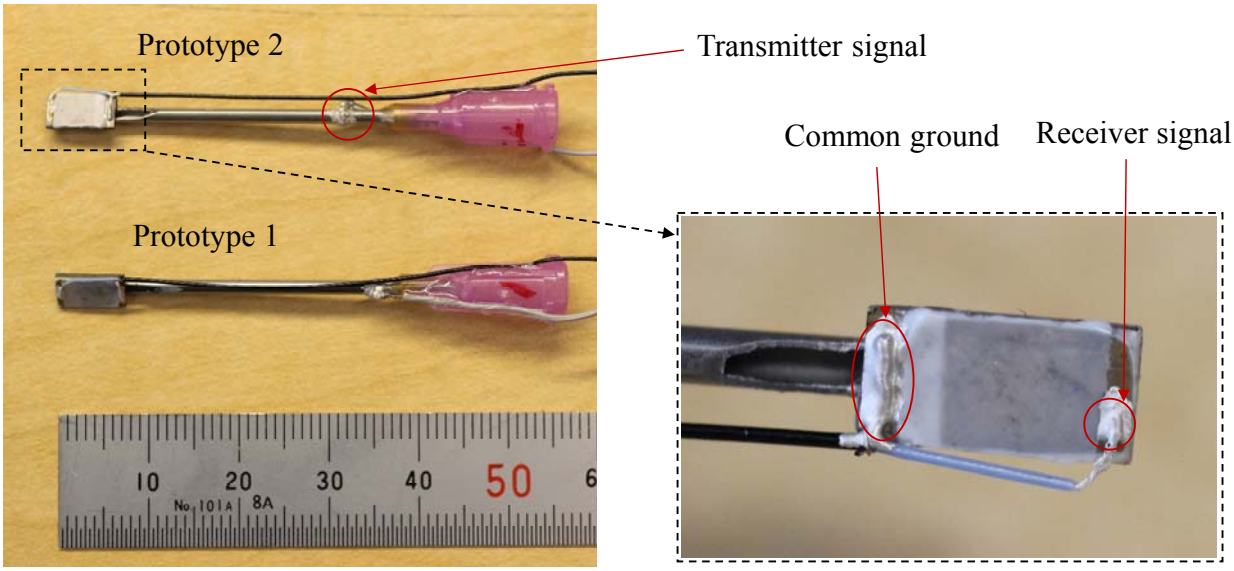

Figure 6. Photograph pictures of dual-frequency transducer prototypes.

Prototype dual-frequency PC-MUT array fabrication

A prototype of the dual-frequency array was fabricated according to the design parameters. First, a PZT plate of 500 μm (for low frequency TX) was cleaned and deposited with Ti/Au on both

sides. The top electrode was then attached with the conductive epoxy (E-solder 3022, Von Roll Isola, Inc. New Haven, CT). The material was cured at room temperature for 24 hours. After E-solder was carefully lapped to 30 μm thick, the RX material, 2-2 composites, was bonded to the TX layer using Epo-Tek 301 (Epoxy Technologies, Billerica, MA), and then lapped to the thickness of 100 μm for 15 MHZ resonance (Figure 7). Finally, the conductive layer, Ti/Au, was sputtered to the top receiving layer.

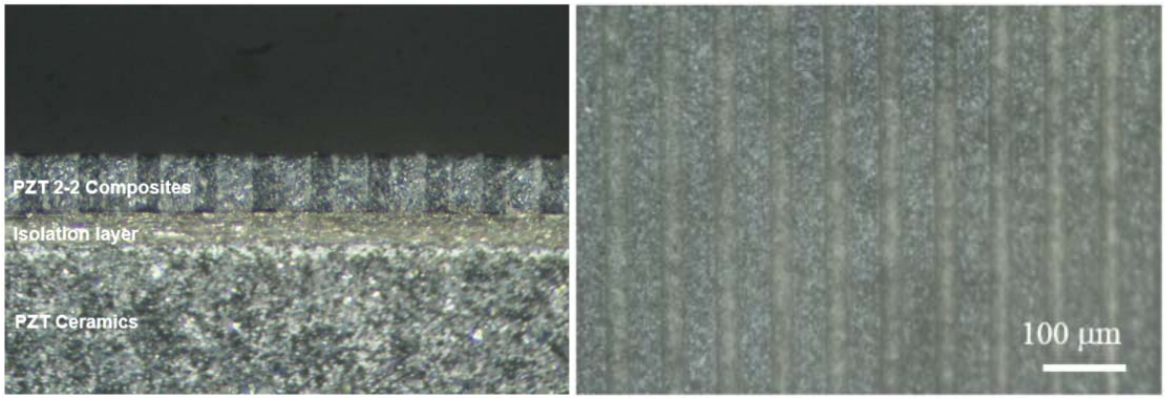

Figure 7 The photograph of the multi-layer stack, side view (left) and top view (right).

The flex circuits for TX and RX were then bonded to both sides of the stack. After the epoxy was fully cured, the dicing process was performed according to the pitch design. Finally, the array was interconnected with the PCB for the further test (Figure 8, Li 2015).

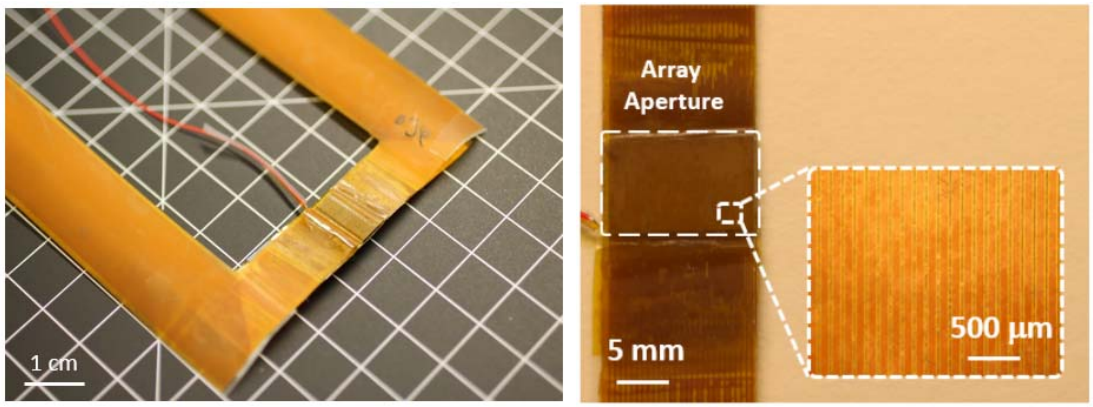

Figure 8 Photograph pictures of dual-frequency array prototype.

Task 3 Characterization of dual frequency PC-MUT co-linear array (Months 15-27)

Electrical and acoustic characterizations will be performed under this task to evaluate the prototyped dual frequency co-linear array.

Subtask 3.1 Electrical characterization (Months 15-21)

Resonant frequency, capacitance, and electrical impedance of single element and a group of elements will be measured using an impedance analyzer. The measured values will be compared with the modeling results.

Subtask 3.2 Acoustic characterization (Months 21-27)
Transducer characterization will be performed under this subtask. The prototype array will be driven with the multi-channel Verasonics programmable ultrasound pulser/receiver). Pulse-echo and hydrophone (HNC-0200, Onda Corp) characterization will be performed in water tank to obtain the transmission characteristics of the 5 MHz transmitter, and the receiving sensitivity and bandwidth of the 20 MHz receiver.

Methods and Results for Task 3:

Electrical Characterization of single element prototype

The electrical impedance of both transmitters and receivers of the prototypes were measured using an Agilent 4294A precision impedance analyzer (Agilent Technologies Inc., Santa Clara, CA). Figure 9 and Figure 10 show the electrical impedance and phase spectra of prototype 1 and prototype 2, respectively. Both prototypes showed the transmitting and receiving frequencies at the designed ranges (Kim 2015).

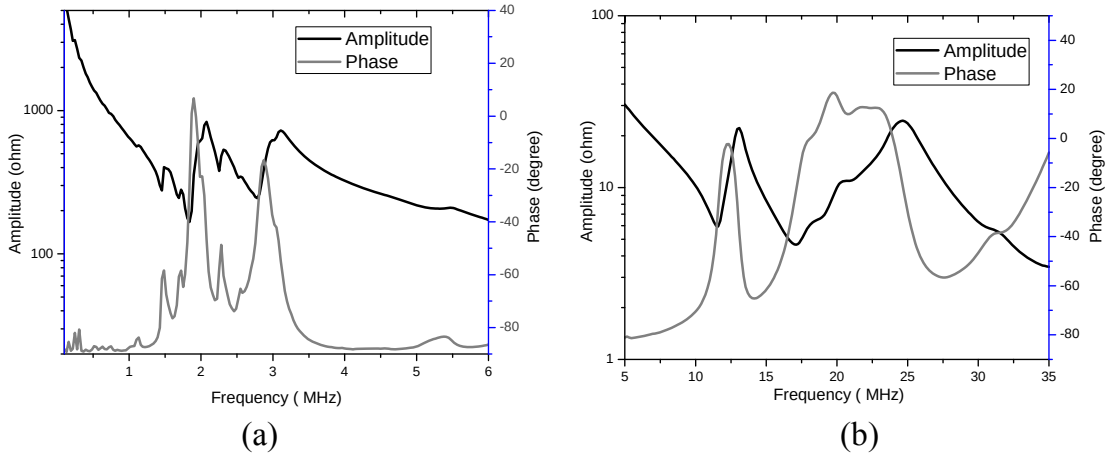

Figure 9. Impedance and phase spectra of the prototype 1: (a) Transmitter; (b) Receiver.

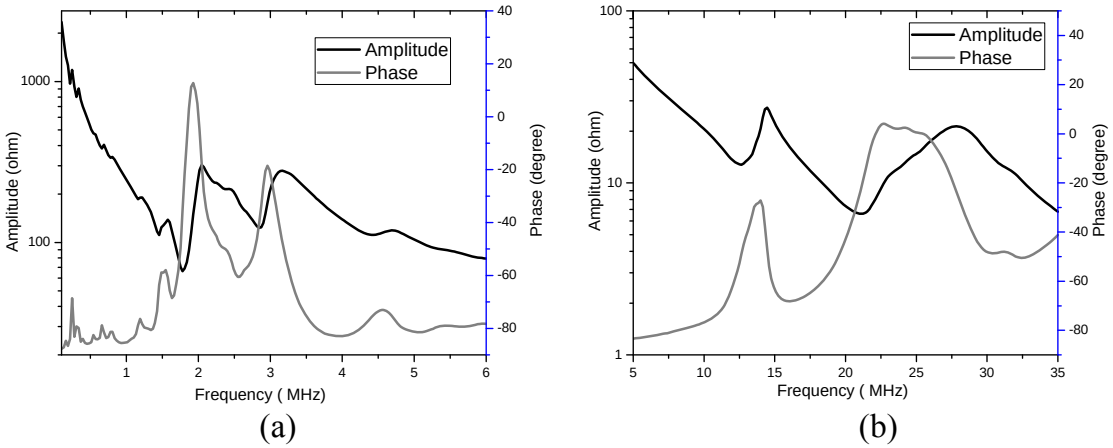

Figure 10. Impedance and phase spectra of the prototype 2: (a) Transmitter; (b) Receiver.

Electrical characterization of array prototype

The electrical impedance of selected elements of the array were measured using an Agilent 4294A precision impedance analyzer (Agilent Technologies Inc., Santa Clara, CA). The transmission element exhibits the fundamental resonant frequency of 3.7 MHz, and the resonant of the receiving element are 13.8 MHz (Figure 11).

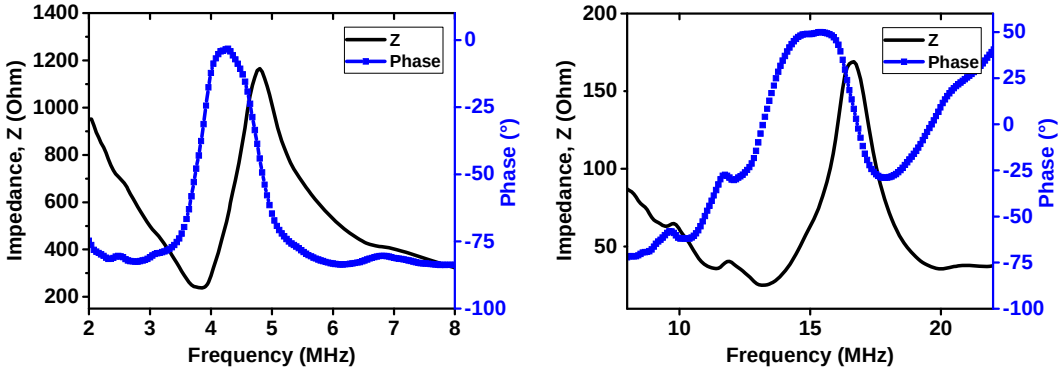

Figure 11. Electrical response of transducer at transmission (left) and receiving (right)

Acoustic characterization of single element prototype

The transmitting and receiving performances of prototypes were tested. The pulse-echo signals of both transmitters and the receivers were measured individually and the peak negative pressure value of the transmitters were also measured. A pulser/receiver (5900PR, Panametrics Inc., Waltham, MA) was used in pulse-echo test and energy of 1 μJ and 2 μJ were excited to the

receiver and transmitter, respectively. The cut-off frequency of the low-pass filter was 20 MHz for the transmitter and 50 MHz for the receiver test. The gain and attenuation were not changed during the pulse-echo test. The transmitter of the prototype 1 showed the peak-to-peak voltage of 210 mV and -6 dB bandwidth of 61.1 %, and the receiver showed the peak received echo voltage 430 mV and -6 dB fractional bandwidth of 45.1 % (Figure 12). The pulse-echo results of the prototype 2 is shown in Figure 13. The measured echo peak voltages for the transmitter and receiver are 430 mV_{pp} and 410 mV_{pp}, respectively. The measured -6dB fractional bandwidth for transmitter and receiver were 55.1% and 35.6 %, respectively.

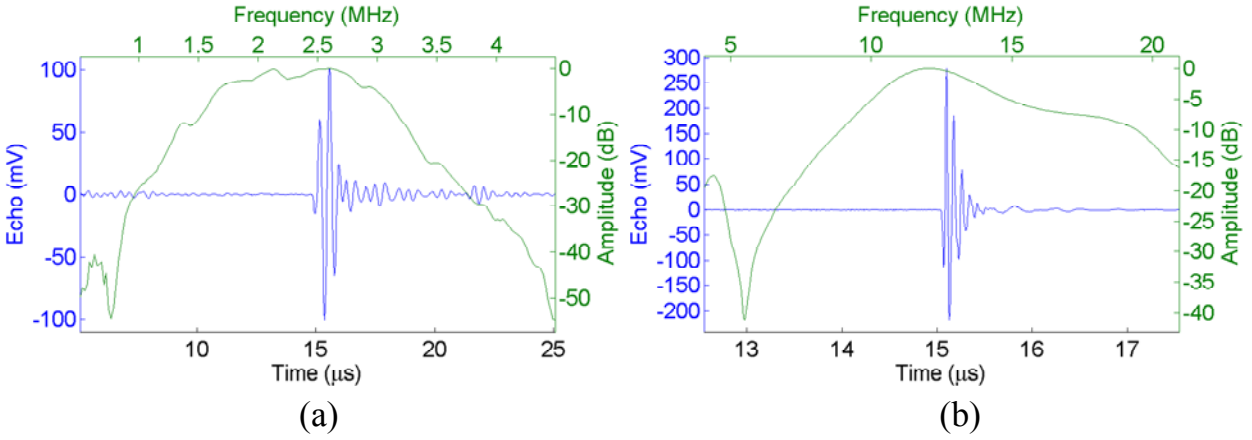

Figure 12. Pulse-echo responses and spectra of the prototype 1: (a) Transmitter, (b) Receiver.

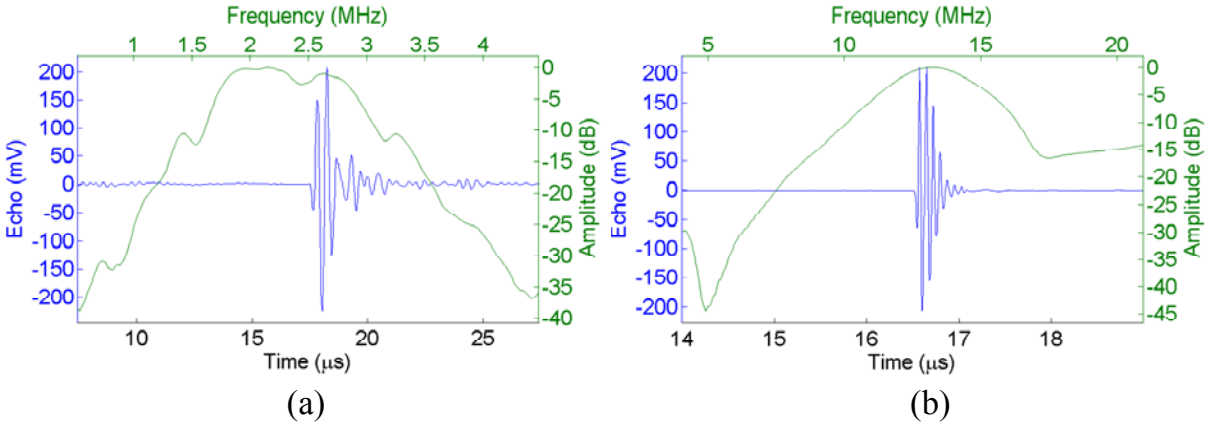

Figure 13. Pulse-echo resposnes and spectra of the prototype 2: (a) Transmitter, (b) Receiver.

The peak negative pressure of prototype 2 was measured using the setup shown in Figure 15. In the set-up, a needle hydrophone (HNA-0400, Onda Corp., Sunnyvale, CA) was located in front the prototyped transducer. The transmitter of the prototype 2 was excited with two cycles of 2 MHz and 300 mV_{pp} sinusoidal input by a function generator (AFG3101, Tektronix Inc., Beaverton, OR) and amplified by 55 dB using a radio-frequency amplifier (Model 3200L, Electronic Navigation Industries Inc., Rochester, NY). The hydrophone was moved laterally and axially and the measured pressure values were processed to obtain the pressure mapping, as shown in Figure 16. The peak negative pressure at the far field was about -1.6 MPa, which is

high enough to excite microbubbles for nonlinear responses. The mechanical index (MI) was calculated to be 1.13, which is within regulated FDA limits for diagnostic ultrasound equipment (Kim 2014).

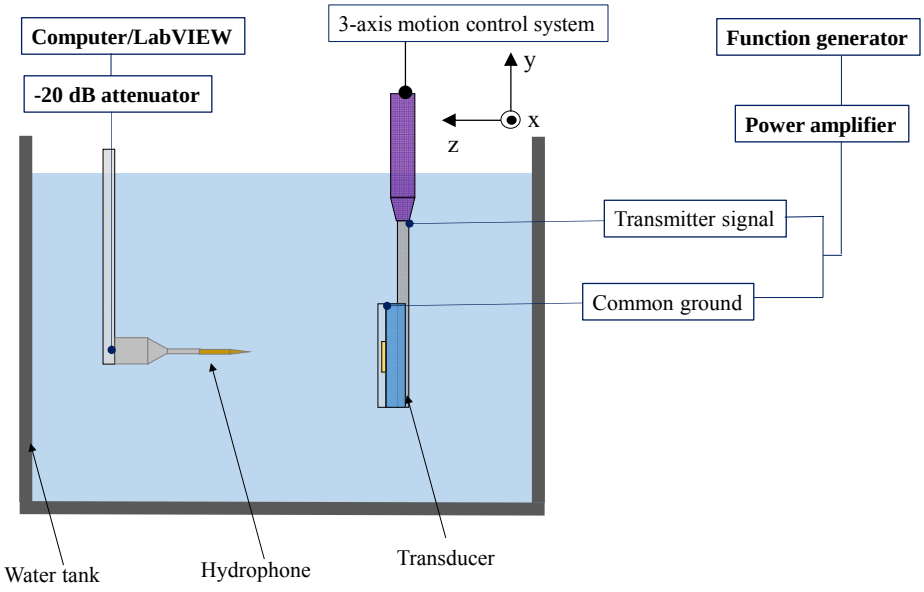

Figure 14. Pressure mapping measurement setup.

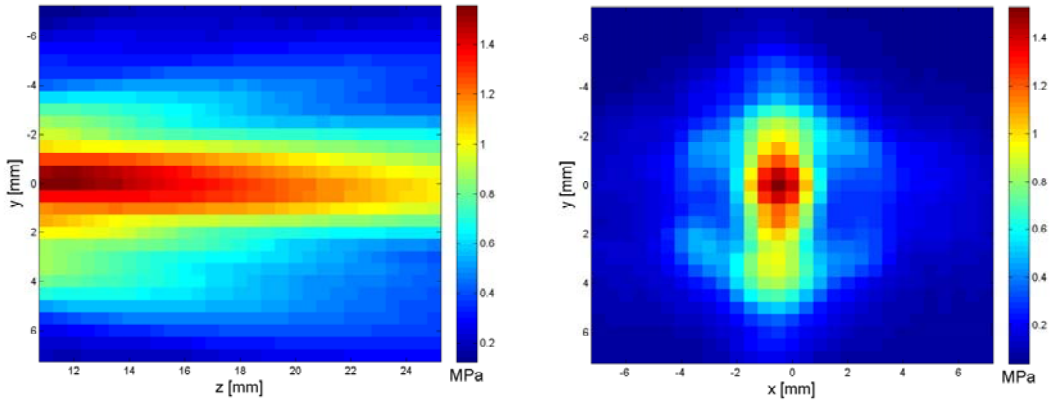

(a) (b)

Figure 15. Pressure mapping results for the prototype 2 transducer (with 2 cycles of the 2 MHz and 300V_{pp} excition): (a) yz-plane; (b) xy-plane at z = 13 mm (Kim 2014).

Acoustic characterization of array prototype

The transmitting and receiving performances of array elements were tested using the pulser/receiver (5900PR and 5077PR, Panametrics Inc., Waltham, MA). The low frequency transmission elements were excited by a 100 V pulse, and showed a peak-to-peak voltage of 45

mV and -6 dB bandwidth of ~45%. The receiving element was excited by 1 μJ pulse and showed ~ 30 mV_{pp} response and ~50% in -6 dB bandwidth , respectively (Figure 16) (Li 2016).

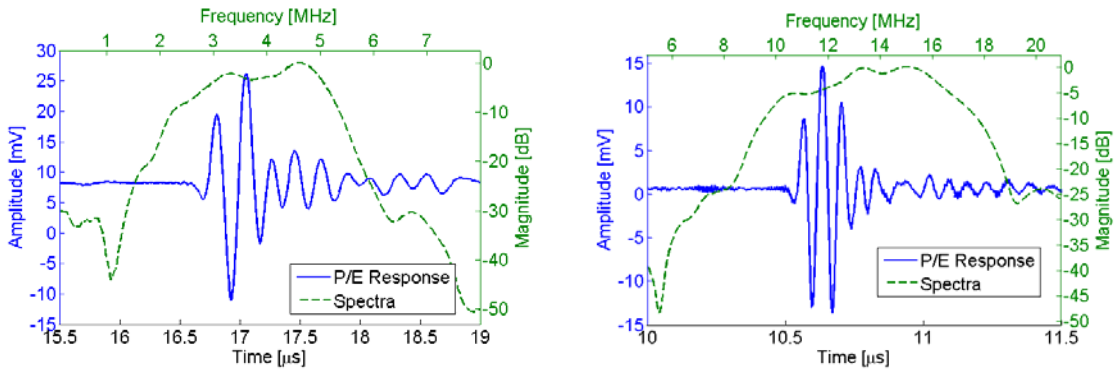

Figure 16. Pulse-echo response of transducers at transmission (a) and receiving (b) (Li 2016)

The peak negative pressure of TX elements with different focal depth were measured, and mapping to show the waveform (Figure 17) and beam profile (Figure 1). In the set-up, a needle hydrophone was located in front the prototyped transducer and moved laterally. The measured pressure values were processed to obtain the pressure mapping. The peak negative pressure at the far field was about -3.5 MPa at focus of 25 mm and -2.5 MPa at focus of 40 mm, which is enough to excite microbubbles for nonlinear responses. The mechanical index (MI) can reach as high as 1.5.

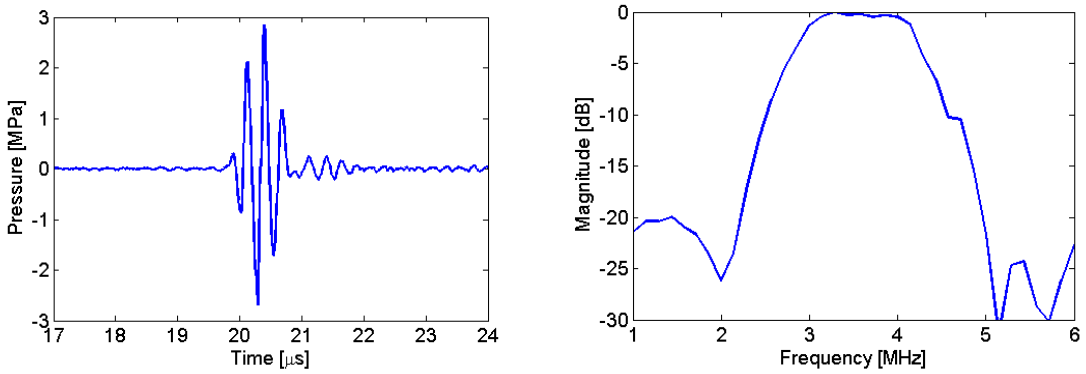

Figure 17 The waveform of TX element, measured by the hydrophone.

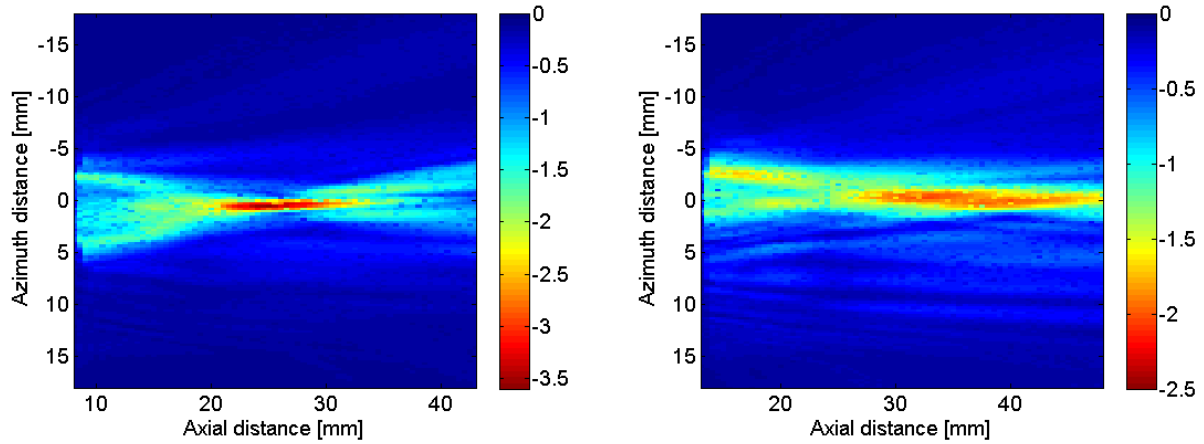

Figure 18 Pressure mapping results for the TX elements with focus at 20 mm (left) and 35 mm (right). The pressure unit in the figure is MPa.

Task 4 Prepare manuscript for data dissemination (Months 30-33)

After completion and characterization of the prototype array transducer, data will be presented in a manuscript for a peer-reviewed journal such as IEEE Ultrasonics, Ferroelectrics, and Frequency Control.

A manuscript on transducer development and characterization was prepared for Transaction of UFFC (Kim 2014).

Task 5 In-vitro testing of dual frequency PC-MUT co-linear array (Months 21-30)

Subtask 5.1 Tissue phantom testing (Months 21-25)

Gelatin based tissue mimicking phantoms will be used with a range of spherical hyperechoic and hypoechoic lesions. A spectrum of lesion detectability parameters will be tested. These lesions will be imaged at several axial depths using our prototype array and the Siemens EV-8C4 clinical TRUS probe. A blinded reader study will be performed and accuracy of the manually defined regions will be assessed between clinical and prototype probes for depth, phantom parameters, and imaging system parameters. Signal to noise ratio will be determined as a function of axial depth into tissue.

Subtask 5.2 Microvascular flow phantom testing (Months 25-30)

Images will be acquired in DFUB mode of microvascular flow phantoms with various diameters. Sinusoidal microvascular phantoms will be imaged at multiple axial depths, as well as with varying flow rates appropriate for simulating tumor microenvironment. A blinded reader study will be performed in which readers rank the sensitivity to slow flow within an added tissue clutter background.

<u>Methods and Results for Task 5:</u> Although much of the in-vitro testing was proposed in year three, we have started these studies in year 2 to provide additional feedback to the design process.

In-vitro contrast testing of dual-frequency PC-MUT transducers in water

The harmonic signals from microbubbles (ultrasound contrast agents) were measured using the set-up shown in Figure 18. The micro tube was positioned at about 8 mm away from the transducer. The transmission condition was same as pressure mapping condition (2 MHz, cycles, 300 mV_{pp}, and 55dB gain). The cellulose tube was filled with water, air, and micro bubbles, respectively, and then the received signals in each case were processed to obtain echo spectrum and filtered signal. The cut-off frequencies of the high and low pass filters were 10 MHz and 20 MHz, respectively, because the center frequency of the receiver is about 14 MHz. When the water was injected to the micro-tube, no high order harmonic signal reflected from the tube was measured in both raw signal and filtered signal (Figure 19). The peak at fundamental transmitting frequency (2 MHz) in frequency spectrum comes from the electrical coupling and very weak reflected signal from the tube.

The air was next injected to the micro-tube. The reflected waves from the tube due to the large acoustic impedance difference between water and air were detected by the high frequency receiver (Figure 20). The frequency spectrum showed that the received signal has no harmonic components but only fundamental transmitting frequency.

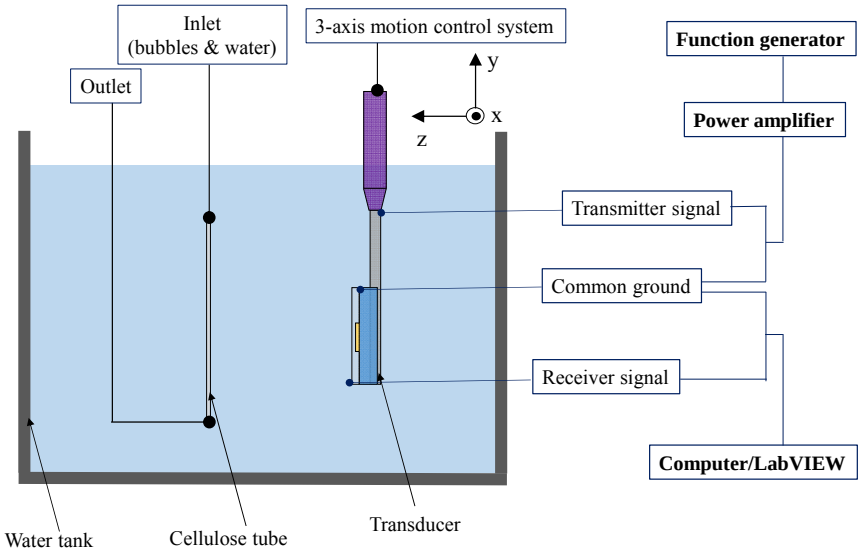

Figure 19. Bubble signal measurement setup.

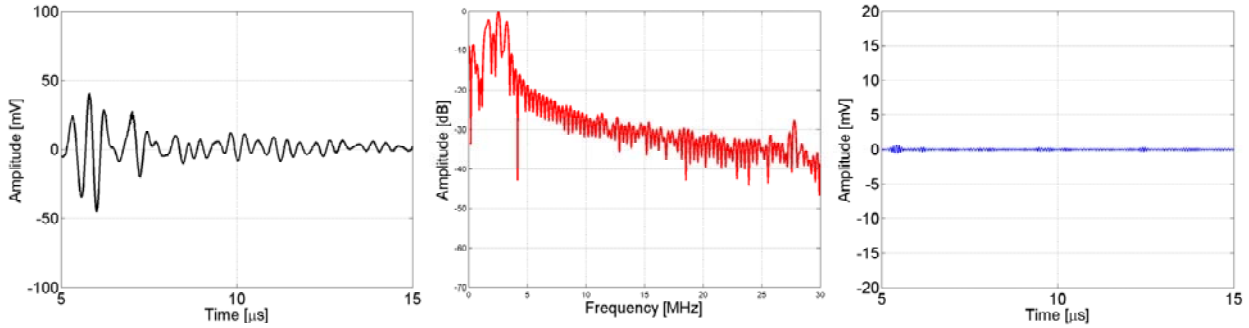

(a) (b) (c)

Figure 20. Received signal from the tube filled with water: (a) raw signal, (b) frequency spectrum, (c) filtered signal (10 to 20 MHz)

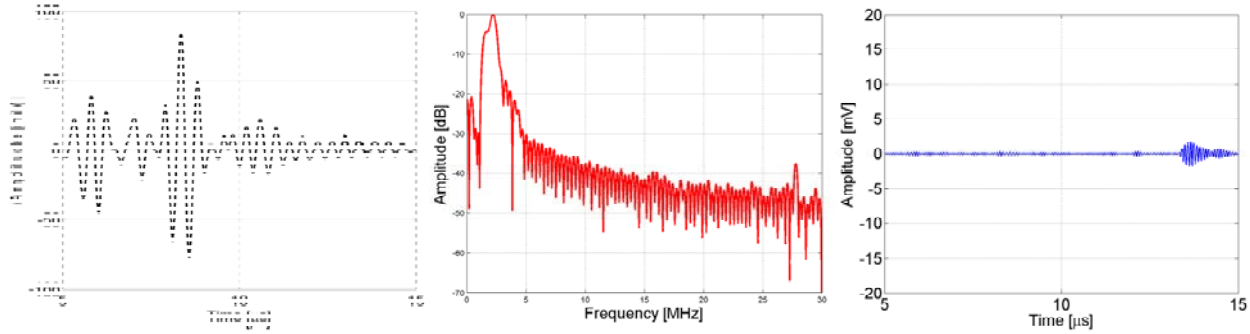

(a) (b) (c)

Figure 21. Received signal from the tube filled with air: (a) raw signal, (b) frequency spectrum, (c) filtered signal (10 to 20 MHz).

The diluted microbubbles were then pumped through the tube during the contrast agent detection test. The receiver successfully detected the fundamental reflection and super harmonic responses from the tube filled with microbubbles (Figure 21). The peak amplitude in the raw signal of was slightly reduced, but the frequency spectrum showed distinctive harmonic components. Although the center frequency of the receiver is 14 MHz which means that the receiver has the highest sensitivity for that frequency range and has very low sensitivity at low frequency range as 1 to 4 MHz, the second harmonic component was comparable to the fundamental frequency (-9 dB). The intended receiving frequency components (~14 MHz) also showed in frequency spectrum, and those were slightly larger than 5~10 MHz components. The filtered signal has a discernable peak but the amplitude was not high (5 mV) in comparison with the noise signal. Thus, the bubble response was measured with 16 dB gain and analog high-pass filter which has a cut-off frequency of 10 MHz (Figure 22). With 16 dB gain the harmonic bubble signal showed higher signal-to-noise ratio.

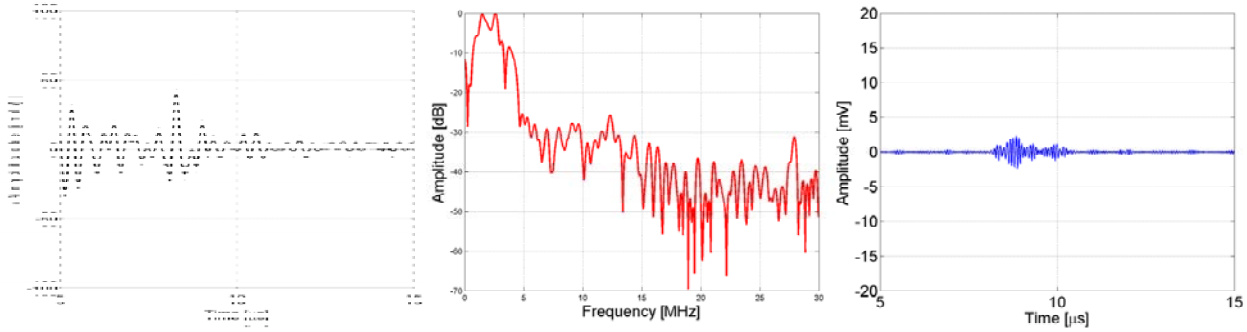

(a) (b) (c)

Figure 22. Received signal from the tube filled with bubbles: (a) raw signal, (b) frequency spectrum, (c) filtered signal (10 to 20 MHz).

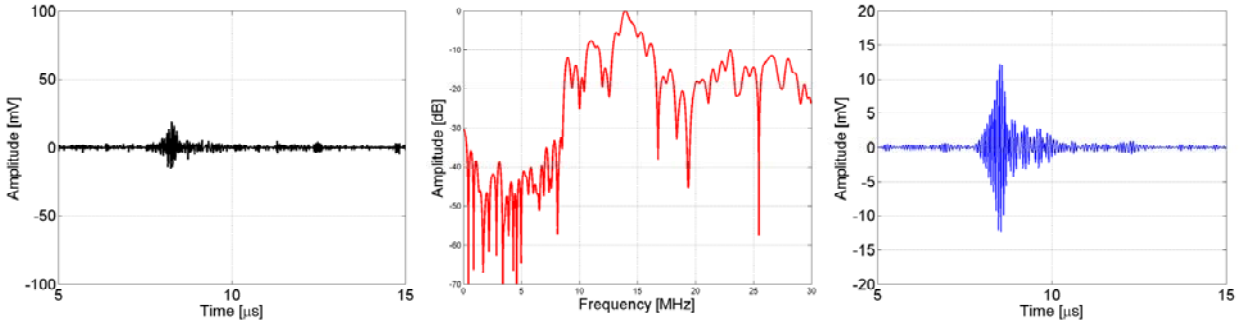

(a) (b) (c)

Figure 23. Received bubble signal with 16dB gain and 10 MHz high pass filter: (a) raw signal, (b) frequency spectrum, (c) filtered signal (10 to 20 MHz).

In-vitro phantom testing of dual-frequency PC-MUT transducers

The bubble test was also conducted with a tissue-mimicking phantom. In this experiment, the micro-tube was placed inside of the tissue phantom, which was positioned in the water tank. Other experimental conditions including experiment set-up, settings, and procedure were as the same as the bubble tests using a micro-tube in water.

Phantom fabrication

A graphite-gelatin phantom was used for this study. The phantom composed of 92.5% de-ionized water, 5% n-propanol (to adjust for speed of sound), 2.5% Kodak Photo-Flo 200 (surfactant), 7.5% g/mL porcine gelatin, and 0.115 g/mL graphite. The concentration of graphite was chosen to match experimental attenuation data of normal human prostate of 0.75 dB/cm/MHz. The ingredients were mixed with a stir bar over a stir plate and simultaneously heated to 40-45°C. Once the liquid phantom cooled back down to 30°C, it was poured into the custom mold and refrigerated for 24 hrs. The design of the mold consisted of two parallel cellulose tubes suspended in a hollow rectangular cup, such that if the opening of the cup faced up, the tubes ran parallel to the ground. The cellulose tubes were bound to a larger diameter polyethylene tube

using a water-proof adhesive. The distance from the cellulose tube to the surface of the phantom was approximately 5mm, with the tubes being in a distance of 5mm from each other (Figure 23).

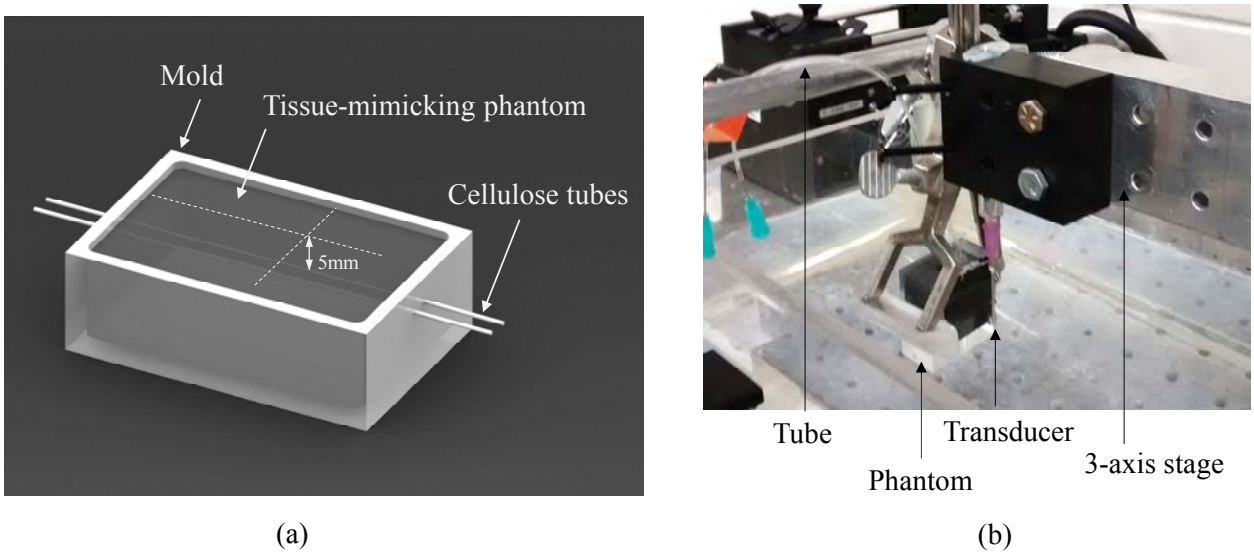

Figure 24. Design of a tissue-mimicking phantom

Bubble test results

The reflected signal from the surface of phantom was observed during the bubble test. If the transducer was too close to the phantom, the ringing of reflected signal from the surface was combined with the target signal from the tube. Therefore, to get a clear signal from tube the distance between the tube and the transducer was adjusted to 11 mm (Figure 23 (b)). Firstly, water was injected into microtubes and there was no received signal at the receiver, since the generated waves were almost perfectly transmitted through the tube filled with water (Figure 24). The tube with air showed clear reflected signal without any harmonic components (Figure 25). The micro-bubble case showed clear 7th harmonic signal, as seen in the frequency spectrum (Figure 17). This super harmonic signal was observed even more clearly in filtered signal, but the amplitude was not very high compared to the noise signal from the amplifier (Figure 26 (c)).

We will continue the contrast tests by using an analog high-pass filter (10M Hz) with proper gain (>10 dB) (Kim 2015).

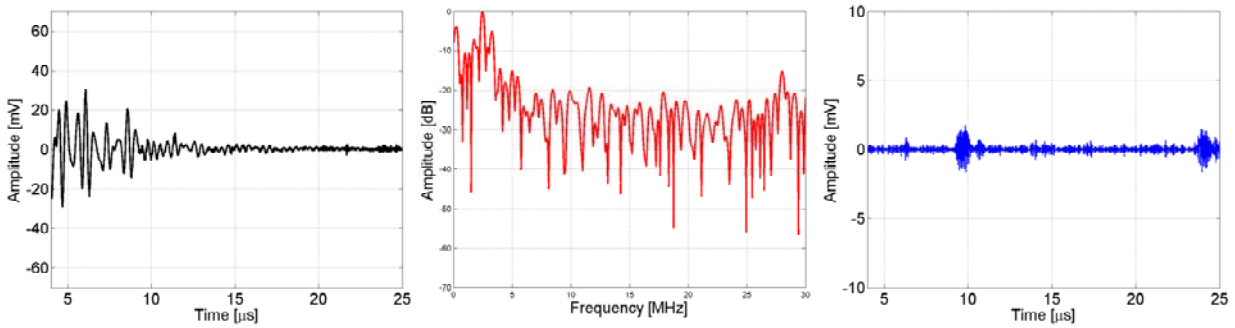

(a) (b) (c)

Figure 25. Received signal from the tube filled with water in a phantom: (a) raw signal, (b) frequency spectrum, (c) filtered signal (10 to 20 MHz)

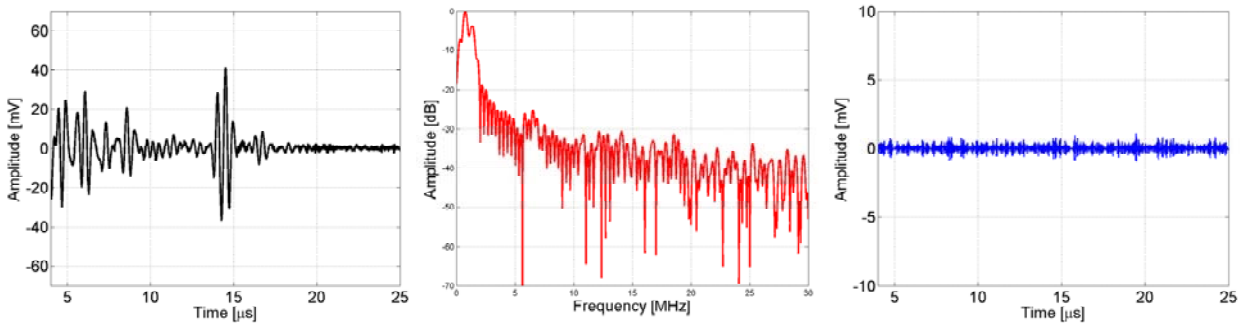

(a) (b) (c)

Figure 26. Received signal from the tube filled with air in a phantom: (a) raw signal, (b) frequency spectrum, (c) filtered signal (10 to 20 MHz)

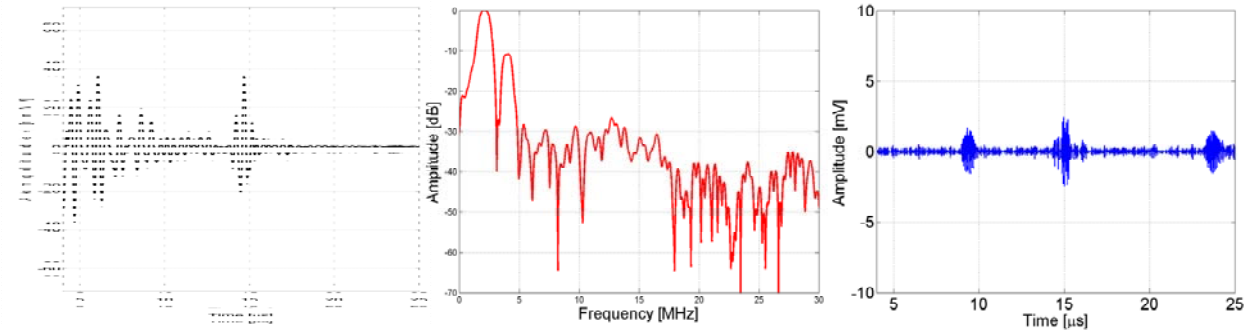

(a) (b) (c)

Figure 27. Received signal from the tube filled with bubbles in a phantom: (a) raw signal, (b) frequency spectrum, (c) filtered signal (10 to 20 MHz)

In-vitro phantom testing of dual-frequency co-linear array

Contrast imaging with the array transducer was conducted in a tissue-mimicking phantom. A 200 μm-diameter cellulose tube with flowing microbubbles (10^8 units/mL) was positioned ~30 mm away from the ultrasound probe (Figure 28).

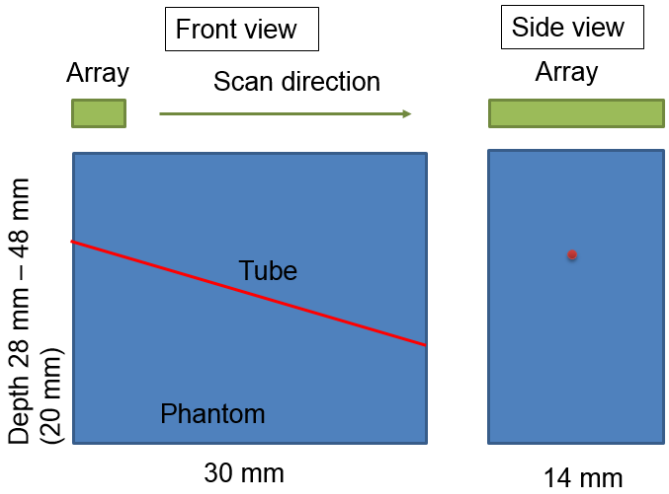

Figure 28 Design of a tissue-mimicking phantom for the array test

A multi-channel imaging system (Verasonics Vantage, Kirkland, WA) was used to drive the array and acquire echoes. For this work, 19 TX elements were fired as a group, and the single RX element at the center of the sub-aperture captured the high frequency superharmonic echoes. Each low frequency TX element was excited with a one-cycle, 37 V pulse. High frequency echoes were filtered with a bandpass filter (9-27 MHz) and time-gain compensation was applied.

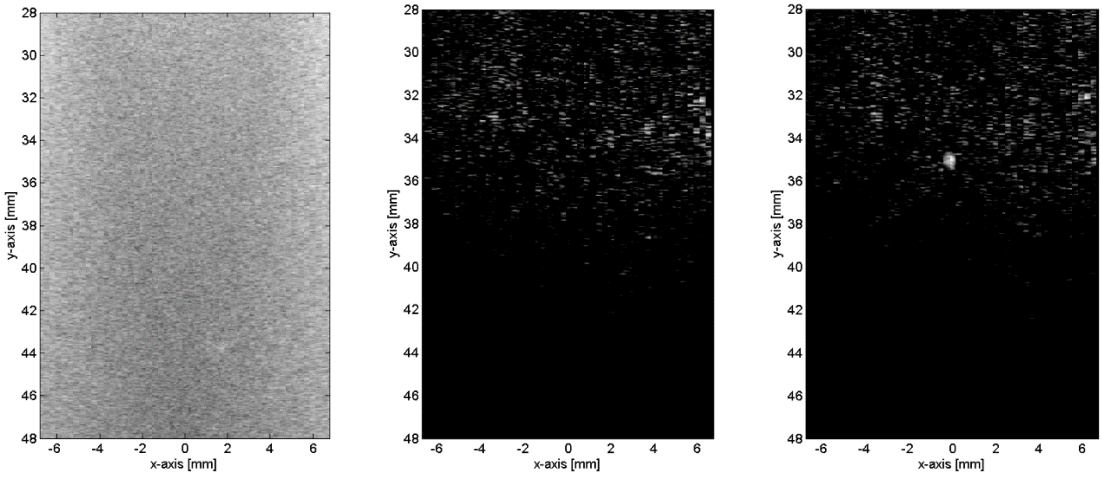

Figure 29 A 2D gray scale image in side view of phantom test in diffrerent mode (left: HF B-mode, middle: contrast mode (without bubble flow), right: contrast mode (with bubble flow))

The array was tested with 3 scenarios, 1. High frequency B-mode imaging; 2. Contrast imaging without microbubbles flowing; and 3. Contrast imaging with microbubbles flowing (Figure 29). In the high frequency B-mode, it showed full of speckles in the image. While the array was operated in the contrast mode, the speckle signal was significantly reduced. When microbubbles were flowing in the tube, the array in contrast mode received the target signal in the image. By combining above three image, the array is capable of acoustic angiography, which shows the

tissue imaging and vessel mapping by operating in B-mode and contrast mode. With positioned by the motion stage, the array was moved along the elevation direction. A set of 3D images were formed (Figure 30).

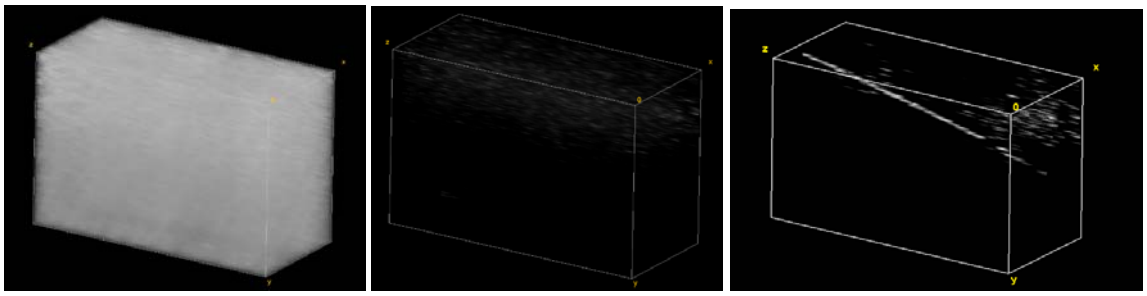

Figure 30 A 3D image of phantom test in different mode (left: HF B-mode, middle: contrast mode (without bubble flow), right: contrast mode (with bubble flow))

With the analysis of the 2D image (Figure 31), the acquired image shows that the co-linear array was able to capture the microbubble signal flowing in the cellulose tube. The received echo beam width in the axial and lateral dimensions were measured to be 400 μm and 600 μm, respectively. The contrast to noise ratio was calculated to be ~20 dB (Li 2016).

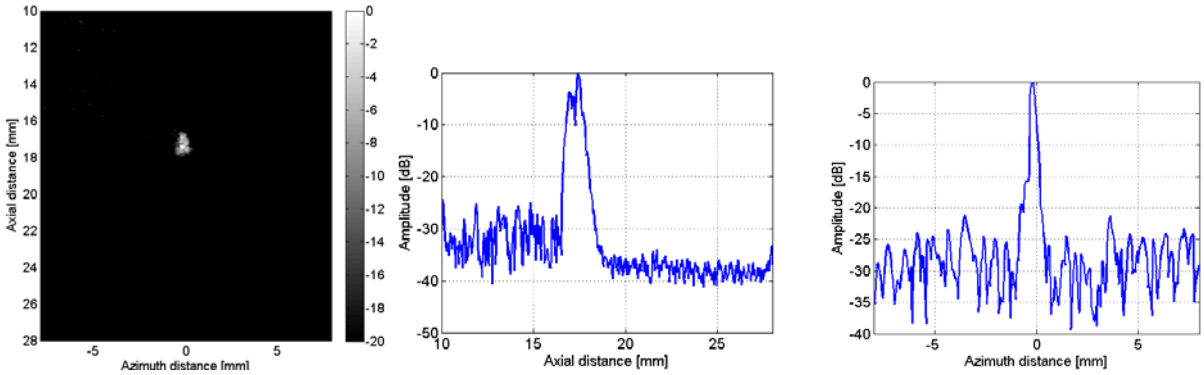

Figure 31 The image of target cellulose tube in contrast mode (left), and its beam width in axial (middle) and azimuth (right) direction (Li 2016).

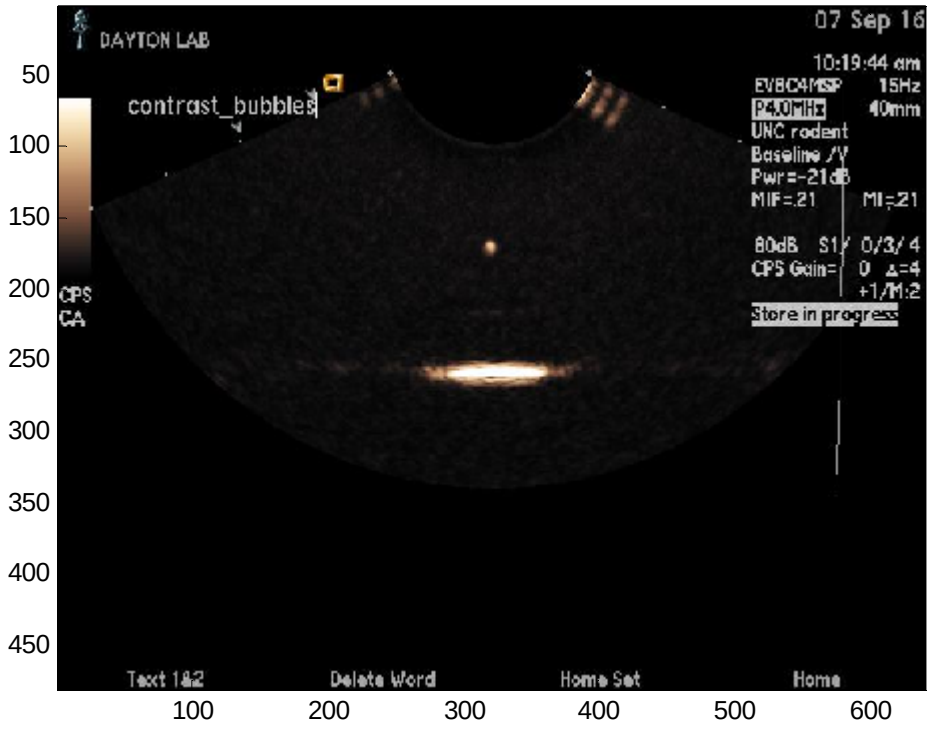

The same phantom with cellulose tube was image with an EV-8C4 Siemens transrectal probe transducer. The received beam widths in the axial and lateral dimensions measured to be 1.33 mm and 1.25 mm, respectively. The contrast to noise ratio was calculated to be approximately 70 dB.

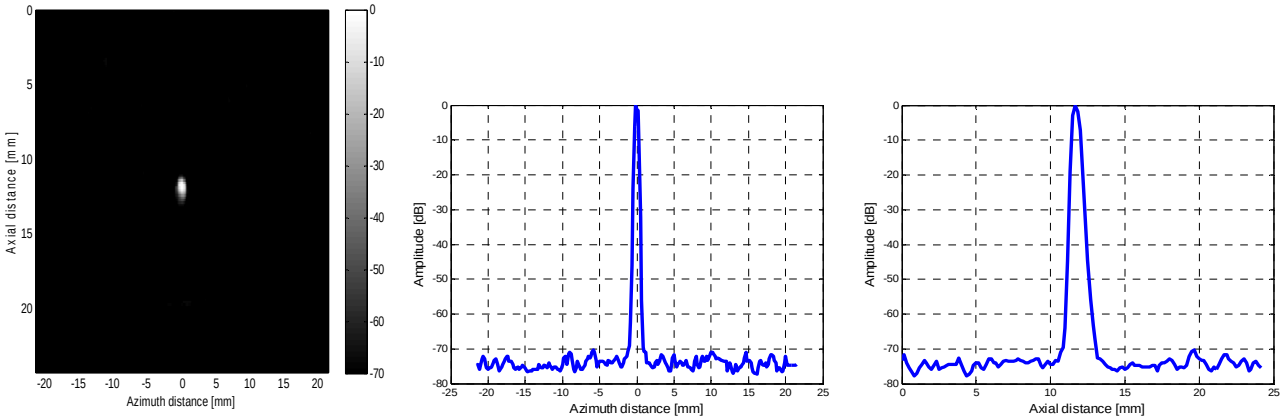

Figure 32 The image of target cellulose tube imaged with a Siemens EV-8C4 in contrast mode (left), and its beam width in axial (middle) and azimuth (right) direction.

Task 6 In-vivo testing of dual frequency PC-MUT co-linear array (Months 1-6, and 24-36)
Subtask 6.1 Prepare for IACUC approval for animal studies (Months 1-6)

Immediately upon project commencement, an appropriate protocol will be prepared for the University of North Carolina *Institutional Animal Care and Use Committee,* for eventual in-vivo imaging studies.

Subtask 6.2 Establish Dunning/Copenhagen rodent prostate cancer model (Months 24-27)
The Dunning R3327 cell line is available from ATCC, from the Johns Hopkins Collection. Twenty 60 day old male Copenhagen Rats (Harlan Indianapolis, IN) will be utilized for in-vivo imaging. Cells will be propagated in culture, and then subcutaneously injected into the flank of each rat. Imaging will be performed starting one week after implantation, and continued until tumors reach approximately 15 mm in diameter, after which animals will be humanely euthanized. For all procedures, animals will be anesthetized using inhaled oxygen and 2% isoflurane. Body temperature will be maintained using a temperature controlled heating pad.

Subtask 6.3 Assess performance of imaging probe in animal model (Months 25-36)
The diagnostic utility of the prototype array to detect cancerous lesions will be assessed in vivo in terms of spatial and temporal sensitivity relative to a conventionally used clinical probe. Two specific imaging approaches will be assessed – ultrasound molecular imaging and microvessel mapping. Spatial sensitivity will be determined by how accurately molecularly targeted contrast agents and microvascular abnormalities conform to the tumor boundaries (relevant to improving biopsy guidance accuracy), while temporal sensitivity will be assessed by observing how these metrics evolve throughout the course of a tumor's growth. The Dunning model will be established in the right flank of 20 male rats (the left flank will serve as a control). To assess the imaging performance of the prototype array as a function of axial depth between 0.5 and 5 cm, tissue mimicking gelatin standoffs will be inserted between the animals' skin and transducer to simulate a deeper lesion depth. Images will be acquired with the clinical probe for contrast imaging of the same tumor and control tissue volumes to compare molecular imaging signal strengths and ability to visualize vascular abnormalities.

Methods and Results for Task 6:

In-vivo 2D and 3D rat imaging using prostate dual-frequency array

Due to challenges with obtaining cell lines to establish the Dunning R3327 rat prostate model, we instead chose to use the fibrosarcoma rat tumor model in female Fisher 344 rats. Tumors were implanted subcutaneously in the right flank of the rat, and grew between 5-10 mm in diameter. Rats were anesthetized with isoflurane and then shaved in the lower abdominal/flank region. The transducer was positioned approximately 5 mm from the surface of the tumor and was coupled to the skin with ultrasound gel. Before contrast injection, B-mode imaging was performed, followed by contrast mode imaging for baseline measurements of the tumor. Then, a constant infusion of a 1:1 dilution of contrast to saline was administered at a rate of 30 μL/min and contrast mode imaging was performed again to detect blood vessels. In order to increase sensitivity to microbubbles, an excitation voltage of 33V (~1 MPa) was delivered to elicit a higher harmonic tissue response. The transducer sensitivity to the broadband microbubble response was not sufficient for detecting contrast enhancement within the tumor. Therefore, we shifted the imaging region to the inguinal area of the rat to image the larger iliac vein and

arteries. From the contrast mode 2D image with microbubbles, there is clear enhancement of microvessels (Figure 34).

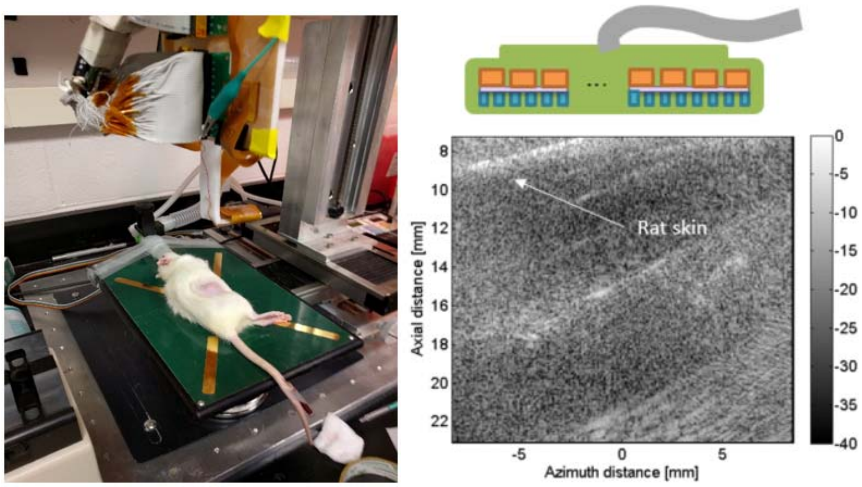

Figure 33 A photograph of experimental setup in animal imaging (left), and the B-mode image on the plane of interest (right)

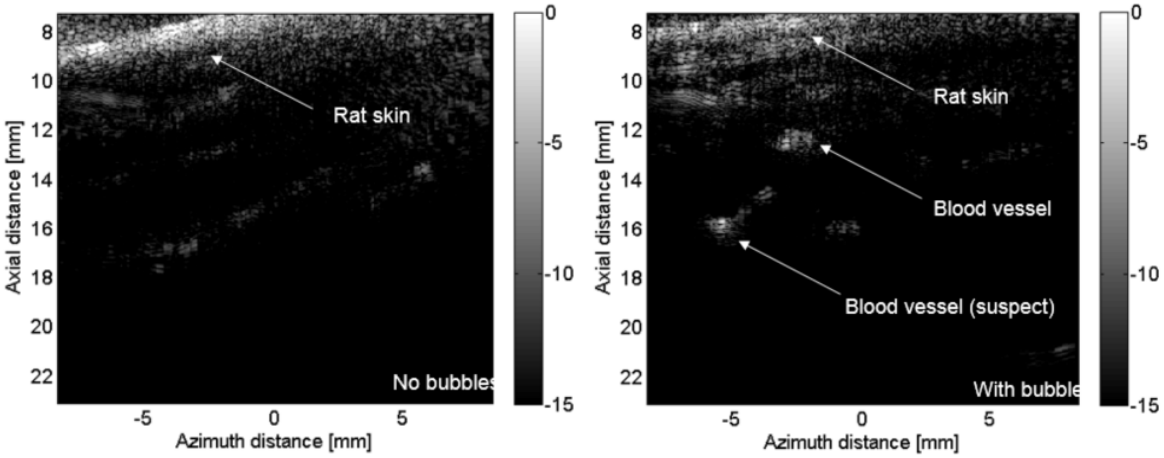

Figure 34 A 2D gray scale image of animal test in different scenarios (left: contrast mode without bubble flow, right: contrast mode with bubble flow)

In a different rat, a 3D image was acquired with an elevational dimension of 1 cm and a 0.5 mm step size. Individual vessels were detected in the 3D pull-back at a depth between 20-30 mm (Figure 35). Further post-processing and refinement of the RF data is required to further remove system noise residual higher-harmonic tissue signal.

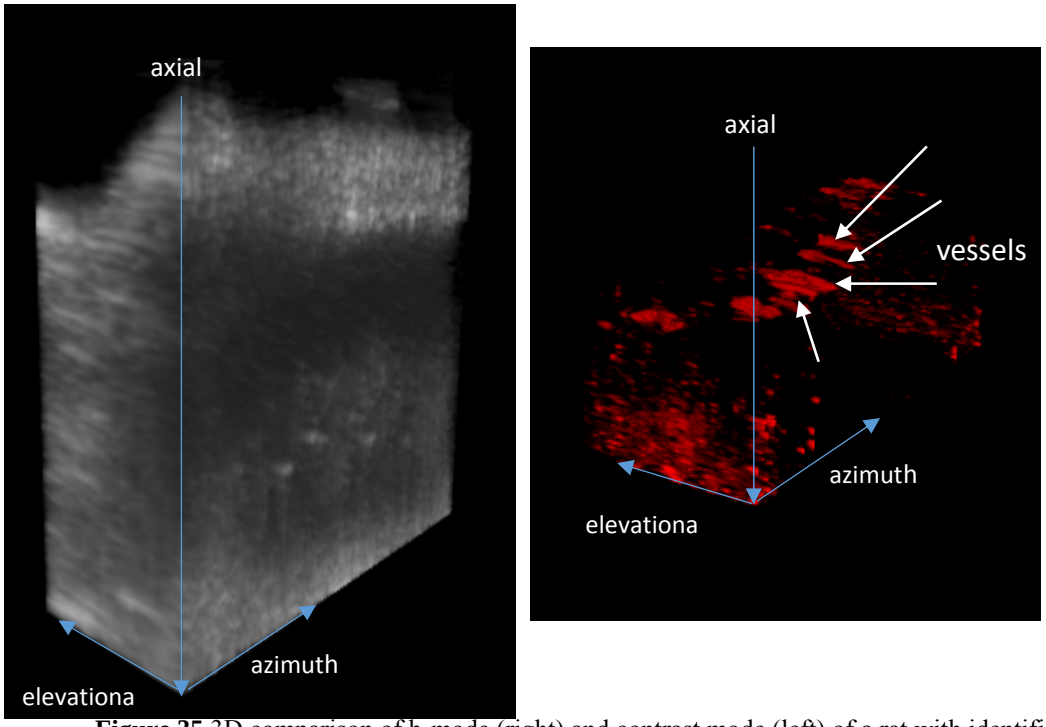

Figure 35 3D comparison of b-mode (right) and contrast mode (left) of a rat with identified vessels.

Task 7 Prepare manuscript for data dissemination (Months 30-36)

Although during this project we made substantial progress on the novel design of dual-frequency transducer arrays for superharmonic imaging, the prototype arrays that were produced during the project period did not demonstrate a sensitivity high enough for high contrast-to-tissue imaging of the microvasculature in vivo. Although we could see some vessels, the probe did not perform well enough to benchmark in-vivo imaging against the Siemens EV-8C4. We still have several arrays that were fabricated with minor modifications to the design, such as adjusting the matching layers, at the end of the project period. We are still testing these transducers despite the fact that the original DoD project has ended. Although this project resulted in 4 other published manuscripts, we have not yet been able to publish in-vivo performance data at this point. However, we are still working towards this aim and are in the progress of soliciting additional funding as this project has been highly encouraging.

Impact/Problems

- Single element dual-frequency transducers have been designed, fabricated and tested for feasibility study. Contrast imaging tests have been conducted and contrast signals have been successfully detected. A 64/128-element dual-frequency 3 MHz/15 MHz linear array transducer has been designed and fabricated, and the initial tests of contrast phantom imaging have been demonstrated the potential for acoustic angiography. An invention disclosure was filed on the dual-frequency transducer technology, patent pending.
    - This was the first dual-frequency stacked array of its kind – all current commercial ultrasound transducers operate within a single bandwidth range, typically less than 100% (ie: a 3 MHz commercial array with a 100% bandwidth would operate with -6dB performance between 1.5 and 4.5 MHz). We overcame several challenges in the fabrication technology to develop our unique dual-frequency configuration, with the resulting transducer operating at a bandwith that extends past 15 MHz when transmitting at 3 MHz – far superior to currently available transducers. The potential impact is that other manufacturers or scientists might now further expand on this technology development to produce newer transducers with even better performance.

- 2D and 3D rat imaging demonstrates the ability to detect individual vessels in the inguinal area of a rat. Further design modification and post-processing is needed to improve image quality and sensitivity to smaller tumor vessels.
    - The impact was that we demonstrated that our dual-frequency transducers could detect microvessels with high contrast to tissue ratio. This is important, because we believe that microvessel imaging will help the detection of cancer, based on cancer's angiogenic signature. One of our challenges was that our array transducer was not as sensitive as we had hoped, which prohibited full analysis of tumor microvasculature. We know that sensitivity could be better because other single element transducers that we use do have sufficient sensitivity to image vessels down to 150 microns with high contrast to tissue.

- Four publications (Martin et al, 2014; Dayton et al; 2014; Kim et al, 2015; Wang et al 2016) and five conference presentations (Kim et al 2014; Kim et al 2015; Kim et al 2015b; Li et al 2015; Li et al, 2016) were presented describing the technology developed from this project.
    - We have disseminated our findings to the community and the impact will be that others will build on and continue our work, to build better transducer systems for cancer imaging. Eventually, it is highly likely that prostate ultrasound will be come a primary tool for assessing prostate cancer non-invasively (ie: without biopsy).

Conclusion

Both single element dual frequency transducers and dual frequency linear array transducers designed towards trans-rectal ultrasound imaging have been successfully prototyped and tested.

A single element dual frequency (2 MHz/14 MHz) was designed, fabricated and tested with microbubbles. It was found that: 1) the dual isolation layer works well to block the unwanted background signals; 2) the 1-3 piezoelectric composite is a useful material for the low frequency transmitter without thick and lossy backer, and results in sufficient transmit pressure and reasonably wide bandwidth; and 3) the prototypes based on this design can detect 7^{th} harmonic signal from the micro bubbles.

A co-linear, dual-frequency (3/15 MHz) transducer was developed for demonstrating the feasibility of transrectal acoustic angiography. This was the first dual mode 3/15 MHz array transducer reported to our knowledge. The acoustic characterization results indicate that our design concept and technique can achieve fractional bandwidths and transmission/receiving sensitivities which are sufficient for superharmonic microbubble imaging. We also used a multi-channel imaging system to demonstrate that the array was capable of inducing a higher harmonic response from microbubble contrast agents at a depth of 30 mm. With a 1-cycle burst excitation, the target widths in axial and lateral directions were 200 μm and 400 μm, respectively, and CTR was ~20 dB. In-vivo animal imaging demonstrated the ability to detect large individual vessels at a depth of 20-30 mm in the inguinal area. Unfortunately, the transducer was not sensitive to detecting smaller vessels (<500 μm) when imaging a tumor in-vivo. Further modifications to the transducer design and post-processing will be required to achieve a sensitivity to vessels in the <500 μm range hypothesized to be involved in prostate tumor angiogenesis. Nevertheless, these results indicate that the co-linear array is capable of detecting superharmonic microbubble signals and suggest that is can be used for acoustic angiography imaging of tissue neovascularization with further improvements to the design.

Overall, our project was highly productive towards the development of dual-frequency array technology. Our team intends to continue testing with devices which were fabricated during the project period, and will pursue additional project funding to further improve the imaging arrays.

Publications, Abstracts, and Presentations

Abstract/Presentations

J. Kim, S. Li, X. Jiang "Development of Transmitters in Dual Frequency Transducers for Interventional Contrast Enhanced Imaging", abstract accepted to 2014 IEEE Ultrasonics Symposium, presented Sept 3-6, 2014.

J. Kim, S. Li, S. Kasoji, P. Dayton, X. Jiang, "Development of Transmitters in Dual-Frequency Transducers for Interventional Contrast Enhanced Imaging and Acoustic Angiography," *IEEE Ultrasonics Symposium Proceedings*, 2015;63:7-15.

J. Kim, S. Li, S. Kasoji, P. A. Dayton, and X. Jiang, "Dual-frequency super harmonic imaging piezoelectric transducers for transrectal ultrasound," in SPIE Smart Structures and Materials+ Nondestructive Evaluation and Health Monitoring, 2015, pp. 943823-943823-10 *(proceedings).*

S. Li, J. Kim, Z. Wang, X. Jiang, S. Kasoji, B. Lindsey, P. A. Dayton., "A 3 MHz/18 MHz dual-layer co-linear array for transrectal acoustic angiography," in Ultrasonics Symposium (IUS), 2015 IEEE International, 2015, pp. 1-4

S. Li, J. Kim, Z. Wang, X. Jiang, S. Kasoji, B. Lindsey, Paul A. Dayton., " A Dual-frequency Co-Linear Array for Prostate Acoustic Angiography," in Ultrasonics Symposium (IUS), 2016 IEEE International, 2016

Publications

K. H. Martin, B Lindsey, J Ma, M. Lee, F. S. Foster, X Jiang, P. A. Dayton, "Dual-frequency piezoelectric transducers for contrast enhanced ultrasound imaging", *Sensors*, 2014; 14(11):20825-42

P.A. Dayton, R.C. Gessner, L. Phillips, et al. The implementation of acoustic angiography for microvascular and angiogenesis imaging. Conf Proc IEEE Eng Med Biol Soc. 2014;2014:4283-5.

J. Kim, S. Li, S. Kasoji, P. Dayton, X. Jiang. "Phantom evaluation of stacked-type dual-frequency 1-3 composite transducers: A feasibility study on intracavitary acoustic angiography." *Ultrasonics 2015.* 63:7-15.

Z. Wang, K.H. Martin, W. Huang, P.A. Dayton, X. Jiang. "Contrast Enhanced Superharmonic Imaging for Acoustic Angiography Using Reduced Form-factor Lateral Mode Transmitters for Intravascular and Intracavity Applications". *IEEE Trans Ultrason Ferroelectr Freq Control*. 2016

Inventions, Patents, and Licenses

Invention: Multi-Frequency Ultrasound Transducers and Arrays for Ultra-Broadband Ultrasound Imaging
Record: 14187
Invention disclosure submitted 4/6/14
Reported on 5/9/14.
No patents filed yet

Reportable Outcomes

Nothing to report

Other Achievements

Nothing to report

References

See above in 'publications'

Report of Personnel Supported During Project Period

Dayton, Paul A, Ph.D.	PI
Jiang, Xiaoning, Ph.D.	co-PI
Fielding, Julia Rose, M.D.	clinical consultant
Johnson, Kennita, Ph.D.	laboratory manager, IACUC manager
Brooks, Lindsey, Ph.D.	post-doc research associate
Novell, Anthony, Ph.D.	post-doc research associate
Sridharan, Anush, Ph.D.	post-doc research associate
Kim, Jinwook	student research associate
Kasoji, Sandeep Kumar	student research associate
Li, Sibo	student research associate
Wang, Zhuochen	student research associate
Guo, Sijia	student research associate
Kim, Kyungrim	student research associate

Appendix 1: Copies of Publications

This article has been accepted for publication in a future issue of this journal, but has not been fully edited. Content may change prior to final publication. Citation information: DOI 10.1109/TUFFC.2016.2619687, IEEE Transactions on Ultrasonics, Ferroelectrics, and Frequency Control

Contrast Enhanced Superharmonic Imaging for Acoustic Angiography Using Reduced Form-factor Lateral Mode Transmitters for Intravascular and Intracavity Applications

Zhuochen Wang, K. Heath Martin, Wenbin Huang, Paul A. Dayton, Xiaoning Jiang, *Member, IEEE*

***Abstract*—Techniques to image the microvasculature may play an important role in imaging tumor-related angiogenesis and vasa vasorum associated with vulnerable atherosclerotic plaques. However, the microvasculature associated with these pathologies is difficult to detect using traditional B-mode ultrasound or even harmonic imaging due to small vessel size and poor differentiation from surrounding tissue. Acoustic angiography, a microvascular imaging technique which utilizes superharmonic imaging (detection of higher order harmonics of microbubble response), can yield a much higher contrast to tissue ratio (CTR) than second harmonic imaging methods. In this work, two dual-frequency transducers using lateral mode transmitters were developed for superharmonic detection and acoustic angiography imaging in intracavity applications. A single element dual-frequency IVUS transducer was developed for concept validation, which achieved larger signal amplitude, better contrast to noise ratio (CNR) and pulse length compared to the previous work. A dual-frequency PMN-PT array transducer was then developed for superharmonic imaging with dynamic focusing. The axial and lateral size of the microbubbles in a 200 µm tube were measured to be 269 µm and 200 µm, respectively. The maximum CNR was calculated to be 22 dB. These results show that superharmonic imaging with a low frequency lateral mode transmitter is a feasible alternative to thickness mode transmitters when final transducer size requirements dictate design choices.**

***Keywords*—Lateral mode transducer, dual-frequency, superharmonic, ultrasound transducer.**

I. Introduction

IMAGING of microvessels with diameters ranging from 2 µm to 200 µm [1] can be used to detect the early phase of tumor development and may also aid in identifying atherosclerotic plaques which cause heart attacks and strokes [2-7]. Traditional B-mode ultrasound (2–20 MHz) is widely used in biomedical diagnostic imaging because of its relative low cost, portability, ease of operation and real-time imaging. However, blood is a poor ultrasound scatterer compared to the surrounding tissues, making it hard to image microvessels [8]. Thus, ultrasound contrast agents (UCAs) (e.g. microbubbles) are used to increase the scattering and thereby improve imaging of blood flow [9].

Although in standard fundamental B-mode imaging, UCAs can result in improved contrast from the blood pool, contrast with surrounding tissue is still limited. Blood is a poor scatterer at diagnostic frequencies (2-20 MHz) typically used in the clinic and vessels appear anechoic during imaging. When contrast agents are administered, the blood vessels opacify due to the increased echogenicity provided by the microbubbles, but the vessel are not easily discernable from the surrounding tissue which has similar backscatter, leading to poor contrast and low CTR [10]. Harmonic imaging of UCAs, transmitting at a lower frequency and receiving the signal from the second harmonic, can yield a higher CTR with less near field artifacts than fundamental B-mode imaging. This imaging technology may be used to improve the visualization and assessment of cavities, large vessels, and bulk blood flow in organs and tissues [11, 12]. Harmonic imaging technology was developed from conventional transabdominal and transthoracic echocardiography, and soon applied in smaller diagnostic transducers, for ophthalmic, urologic, and intravascular ultrasound purposes [13-19].

Most of the echo from the tissue is confined to the fundamental frequency and low order harmonics [20]. In contrast, superharmonic imaging, where higher order harmonics are detected, provides improved differentiation of UCAs from tissue and higher resolution in the resulting images [21]. Some work have been done to study the optimization of microbubble response, including varying pulse window and phase of the signal, changing the bubble size, adjusting the frame number, and controlling the peak negative pressure [22, 23]. Typically, for non-inertial cavitation superharmonic imaging, higher order non-linear responses are maximized by exciting microbubbles with a large peak negative pressure or at a frequency close to the resonant frequency of the microbubble. This resonant frequency depends primarily on bubble diameter, though many other physical factors also play a role in determining resonance [24, 25].

Studies have shown that lower frequency (1-3 MHz) acoustic

Zhuochen Wang and Xiaoning Jiang are from the Department of Mechanical and Aerospace Engineering, North Carolina State University, Raleigh, NC 27695, USA. (e-mail: xjiang5@ncsu.edu).

Wenbin Huang is from the State Key Lab of Mechanical Transmissions, Chongqing University, Chongqing, 400044, China.

K. Heath Martin and Paul A. Dayton are from Joint Department of Biomedical Engineering, University of North Carolina and North Carolina State University, Chapel Hill, NC 27599, USA.

This article has been accepted for publication in a future issue of this journal, but has not been fully edited. Content may change prior to final publication. Citation information: DOI 10.1109/TUFFC.2016.2619687, IEEE Transactions on Ultrasonics, Ferroelectrics, and Frequency Control

waves can excite microbubbles more effectively to generate non-linear responses from microbubbles that are necessary for contrast specific imaging. Kruse et al. received broadband microbubbles response exceeded 45 MHz with short pulses at 2.25 MHz [26]. Gessner et al. reported 3-D contrast imaging of in vivo microvasculature with a dual-frequency transducer (2.5 MHz / 30 MHz) [27]. Lindsey et al showed that CTR of superharmonic imaging can be improved by detecting the non-linear high-frequency signal from microbubbles excited at lower frequencies [28]. Wang et al. reported preliminary superharmonic contrast imaging results with a lateral mode intravascular ultrasound (IVUS) cylindrical transducer array transmitter (2.25 MHz) and commercial piston receivers (15 MHz, 20 MHz and 25 MHz) [29]. Microvascular images produced with transmission between 2–4 MHz and detection between 15–45 MHz have demonstrated very high resolution and CTR, producing images similar to x-ray angiography, and images produced with this dual-frequency ultra-broadband contrast imaging approach have been referred to as "acoustic angiography" [30-33].

Small diagnostic transducers are important for extending the possibilities of intravascular, intracardiac, and transesophageal ultrasound [34]. Superharmonic imaging using a small single element intravascular ultrasound transducer has been demonstrated with a transmission at 6.5 MHz [35], but it is likely that these results may be improved by using a lower transmission frequency (1-3 MHz). Miniaturization of the lower frequency transducer can be achieved by utilizing the lateral excitation mode in developed transducers. Some therapeutic IVUS catheters have been designed using lateral mode excitation for thermal ablation and drug delivery previously [36-38]. Transducer arrays have several benefits over single-element transducers, such as electrical scan and dynamic focusing, which can result in higher frame rates and decreased point spread functions, respectively [39]. Despite these advantages, early studies comparing commercial transducers favored single-elements over array designs in terms of image quality [40], suggesting array design in IVUS may be improved. Under the same input voltage, a lateral mode transducer having a smaller thickness between electrodes would have a higher electric field compared to a thickness mode transducer at the same frequency. Lateral mode transmitters are also suitable for developing an array.

In this work, two dual-frequency transducers with lateral mode, low frequency transmitters are demonstrated for superharmonic imaging (over 12th harmonic). First, a dual-frequency single element IVUS transducer with a lateral mode low frequency transmitter was developed for contrast enhanced intravascular ultrasound (CE-IVUS) imaging and to validate the concept. Next, a dual-frequency PMN-PT array using a lateral mode low frequency transmitter was developed for superharmonic imaging in larger cavities (e.g. intracardiac and transesophageal ultrasound). In both cases, the center frequency of the transmitters was selected to be 2.25 MHz to excite microbubbles effectively, while the center frequency of the receivers was 30 MHz. The dual-frequency transducers were used for superharmonic contrast testing and real-time superharmonic imaging.

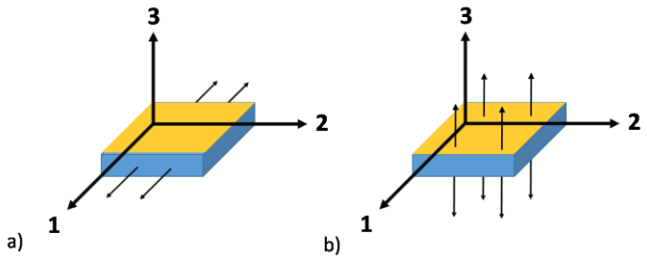

Fig. 1. a) Lateral mode transducer and b) thickness mode transducer.

II. Methods

A. *Lateral mode transmitter*

Low frequency (1-3 MHz) acoustic wave excitation is a promising method for contrast imaging because it can generate non-linear microbubbles responses more effectively from large bubbles by exciting them near their resonant frequency. However, low frequency transducers in conventional thickness mode require a large dimension in thickness and may not be suitable for some applications with limited accessible space (e. g. intravascular, intracardiac, and transesophageal). For example, a 2.25 MHz thickness mode transmitter would require a thickness of approximately 1 mm for $Pb(Mg_{1/3}Nb_{2/3})O_3]$ -x[$PbTiO_3$] (PMN-PT). This dimension would not suitable for an IVUS transducer (3 French = 1 mm) after integration with matching layer, backing layer and housing.

In addition to the thickness vibration mode, ultrasound transducers can be designed to operate in lateral vibration modes (Figure. 1). In a lateral vibration mode, the resonant frequency is determined by the width or length of the piezoelectric layer rather than the thickness [35]. The coupling coefficients of lateral mode (k_{31}=0.51) of PMN-PT is smaller than the coupling coefficients of thickness mode (k_t=0.62, and k_{33}=0.91), leading to a reduction in performance of the transducer in regards to sensitivity and bandwidth [41]. While because of high elastic compliance of PMN-PT (s_{11}^E = 59.7 pm^2/N), the transverse frequency coefficient (N_{31}) of PMN-PT is much lower than the thickness frequency coefficient (N_t) (721 vs 2002 m•Hz).

$$N_{31} = 1/2\sqrt{1/(\rho \bullet s_{11}^E)} \quad (1)$$

$$N_t = 1/2\sqrt{c_{33}^E/\rho} \quad (2)$$

where N_{31} is the transverse frequency coefficient, N_t is the thickness frequency coefficient, ρ is the density = 8050 kg/m^3, s_{11}^E is the elastic compliance, c_{33}^E is the elastic stiffness = 129 GPa.

As a result, the lateral mode transducer can achieve a low resonant frequency with small dimensions in both thickness and width. Compared to the conventional thickness mode transducer, the aspect ratio (width/thickness) of a lateral mode transducer can be larger, resulting in lower electrical impedances at low frequencies. Furthermore, the electric field developed in a lateral mode transducer would be higher than a thickness mode transducer at same frequency due to the

This article has been accepted for publication in a future issue of this journal, but has not been fully edited. Content may change prior to final publication. Citation information: DOI 10.1109/TUFFC.2016.2619687, IEEE Transactions on Ultrasonics, Ferroelectrics, and Frequency Control

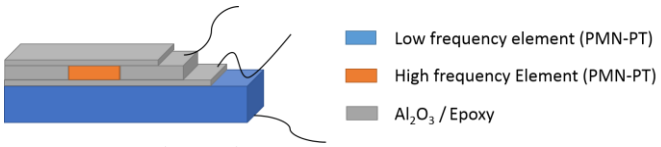

Fig. 2. Structure of a dual-frequency IVUS transducer.

decreased dimension (thickness) between the electrodes. Consequently, lower input voltages can be used to achieve the same electric field. Therefore, in order to develop a low frequency (e.g. 2 MHz) transmitter without increasing the size of the transducer, the lateral mode design approach was selected to achieve efficient low frequency ultrasound output.

B. Dual-frequency Single Element IVUS Transducer

1) Transducer Design and Characterization

The dual-frequency IVUS transducer consists of a low frequency transmitter (2.25 MHz) at the bottom and a high frequency receiver (30 MHz) layered on top of it (Figure. 2). As the elements were aligned overlapped in stack structure [42-44], the beam of both frequencies will overlap as well, making it suitable for superharmonic imaging. In the stack structure, the two active layers cannot be bonded together directly as this would cause aliasing echoes to be generated that can shift the resonant frequencies of both layers and impact the bandwidth [45]. In order to prevent this, a frequency-selective isolation layer that functions as a quarter wavelength anti-matching layer has to be placed in between the two elements in order to isolate the top layer from the bottom layer in the high frequency mode [46]. PMN-PT was selected as the active material because of its high coupling coefficients, high dielectric constant and low transverse frequency coefficient (Table I).

The isolation layer thickness and the material selection, as well as the pulse-echo response of the high frequency receiver, were designed using the KLM model [47]. For low frequency lateral mode transmitter, the frequency response of the electric impedance was simulated with COMSOL (COMSOL, Inc., Burlington, MA). After the transducer design and fabrication, the transducer was characterized by measuring electrical impedance, the pulse-echo response of the high frequency receiver, and the acoustic output of the low frequency transmitter. The detailed method of transducer design, fabrication, and transducer characterizations can be found in [48].

2) Contrast Test

Contrast tests were conducted in a water tank using poly-dispersed (1-10 μm diameter) lipid coated microbubbles, prepared in-house [49], at diluted concentrations (2 x 107 MBs/mL). Microbubbles were pumped through a micro tube made of acoustically transparent material with a diameter of 200 μm. The distance between the transducer and the micro tube was matched to the depth used for pressure measurements (2 mm). The experimental setup is depicted in Figure 3.

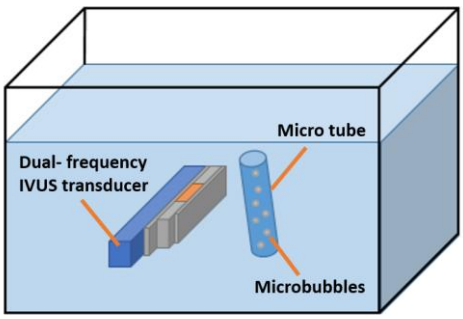

Fig. 3. Experimental setup of the contrast test.

TABLE I
MATERIAL PROPERTIES OF DIFFERENT ACTIVE MATERIALS

	k_{33}	k_t	k_{31}	ε_r	N_t	N_{31}
PMN-PT	0.91	0.62	0.51	8266	2002	721
PZT-5H	0.78	0.51	0.43	3400	1975	1421
PZT-4	0.7	0.49	0.33	1300	1958	1646

Microbubbles in the micro tube were excited by the low frequency transmitter using a 2.25 MHz, 1-cycle sine burst excitations generated by an arbitrary function generator (AFG3101, Tektronix Inc., Beaverton, OR) and a radio-frequency amplifier (Model 3200L, Electronic Navigation Industries Inc., Rochester, NY). The superharmonic non-linear responses from excited microbubbles were then detected by the high frequency receiver and recorded using an in-house LabVIEW (National Instruments Co., Austin, TX) data acquisition system and A/D card (Signatec PDA14, Corona, CA) at 100 MHz sampling rate. 24 dB of gain was applied on the high frequency response. The superharmonic signal, contrast to noise ratio (CNR) and pulse length of superharmonic echo were measured. The CNR of the single element IVUS transducer was measured as the ratio between maximum microbubble response and the mean noise level. Experimental results were recorded as a function of different excitation voltages (e.g. 20V, 40V, 60V and 80V).

C. Dual-Frequency Array Transducer

1) Transducer Design and Characterization

This dual-frequency array consists of 8 low frequency lateral mode transmission sub-elements and 32 high frequency receiving elements (Figure. 4). The center frequency of the transmitter was selected to be 2.25 MHz to excite microbubbles more effectively, while the frequency of the receivers was designed to be 30 MHz for high image resolution. The width to height aspect ratio of each layer is important for the lateral mode transducer. For the low frequency transmitter, the aspect ratio was designed close to 1 to enhance the lateral mode, by using COMSOL simulation; while the aspect ratio of the high frequency layer was designed to be greater than 2 to promote thickness mode operation, which was simulated by using KLM model. An acoustic isolation layer was also placed in between the two PMN-PT active layers to reduce the ringdown of the high frequency receiver layer and to improve the performance.

The pulse-echo response of high frequency receiving layer, acoustic pressure and acoustic mapping of low frequency

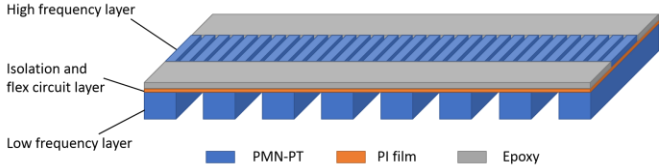

Fig. 4. Structure of a dual-frequency array transducer.

transmitter were tested to evaluate the performance of the dual-frequency array. The detailed method of design, electrical and acoustical characterization of this dual-frequency array transducer were reported in [50].

2) Real-time Contrast Imaging

Real-time contrast imaging was conducted with the Verasonics programmable ultrasound system (Verasonics Vantage, Redmond, WA). The Verasonics sampling frequency (quadruple of the base frequency) was set to be 62.5 MHz (15.6 MHz as base frequency), which is the maximum frequency setting of our Verasonics System. Since the maximum sampling rate of the Verasonics system is 62.5 MHz, the upper band of the receiving signal is limited to 31.25 MHz. The contrast images were rendered using a proprietary Verasonics linear scan beamforming algorithm and a built-in bandpass filter (19-30 MHz). A plane wave generated from 8 low frequency sub-elements first excites the microbubble contrast agents; then higher order non-linear microbubble responses were collected with high frequency receivers; the position and amplitude information of microbubble response were reconstructed with dynamic receive focusing of filtered signals. The constant f-number on the receivers was set to be 1.26. The maximum voltage of the low frequency transmitter is 55 V due to the limitation of the Verasonics system at the functional frequency.

Contrast tests were conducted in a water tank using lipid coated microbubbles (1-10 μm diameter) at diluted concentrations (1 ×108 MBs/mL). Contrast agents were passed through a micro tube made of acoustically transparent material with a diameter of 200 μm. The flow rate was set to be 10 mL/hr. The distance between the transducer and the micro tube was set to be 5.5 mm (Figure. 5).

Microbubbles in the micro tube were excited by the low frequency transmitter with a 2.23 MHz, 1-cycle burst using either 55 V or 35 V excitation for comparison. The superharmonic non-linear responses from excited microbubbles were then detected by the high frequency receivers. The real-time contrast imaging, average of 10 images, was observed from the monitor and saved for later offline evaluation. The axial and lateral superharmonic image resolutions were calculated quantitatively from the axial and lateral profile of the microbubbles responses. The CNR of the array transducer was measured as the ratio between maximum microbubble response and the mean of the noise in an area of 3 mm by 3 mm.

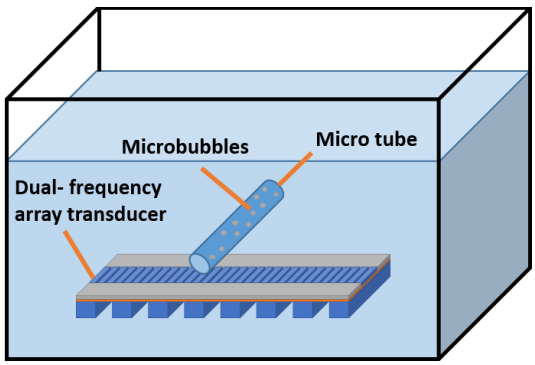

Fig. 5. Experimental setup of the real-time superharmonic imaging.

3) Electric Matching

The electrical impedance of the transducer at resonance is inversely proportional to the capacitance of the transducer or, in another words, the surface area of the piezoelectric element.

$$Z \propto 1/C = d/(\varepsilon \bullet A) \quad (3)$$

where Z is the electrical impedance, C is the capacitance, d is the thickness and A is the surface area of the piezoelectric element.

Since the aperture size of each high frequency receiver is small in the array design, the electrical impedance of the high frequency receiver is large (~ 200 Ω) and not compatible with most high frequency systems (50 Ω). Additionally, because of the high capacitive reactance, the electrical impedance of the high frequency receivers is highly capacitive at resonance.

Transmission line theory allows a coaxial cable to function as an impedance transformer so that the device can be electrically matched to the electronics to avoid reflections and reduced power delivery [51]. Hence, a coaxial cable was used to connect the transducer array to the Verasonics system (Verasonics, Redmond, VA), and the electric impedance between the transducer element and the Verasonics system can then be matched [52].

III. Results and Discussion

A. Dual-frequency Single Element IVUS Transducer

Based on the finite element analysis and KLM simulation, the material and dimension of the transducer was selected (Table II). The size of the low frequency transmitter was 5 mm × 0.37 mm × 0.3 mm. The high frequency receiver was designed with an aperture size of 0.5 mm ×0.37 mm ×0.07 mm with a 20 μm thick matching layer (Al2O3/ Epo-tek 301 (Epoxy Technology Inc, Billerica, MA)). A 20 μm thick Al2O3/ Epo-tek 301 layer for frequency selective isolation was placed in between the two piezoelectric layers. This suppressed the ringdown and aliasing echo of the high frequency receiver operating in pulse-echo mode. The presence of the isolation layer did not significantly alter the low frequency transmitted pressure because the isolation layer was thin compared to the wavelength of the low frequency mode (1244 μm) [53-55].

This IVUS transducer achieves low frequency transmission

TABLE II
Design Parameters of Single Element Dual-frequency IVUS Transducer

Parameter	Transmission layer	Receiving layer
Center Frequency	2.25 MHz	30 MHz
Material	PMN-PT	PMN-PT
Impedance (MRayl)	32	32
Width (mm)	0.37	0.37
Length (mm)	5	0.6
Thickness (μm)	300	70
Matching/Isolation Material	Al2O3/epoxy	Al2O3/epoxy
Impedance (MRayl)	5.5	5.5
Matching Thickness (μm)	110	20
Isolation layer Thickness (μm)	-	20

This article has been accepted for publication in a future issue of this journal, but has not been fully edited. Content may change prior to final publication. Citation information: DOI 10.1109/TUFFC.2016.2619687, IEEE Transactions on Ultrasonics, Ferroelectrics, and Frequency Control

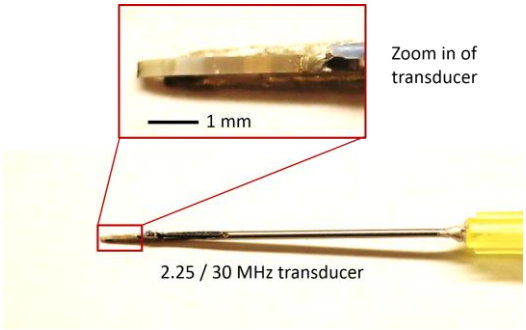

Fig. 6. Prototype dual-frequency IVUS transducer housed on the tip of a 20 gauge needle.

at a size that is applicable for use in interventional procedures and meets the size requirements for typical 3 Fr coronary catheters (Figure 6). The -6 dB fractional bandwidth of the high frequency receiver was measured to be 32 % with a center frequency of 32 MHz, covering a frequency span of 27 – 37.3 MHz [48]. When a 1 cycle burst excitation at 2.25 MHz was applied to the low frequency transmitter, the peak negative pressure at 2 mm reached 575 kPa at 80 V [48], which is enough to excite the microbubbles. Further details of the transducer fabrication and characterization can be found elsewhere [48].

The high frequency response of microbubbles was successfully detected by the high frequency receiver with a CNR of 13 dB (Figure 7a). Microbubbles responses under different excitation voltages were compared in Figure 7b. Significant microbubbles responses were detected with 1 cycle burst excitation of 60 V and 80 V. When the excitation voltage was lower than 40 V, no microbubble signal could be detected. The contrast signal with an amplitude of 45 mV under 24 dB gain (or 2.8 mV without gain) and an -6 dB pulse length of 150 μm (0.1 μs) were achieved.

Compared to our previous thickness mode dual-frequency IVUS transducer (6.5 MHz / 30 MHz) [35], this dual-frequency IVUS transducer (2.25 MHz / 30 MHz) with a lateral mode transmitter has improved performance in signal amplitude, CNR and pulse length of the superharmonic echo (Table III). Moreover, the required peak negative pressure to produce detectible nonlinear microbubble response has been cut in half to 450 kPa (under 60 V excitation), with a relative low mechanical index (0.3) [48].

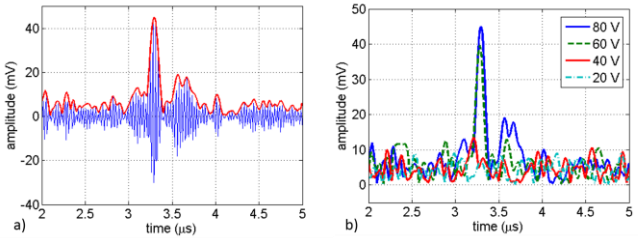

Fig. 7. a) Contrast test result under 80V 1-cycle burst excitation. b) Contrast test results under different voltages.

TABLE III
PERFORMANCE OF SINGLE ELEMENT TRANSDUCERS IN CONTRAST TEST

Transducer	# of Cycles	Applied voltage	Superharmonic echo amplitude	CNR (dB)	-6 dB pulse length
2.25 MHz / 30 MHz	1	80 V	2.8 mV	13	0.1 μs
6.5 MHz / 30 MHz	1	98 V	~ 1.2 mV	~ 6	-
	2	98 V	~ 1.9 mV	~ 10	~ 0.4 μs
	5	98 V	~ 2.1 mV	~ 11	~ 0.8 μs

The lower transmission frequency (2.25 MHz) can excite our standard microbubble population near resonance to produce more nonlinear signals at a given pressure than other frequencies. With lower excitation frequency (2.25 MHz vs 6.5 MHz), the receiver (30 MHz) can collect higher order harmonic responses, which isolates the UCA response with less tissue contamination, and achieves a higher CNR. Also, since the 2.25 MHz transmission excited microbubbles more efficiently, the pulse length can be reduced.

With a lateral mode transmitter, the dual-frequency IVUS transducer achieved 2.25 MHz / 30 MHz with a diameter less than 1 mm, which is suitable for IVUS application. The aperture size of this dual-frequency IVUS transducer is 3 mm by 0.37 mm. Because of our bonding capability, the rigid length of this prototyped transducer is enlarged to 5 mm, which is larger than commercial IVUS transducers, and may cause difficulty to navigate in some narrow vessels. The rigid length of the prototyped transducer is still less than Volcano Eagle Eye IVUS array, which is with 8 mm in the total rigid length. In the future work, we will reduce the size of bonding area to make the transducer smaller and more suitable for IVUS applications.

The results showed that this lateral mode dual-frequency IVUS transducer can be used to detect super-harmonic signals (12th to 15th harmonic) with a shorter pulse length, higher CNR and a relatively low mechanical index, suggesting a good potential for clinical applications.

B. Dual-frequency Array Transducer

In order to achieve lateral mode transmission at 2.25 MHz, the element size of the low frequency layer was designed as 6 mm × 0.35 mm × 0.3 mm, with a pitch of 0.65 mm, which is smaller than one wavelength at 2.25 MHz. Each high frequency receiver was designed with dimensions of 1 mm × 0.13 mm × 0.06 mm to obtain a center frequency of 30 MHz. The pitch of high frequency receivers was design to be 160 micron, which is larger than three wavelength at 30 MHz. This pitch size is an compromise of desired aspect ratio (> 2) and crystal volume fraction (80 %) based on our fabrication capability (Table IV).

A polyimide (PI) film based single layer flexible printed circuit (FPC) was used for both electrical connectivity and as the isolation layer of the high frequency receivers because of its low acoustic impedance. The thickness of the PI substrate is 12.5 μm and a 2 μm copper circuit was patterned on it. As mentioned previously, the isolation layer does not significantly alter the low frequency transmission because the isolation layer is thin compared to the wavelength of the low frequency mode. Similarly, it was expected that the 2 μm thick copper electrode would not impact the isolation function since it is negligibly thin compared to the wavelength of the receiving array in copper (170 μm).

The dual-frequency array transducer was prototyped as shown in Figure. 8. The flex circuits, PCB board, and additional

This article has been accepted for publication in a future issue of this journal, but has not been fully edited. Content may change prior to final publication. Citation information: DOI 10.1109/TUFFC.2016.2619687, IEEE Transactions on Ultrasonics, Ferroelectrics, and Frequency Control

TABLE IV
DESIGN PARAMETERS OF DUAL-FREQUENCY ARRAY

Parameter	Transmission layer	Receiving layer
Center Frequency	2.25 MHz	30 MHz
Material	PMN-PT	PMN-PT
Impedance (MRayl)	32	32
Width (mm)	0.35	0.13
Length (mm)	6	1
Thickness (μm)	300	65
Matching/Isolation Material	8 sub-elements	32 elements
Impedance (MRayl)	650	160
Matching Thickness (μm)	350	130
Isolation layer Impedance (MRayl)	-	3.5
Isolation layer Thickness (μm)	-	12.5

wires were used for cable wiring between the elements and the Verasonics connector (DL260, ITT Corporation, Santa Ana, CA). A 75 Ω multi-core coaxial cable with a length of 2 m, would act as a quarter-wave impedance transformer at 30 MHz and was used to match the impedance of the transducer to around 30 Ω for better electrical impedance matching between the Verasonics system and the receiving layer of the transducer (Figure 9).

With a 2-meter coaxial cable (75 Ω), the -6 dB fractional bandwidth of the high frequency receiver was measured to be 23 % with a center frequency of 29 MHz [50]. The center frequency and -6 dB fractional bandwidth of the low frequency transmitter were measured to be 2.6 MHz and 37%, respectively. The peak negative pressure generated by the low frequency transmitter with the 55 V, 2.25MHz, 2-cycle burst excitation is over 800 kPa at 5 mm axially from the transducer surface, which is high enough to excite the microbubbles for superharmonic imaging purposes. Acoustic mapping of the low frequency transmitter at 5.5 mm away from the aperture showed that the pressure is almost uniform in the interested area, which corresponds to the sensitive region of the receivers [50]. Further information of the transducer fabrication and characterization has been previously reported [50].

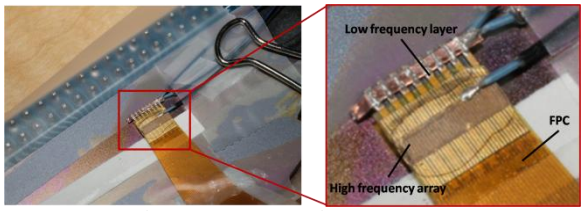

Fig. 8. Photograph of the prototype dual-frequency array.

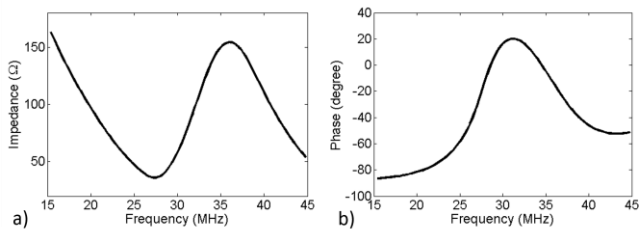

Fig. 9. High frequency array with 2-meter cable, b) electric impedance and b) phase spectrum.

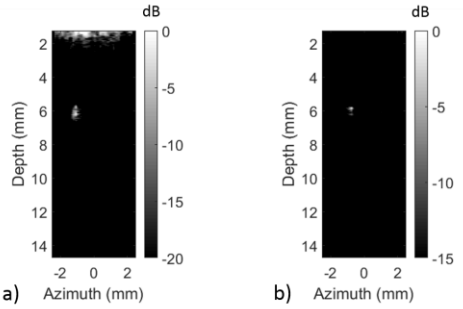

Fig. 10. Real-time superharmonic imaging. a) Under 55V. b) Under 35V.

The superharmonic images of a 200 μm micro tube with the dual-frequency array under different excitation voltages are shown in Fig. 10. With 1 cycle burst 55 V excitation and 627 kPa in PNP, the signal is clear but axial resolution is even worse than the lateral resolution (Figure 10a). That is because there was not a backing layer nor a good matching layer for our low frequency transmitter, leading a longer pulse length and ring down. Besides of the main negative peak of the transmission wave form, the other peaks also exceed the threshold and can excite the microbubbles to generate high order non-linear response; thus producing some axial aliasing of the micro tube and impacts the axial resolution. The axial resolution can be improved with a lower excitation amplitude, hence the only main peak of the transmission waveform can excite the microbubbles. With a 1 cycle burst at 35 V and 400 kPa in PNP, only one spot can be observed, with a higher axial resolution (Figure 10b). As expected, with lower excitation amplitude, the CNR will be lower.

The axial and lateral estimates of the image resolution using different excitation voltages were calculated by measuring the full-width half-maximum (FWHM) of the microbubbles responses from the enveloped and log compressed image data. Raw pixel data from superharmonic imaging were saved and processed with Matlab (MathWorks, Natick, MA.). Dimensions of microbubble responses along the depth and lateral directions were calculated separately to estimate the axial and lateral FWHM. The axial and lateral microbubbles responses under different excitation voltages are shown in Figure 11 (under 55 V excitation) and Figure 12 (under 35 V excitation).

Under 55 V excitation there were two peaks above -6 dB in amplitude measured axially. The -6 dB response of the main peak was 295 μm and the total axial FWHM was 600 μm. In the lateral direction, the -6 dB response shows that the lateral FWHM was 271 μm. The decreased CNR in the lateral direction may be attributed to the pitch size of the receiving array being larger than 3 wavelengths, which would produce grating lobes. Additionally, cross talk between adjacent elements may introduce noise that would have reduced the CNR and resolution of the system. Overall, the CNR of the microbubbles response was about 22 dB.

The axial FWHM using 35 V for the excitation was measured as 269 μm and the lateral FWHM was measured as 200 μm. As expected, the measurements using a lower excitation voltage were better, especially considering the

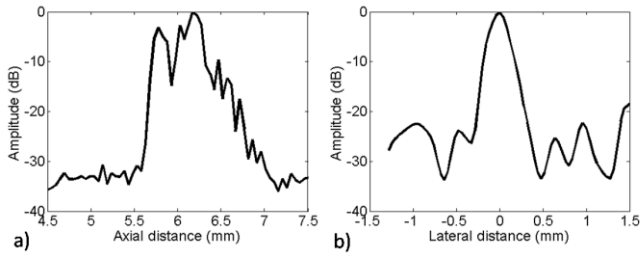

Fig. 11. Microbubble response under 55 V and 627 kPa. a) Axial; b) Lateral.

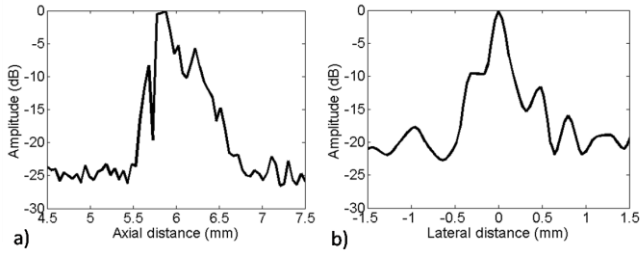

Fig. 12. Microbubble response under 35 V and 400 kPa. a) Axial; b) Lateral.

elimination of multiple images of the tube when using lower voltages. On the other hand, the lower excitation voltage had a lower CNR. The CNR was about 17 dB.

It must be noted that the micro tube resolution results represent the combined performance of both the transducer and the chosen beamformer, which in this work was the Verasonics' pixel-based beamformer. The calculated FWHM is not the real resolution but the microbubble responses in a micro tube which size is not negligible compared to the wavelength of the receiver. Also, the FWHM was calculated based on the microbubble response, which may not fill the entire chamber of the micro tube. Furthermore, because of the frequency limitation of the Verasonics system, the frequency components above 31.25 MHz were cut off which will likely impact the reported values of FWHM. Even with this limitation, the dual-frequency array can detect the superharmonic response of microbubbles using a relatively low excitation voltage.

IV. Conclusion

This paper reports the use of lateral mode transmitters both in single element and in an array fabrication in order to detect the higher order harmonics for contrast enhanced ultrasound. A dual-frequency single element IVUS transducer (2.25 MHz / 30 MHz) with a lateral mode transmitter was developed and characterized by superharmonic contrast testing for concept validation before extending this approach to an array. This transducer was small enough for use in IVUS catheter sizes typically used for coronary interventions (<3 Fr). Additionally, a dual-frequency array transducer (2.25 MHz / 30 MHz) with small lateral mode transmitter (300 μm in thickness) for superharmonic imaging was developed and tested. Real-time contrast imaging was conducted with a Verasonics system.

The contrast test of the dual-frequency single element IVUS transducer shows that the higher order non-linear response (12th to 15th harmonic) was large enough to be detected with low pressure, 1-cycle burst excitation. Compared to our initial 6.5 MHz/ 30 MHz IVUS transducer design, this dual-frequency IVUS transducer with a lateral mode transmitter (2.25 MHz / 30 MHz) had larger signal amplitude, better CNR and better pulse length in contrast tests.

The dual-frequency array transducer with a lateral mode transmitter can be used for real time superharmonic imaging with a low frequency, 1 cycle burst excitation. The axial and lateral FWHM of a 200 μm contrast-filled tube operating in superharmonic imaging mode were measured to be 269 μm and 200 μm, respectively. The maximum CNR was calculated to be 22 dB. The imaging results show that superharmonic imaging with a low frequency lateral mode transmitter is feasible and may be used in future applications for contrast agent detection in medical ultrasound.

Acknowledgment

This work was supported by the National Institutes of Health grant R01EB015508 and the Department of Defense W81XWH-12-1-0303.

Declaration

P.A.D. is a co-inventor on a patent application US 20120220869 which describes superharmonic imaging with dual-frequency transducers, and a co-founder of SonoVol, Inc., which has licensed this patent.

References

[1]. J. C. Sluimer and M. J. Daemen, "Novel concepts in atherogenesis: angiogenesis and hypoxia in atherosclerosis," *J. Pathol.*, vol. 218, no. 1, pp. 7-29, 2009.

[2]. J. E. Chomas, R. E. Pollard, A. R. Sadlowski, S. M. Griffey, E. R. Wisner, and K. W. Ferrara, "Contrast-enhanced US of microcirculation of superficially implanted tumors in rats," *Radiology*, vol. 229, no. 2, pp. 439–446, Nov. 2003.

[3]. F. S. Foster, P. N. Burns, D. H. Simpson, S. R. Wilson, D. A. Christopher, and D. E. Goertz, "Ultrasound for the visualization and quantification of tumor microcirculation," *Cancer Metastasis Rev.*, vol. 19, no. 1–2, pp. 131–138, 2000.

[4]. R. Virmani, F. D. Kolodgie, A. P. Burke, A. V. Finn, H. K. Gold, T. N. Tulenko, S. P. Wrenn, and J. Narula, "Atherosclerotic plaque progression and vulnerability to rupture: angiogenesis as a source of intraplaque hemorrhage," *Arterioscler. Thromb. Vasc. Biol.*, vol. 25, no. 10, pp. 2054–2061, 2005.

[5]. M. Naghavi, P. Libby, E. Falk, S. W. Casscells, S. Litovsky, J. Rumberger, J. J. Badimon, C. Stefanadis, P. Moreno, G. Pasterkamp, and Z. Fayad, "From vulnerable plaque to vulnerable patient a call for new definitions and risk assessment strategies: part I." Circulation 108, no. 14 pp. 1664-1672, 2003.

[6]. L. G. Spagnoli, A. Mauriello, G. Sangiorgi, S. Fratoni, E. Bonanno, R. S. Schwartz, D. G. Piepgras, R. Pistolese, A. Ippoliti, and D. R. Holmes, "Extracranial thrombotically active carotid plaque as a risk factor for ischemic stroke." *Jama*, vol. 292, no. 15, pp. 1845-1852, 2004.

[7]. S. E. Shelton, Y. Z. Lee, M. Lee, E. Cherin, F. S. Foster, S. R. Aylward, P. A. Dayton," Quantification of Microvascular Tortuosity during Tumor Evolution Using Acoustic Angiography." *Ultrasound Med. Biol.*, vol. 41, no. 7, pp.1896-904, 2015.

[8]. K. K. Shung and G. A. Thieme, "Ultrasonic Scattering in Biological Tissues," *CRC Press*, 1992.

[9]. R. Gramiak, and P. M. Shah. "Echocardiography of the aortic root." *Invest. Radiol.*, vol. 3, no. 5, pp. 356-366, 1968.

[10]. P. J. A. Frinking, A. Bouakaz, J. Kirkhorn, F. J. ten Cate, and N. de Jong, "Ultrasound contrast imaging: current and new potential methods." *Ultrasound Med. Biol.*, vol. 26, no. 6, pp. 965-975, 2000.

[11]. N. de Jong, P. J. Frinking, A. Bouakaz, and F. J. ten Cate, "Detection procedures of ultrasound contrast agents," *Ultrasonics*, vol. 38, no.1, pp. 87-92, 2000.

[12]. M. X. Tang, H. Mulvana, T. Gauthier, A. K. P. Lim, D. O. Cosgrove, R. J. Eckersley, and E. Stride, "Quantitative contrast-enhanced ultrasound imaging:

a review of sources of variability." *Interface Focus*, vol. 1, no. 4, pp. 520-539, 2011.
[13]. R. H. Silverman, D. J. Coleman, J. A. Ketterling, and F. L. Lizzi, "High-frequency harmonic imaging of the eye." In *Medical Imaging, SPIE*, 2005, pp. 16-25.
[14]. E. J. W. Merks, A. Bouakaz, N. Bom, C. T. Lancee, A. T. F. van der Steen, and N. de Jong, "Design of a multilayer transducer for acoustic bladder volume assessment." *IEEE Trans. Ultrason. Ferroelectr. Freq. Control*, vol. 53, no. 10, pp. 1730-1738, 2006.
[15]. H. J. Vos, M. A. Frijlink, E. Droog, D. E. Goertz, G. Blacquiere, A. Gisolf, N. de Jong, and A. F. W. van der Steern, "Transducer for harmonic intravascular ultrasound imaging," I*EEE Trans. Ultrason. Ferroelectr. Freq. Control*, vol. 52, no. 12, pp. 2418–2422, 2005.
[16]. M. E. Frijlink, D. E. Goertz, L. C. A. van Damme, R. Krams, and A. F. W. van der Steen, "Intravascular ultrasound tissue harmonic imaging in vivo." *IEEE Trans. Ultrason. Ferroelectr. Freq. Control*, vol. 53, no. 10, pp. 1844–1852, 2006.
[17]. M. E. Frijlink, D. E. Goertz, H. J. Vos, E. Tesselaar, G. Blacqui ère, A. Gisolf, R. Krams, and A. F. W. van der Steen, "Harmonic intravascular ultrasound imaging with a dual-frequency catheter," *Ultrasound Med. Biol.*, vol. 32, no. 11, pp. 1649–1654, 2006.
[18]. D. E. Goertz, M. E. Frijlink, D. Tempel, L. C. van Damme, R. Krams, J. A. Schaar, J. Folkert, P. W. Serruys, N. de Jong, and A. F. van der Steen, "Contrast harmonic intravascular ultrasound: a feasibility study for vasa vasorum imaging," *Invest. Radiol.*, vol. 41, no. 8, pp. 631–638, 2006.
[19]. D. Maresca, I. Skachkov, G. Renaud, K. Jansen, G. van Soest, N. de Jong, and A. F. W. van der Steen, "Imaging Microvasculature with Contrast-Enhanced Ultraharmonic Ultrasound," *Ultrasound Med. Biol.*, vol. 40, no. 6, pp. 1318–1328, 2014.
[20]. M. Averkiou, "Tissue harmonic imaging," in *IEEE Int. Ultrason. Symp.*, 2000, vol. 2, pp. 1563–1572.
[21]. A. Bouakaz, S. Frigstad, F. J. T. Cate, and N. de Jong, "Super harmonic imaging: a new imaging technique for improved contrast detection," *Ultrasound in Med. & Biol.*, vol. 28, pp. 59 - 68, 2002.
[22]. B. D. Lindsey, S. E. Shelton, and P. A. Dayton, "Optimization of Contrast-to-Tissue Ratio Through Pulse Windowing in Dual-Frequency "Acoustic Angiography" Imaging." *Ultrasound in Med. & Biol.*, vol. 41, no. 7, pp. 1884-1895, 2015.
[23]. B. D. Lindsey, J. D. Rojas, and P. A. Dayton, "On the relationship between microbubble fragmentation, deflation and broadband superharmonic signal production." *Ultrasound in Med. & Biol.*, vol. 41, no. 6, pp. 1711-1725, 2015.
[24]. E. Talu, K. Hettiarachchi, S. Zhao, R. L. Powell, A. P. Lee, M. L. Longo, and P. A. Dayton, "Tailoring the size distribution of ultrasound contrast agents: Possible method for improving sensitivity in molecular imaging," *Mol. Imaging*, vo. 6, no. 6, pp. 384–392, 2007.
[25]. J. E. Streeter, R. Gessner, I. Miles, and P. A. Dayton, "Improving sensitivity in ultrasound molecular imaging by tailoring contrast agent size distribution: In vivo studies," *Mol. Imaging*, vol. 9, no. 2, pp. 87–95, 2010.
[26]. D. E. Kruse and K. W. Ferrara, "A new imaging strategy using wideband transient response of ultrasound contrast agents," *IEEE Trans. Ultrason. Ferroelectr. Freq. Control*, vol. 52, no. 8, pp. 1320–1329, 2005.
[27]. R. C. Gessner, M. Lukacs, M. Lee, E. cherin, F. S. Foster, and P. A. Dayton, "High-resolution, high-contrast ultrasound imaging using a prototype dual-frequency transducer: In vitro and in vivo studies," *IEEE Trans. Ultrason. Ferroelectr. Freq. Control*, vol. 57, no. 8, pp. 1772–1781, 2010.
[28]. B. D. Lindsey, J. D. Rojas, K. H. Martin, S. E. Shelton, and P. A. Dayton, "Acoustic characterization of contrast-to-tissue ratio and axial resolution for dual-frequency contrast-specific acoustic angiography imaging," *IEEE Trans. Ultrason. Ferroelectr. Freq. Control*, vol. 61, no. 10, pp. 1668-1687, 2014.
[29]. Z. Wang, J. Ma, X. Jiang, K. H. Martin, and P. A. Dayton, "An array transmitter for dual-frequency contrast enhanced intravascular ultrasound imaging." in *IEEE Int. Ultrason. Symp.*, 2014, pp. 2104-2107.
[30]. R. C. Gessner, S. R. Aylward, and P. A. Dayton, "Mapping microvasculature with acoustic angiography yields quantifiable differences between healthy and tumor-bearing tissue volumes in a rodent model," *Radiology*, vol. 264, no. 3, pp. 733–740, 2012.
[31]. R. C. Gessner, C. B. Frederick, F. S. Foster, and P. A. Dayton, "Acoustic angiography: A new imaging modality for assessing microvasculature architecture," *Int. J. Biomed. Imaging*, vol. 2013, art. no. 936593, 2013.
[32]. K. H. Martin, and P. A. Dayton, "Current status and prospects for microbubbles in ultrasound theranostics." *Wiley Interdiscip. Rev. Nanomed. Nanobiotechnol.*, vol. 5, no. 4, pp. 329-345, 2013.
[33]. K. H. Martin, B. D. Lindsey, J. Ma, M. Lee, S. Li, F. S. Foster, X. Jiang, and P. A. Dayton, "Dual-frequency piezoelectric transducers for contrast enhanced ultrasound imaging," *Sensors*, vol. 14, no. 11, pp. 20825-20842, 2014.
[34]. T. L. Szabo, and P. A. Lewin, "Ultrasound transducer selection in clinical imaging practice." *J. Ultrasound Med.*, vol. 32, no. 4, pp. 573-582, 2013.
[35]. J. Ma, K. H. Martin, P. A. Dayton, and X. Jiang, "A preliminary engineering design of intravascular dual-frequency transducers for contrast-enhanced acoustic angiography and molecular imaging," *IEEE Trans. Ultrason. Ferroelectr. Freq. Control*, vol. 61, no. 5, pp. 870-880, 2014.
[36]. C. D. Herickhoff, C. M. Wilson, G. A. Grant, G. W. Britz, E. D. Light, M. L. Palmeri, P. D. Wolf, and S. W. Smith, "Dual-Mode IVUS Transducer for Image-Guided Brain Therapy: Preliminary Experiments," *Ultrasound Med. Biol.*, 2011.
[37]. C. D. Herickhoff, G. A. Grant, G. W. Britz, and S. W. Smith, "Dual-mode IVUS catheter for intracranial image-guided hyperthermia: Feasibility study," *IEEE Trans. Ultrason. Ferroelectr. Freq. Control*, vol. 57, no. 11, pp. 2572–2584, 2010.
[38]. J. Kilroy, A. Patil, J. Rychak, and J. Hossack, "An IVUS transducer for microbubble therapies." *IEEE Trans. Ultrason. Ferroelectr. Freq. Control*, vol. 61, no. 3, pp. 441-449, 2014.
[39]. A. Macovski, "Ultrasonic imaging using arrays." *Proc. IEEE*, vol. 67, no. 4, pp. 484-495, 1979.
[40]. S. Fort, N. A. Freeman, P. Johnston, E. A. Cohen, and F. S. Foster. "In vitro and in vivo comparison of three different intravascular ultrasound catheter designs." *Catheter Cardiovasc. Interv.*, vol. 52, no. 3, pp. 382-392, 2001.
[41]. C. H. Sherman, and J. L. Butler, "Transducers and arrays for underwater sound." *Springer*, 2007.
[42]. J. A. Hossack and B. A. Auld, "Improving the characteristics of a transducer using multiple piezoelectric layers," *IEEE Trans. Ultrason. Ferroelectr. Freq. Control*, vol. 40, no. 2, pp. 131–139, 1993.
[43]. J. A. Hossack, P. Mauchamp, and L. Ratsimandresey, "A high bandwidth transducer optimized for harmonic imaging," in *IEEE Ultrason. Symp.*, 2000, vol. 2, pp. 1021-1024.
[44]. Z. Wang, S. Li, T. J Czernuszewicz, C. M. Gallippi, R. Liu, X. Geng, and X. Jiang, "Design, fabrication and characterization of a bi-frequency co-linear array", *IEEE Trans. Ultrason. Ferroelectr. Freq. Control*, vol. 63, no. 2, pp. 266-274, 2016.
[45]. T. Azuma, M. Ogihara, J. Kubota, A. Sasaki, S. Umemura, and H. Furuhata, "Dual-frequency ultrasound imaging and therapeutic bilaminar array using frequency selective isolation layer," *IEEE Trans. Ultrason. Ferroelectr. Freq. Control*, vol. 57, pp. 1211-1224, 2010.
[46]. J. Souquet, P. Defranould, and J. Desbois, "Design of low-loss wide-band ultrasonic transducers for noninvasive medical application." *IEEE Trans. Sonics Ultrason.*, vol. 26, no. 2, pp. 75-80, 1979.
[47]. R. Krimholtz, D. A. Leedom, and G. L. Mattaei, "New equivalent circuits for elementary piezoelectric transducers," *Electron. Lett.*, vol. 41, pp. 398-399, 1970.
[48]. Z. Wang, K. H. Martin, P. A. Dayton, and X. Jiang, "A dual frequency IVUS transducer with a lateral mode transmitter for contrast enhanced intravascular ultrasound imaging", *processing in ASME Int. Mech. Eng. Congress*, 2015.
[49]. M. A. Borden, M. R. Sarantos, S. M. Stieger, S. I. Simon, K. W. Ferrara, and P. A. Dayton, "Ultrasound radiation force modulates ligand availability on targeted contrast agents," *Mol. Imaging*, vol. 5, pp. 139–147, 2006.
[50]. Z. Wang, W. Huang, X. Jiang, K. H. Martin, and P. A. Dayton, "Dual-frequency IVUS array for contrast enhanced intravascular ultrasound imaging." in *IEEE Int. Ultrason. Symp.*, 2015.
[51]. A. P. Albrecht, "Transmission lines," in *Electronic Designer's Handbook*, McGraw-Hill, 1977, pp. 8.1–8.78.
[52]. J. M. Cannata, T. Ritter, WH Chen, R. H. Silverman, and K. K. Shung, "Design of efficient, broadband single-element (20-80 MHz) ultrasonic transducers for medical imaging applications." *IEEE Trans. Ultrason. Ferroelectr. Freq. Control*, vol. 50, no. 11, pp. 1548-1557, 2003.
[53]. J. Ma, S. Li, Z. Wang, and X. Jiang, "Anti-matching design for wave isolation in dual frequency transducer for intravascular super-harmonic imaging," in *ASME Int. Mech. Eng. Congress. Expo.*, pp. V003T03A084.
[54]. J. Ma, M. B. Steer, and X. Jiang, "An acoustic filter based on layered structure," *Appl. Phys. Lett.*, vol. 106, no. 11, 2015.
[55]. J. Ma, K. H. Martin, Y. Li, P. A. Dayton, K. K. Shung, Q. Zhou, and X. Jiang, "Design factors of intravascular dual frequency transducers for super-harmonic contrast imaging and acoustic angiography," *Phys. Med. Biol.*, vol. 60, no. 9, pp. 3441, 2015.

Zhuochen Wang was born in Tianjin, China, in 1984. He received his B.S. degree in mechanical engineering from Tianjin University in 2005, and his M.S. degree in mechanical engineering from University of Akron in 2012. Zhuochen joined Dr. Xiaoning Jiang's Micro/Nano Engineering Lab at North Carolina State University in 2012, working on the design, fabrication and imaging of piezoelectric ultrasound transducers. He has a broad research interest in intravascular ultrasound (IVUS) transducer, dual frequency ultrasound transducer, transducer array and acoustic radiation force impulse imaging (ARFI) application.

K. Heath Martin obtained his B.S.E. degree in 2009 from Mercer University in biomedical engineering and then joined a defense contractor performing finite element analysis. He obtained his Ph. D. from the Joint Department of Biomedical Engineering of North Carolina State University and the University of North Carolina in 2016 regarding his work in the field of contrast specific imaging in intravascular ultrasound. His research interests include cardiovascular device design and signal processing methods for superharmonic ultrasound imaging.

Wenbin Huang received the B.S. degree in mechanical engineering from the University of Science and Technology of China, Hefei, China, in 2010, and the Ph.D. degree in mechanical engineering from the North Carolina State University, Raleigh, NC, USA, in 2014. He is currently a Researcher with the State Key Lab of Mechanical Transmissions of Chongqing University, Chongqing, China. His research fields include the fundamental study of flexoelectricity and its various sensing applications, especially for structural health monitoring, piezoelectric sensors and actuators, ultrasound transducers for medical imaging and non-destructive testing applications, and micro and nano electromechanical integrated systems. He has authored and co-authored more than 20 peer-reviewed journal papers and two book chapters in related fields.

Paul A. Dayton received his B.S. degree in physics from Villanova University in 1995, his M.E. degree in electrical engineering from the University of Virginia in 1998, and his Ph.D. degree in biomedical engineering in 2001, also from the University of Virginia. He pursued postdoctoral research and was later research faculty at the University of California, Davis. Much of Dr. Dayton's training was under the mentorship of Dr. Katherine Ferrara; his initial studies involved high-speed optical and acoustical analysis of individual contrast agent microbubbles. In 2007, Dr. Dayton moved to the Joint Department of Biomedical Engineering at UNC–Chapel Hill and NC State University, Raleigh, where he is now Professor and Associate Department Chair. Dr. Dayton is currently Associate Director for Education for the Biomedical Imaging Research Center, and his research interests involve contrast ultrasound imaging, ultrasound-mediated therapies, and medical devices. Dr. Dayton is a member of the technical program committee for the IEEE UFFC Society, and a member of the editorial boards for the journals IEEE Transactions on Ultrasonics, Ferroelectrics, and Frequency Control; Molecular Imaging; and Bubble Science, Engineering, and Technology.

Xiaoning Jiang received his B.S. in mechanical engineering from Shanghai Jiaotong University in 1990, his M.S. in mechanical engineering from Tianjin University in 1992, and his Ph.D. in precision instruments from Tsinghua University in 1997. He received Postdoctoral trainings from Nanyang Technological University and the Pennsylvania State University from 1997 to 2001. He joined Standard MEMS, Inc. as a R&D Engineer in 2001 and then worked for TRS Technologies, Inc. as a Research Scientist, Senior Scientist, Chief Scientist and Vice President for Technology before joining North Carolina State University in 2009. He is now a Professor of Mechanical and Aerospace Engineering and an Adjunct Professor of Biomedical Engineering. Dr. Jiang is the author and co-author of two book chapters, one book, 9 issued US patents, and over 60 peer reviewed journal papers and over 60 conference papers on piezoelectric composite micromachined ultrasound transducers, ultrasound for medical imaging and therapy, drug delivery, ultrasound NDT/NDE, smart materials and structures and M/NEMS. Dr. Jiang is a member of the technical program committee for IEEE Ultrasonics Symposium, UFFC representative to IEEE Nanotechnology Council, and an editorial board member for the journal Sensors.

Ultrasonics 63 (2015) 7–15

Contents lists available at ScienceDirect

Ultrasonics

journal homepage: www.elsevier.com/locate/ultras

Phantom evaluation of stacked-type dual-frequency 1–3 composite transducers: A feasibility study on intracavitary acoustic angiography

Jinwook Kim [a], Sibo Li [a], Sandeep Kasoji [b], Paul A. Dayton [b], Xiaoning Jiang [a,*]

[a] Department of Mechanical & Aerospace Engineering, The North Carolina State University, Raleigh, NC 27695, USA
[b] Joint Department of Biomedical Engineering, University of North Carolina and North Carolina State University, Chapel Hill, NC 27599, USA

ARTICLE INFO

Article history:
Received 23 January 2015
Received in revised form 8 June 2015
Accepted 10 June 2015
Available online 15 June 2015

Keywords:
Dual-frequency transducer
1–3 composite transducer
Superharmonic imaging
Ultrasound contrast agents
Intracavitary probe

ABSTRACT

In this paper, we present phantom evaluation results of a stacked-type dual-frequency 1–3 piezoelectric composite transducer as a feasibility study for intracavitary acoustic angiography. Our previous design (6.5/30 MHz PMN–PT single crystal transducer) for intravascular contrast ultrasound imaging exhibited a contrast-to-tissue ratio (CTR) of 12 dB with a penetration depth of 2.5 mm. For improved penetration depth (>3 mm) and comparable contrast-to-tissue ratio (>12 dB), we evaluated a lower frequency 2/14 MHz PZT 1–3 composite transducer. Superharmonic imaging performance of this transducer and a detailed characterization of key parameters for acoustic angiography are presented. The 2/14 MHz arrangement demonstrated a −6 dB fractional bandwidth of 56.5% for the transmitter and 41.8% for the receiver, and produced sufficient peak-negative pressures (>1.5 MPa) at 2 MHz to induce a strong nonlinear harmonic response from microbubble contrast agents. In an in-vitro contrast ultrasound study using a tissue mimicking phantom and 200 μm cellulose microvessels, higher harmonic microbubble responses, from the 5th through the 7th harmonics, were detected with a signal-to-noise ratio of 16 dB. The microvessels were resolved in a two-dimensional image with a −6 dB axial resolution of 615 μm (5.5 times the wavelength of 14 MHz waves) and a contrast-to-tissue ratio of 16 dB. This feasibility study, including detailed explanation of phantom evaluation and characterization procedures for key parameters, will be useful for the development of future dual-frequency array transducers for intracavitary acoustic angiography.

1. Introduction

Acoustic angiography is a contrast enhanced ultrasound imaging technique based on superharmonic bubble imaging. This technique provides high-resolution (<200 μm) images of microvasculature with suppression of tissue background [1,2]. When coupled with an analysis of microvascular morphology and vessel density, data obtained with acoustic angiography can be used as a tool to assess solid tumors based on their vasculature rather than the tumor mass itself [3,4]. In order to perform this imaging technique, a transducer arrangement with an ultra-wide bandwidth (from a fundamental resonance to >3rd harmonics) is required, and typically multi-element transducers are used [5]. One such arrangement is to utilize a transmitter (center frequency of 1–5 MHz) for excitation of microbubbles near their resonance frequency, and a receiver for detection of superharmonic microbubble echoes (>3rd harmonics) [5,6]. However, the main challenge of acoustic angiography has been the lack of customized dual-frequency transducers which can perform satisfactorily across this wide bandwidth.

To date, several groups have demonstrated dual-frequency arrays [7] or mechanically scanned systems [8] for transmit-low, receive-high imaging. However, no dual-frequency transducer able to perform acoustic angiography has yet been optimized for intracavitary ultrasound imaging applications such as transrectal and transvaginal ultrasound. We hypothesize that such a transducer could provide valuable information regarding microvascular density and morphology associated with prostate, ovarian, and other cancers accessible by intracavitary probes.

For the application of contrast enhanced intravascular ultrasound (CE-IVUS), a 6.5/30 MHz dual-frequency transducer was developed with a small aperture size (0.6 × 3 mm aperture and <600 μm thickness). The 6.5 MHz-PMN–PT single crystal transmitter with an aperture size of 600 μm (1λ) × 3 mm (5λ) and a thickness of 300 μm (0.5λ) was stacked with a 30 MHz-crystal receiver with an aperture size of 600 μm (5λ) × 500 μm (4λ) and a thickness of 65 μm (0.5λ), where λ denotes the respective wavelength of each

* Corresponding author.
E-mail address: xjiang5@ncsu.edu (X. Jiang).

http://dx.doi.org/10.1016/j.ultras.2015.06.009
0041-624X/

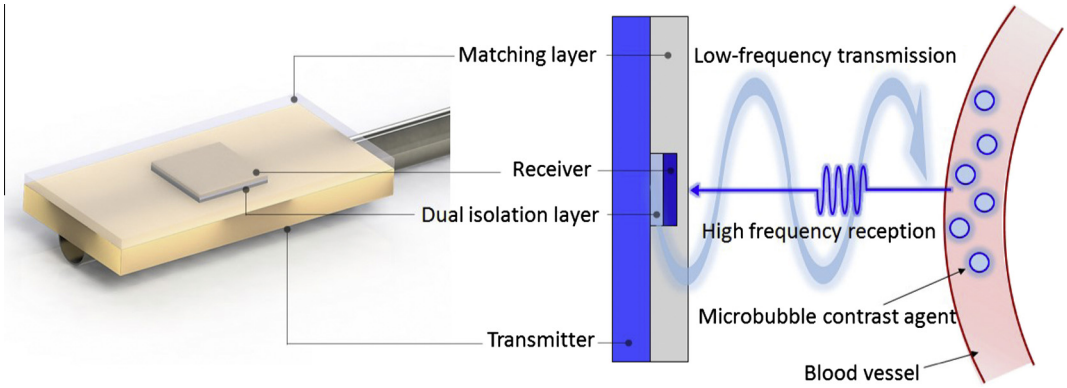

Fig. 1. Schematic of the stacked-type dual-frequency transducer for acoustic angiography.

acoustic medium [3]. This CE-IVUS transducer was designed with a compact and simple form-factor, and yielded results with a contrast-to-tissue ratio (CTR) of 12 dB. However, the transducer size, frequency combination, and penetration depth (2.5 mm, or 50λ with respect to the 30 MHz receiver) were optimized only for IVUS applications, and hence are not applicable to the intracavitary applications mentioned above.

In order to achieve deeper imaging penetration with a form-factor suitable for intracavitary use, we have recently developed 2/14 MHz dual-frequency transducers with a lateral dimension of $8 \times 4\ mm^2$ and a total thickness of 1 mm (Fig. 1). A 2 MHz-1–3 composite transmitter with an aperture size of 3.8 mm (2λ) × 7 mm (3.8λ) and a thickness of 710 μm (0.4λ) was stacked with a 14 MHz-composite receiver with an aperture size of 2 mm (7.5λ) × 2 mm (7.5λ) and a thickness of 90 μm (0.35λ) [9]. Although the design concept was briefly introduced in our previous work [9], experimental superharmonic imaging performance was not evaluated.

Hence, in this paper, we present in-vitro phantom imaging results using a prototype stacked-type dual-frequency 1–3 composite transducer. The purpose of this study is to assess the feasibility of this new dual-frequency transducer design for intracavitary acoustic angiography through acoustic characterization of transducer performance.

2. Materials and methods

2.1. Piezoelectric materials and design methods

A PZT-5H 1–3 piezoelectric composite (volume fraction of 60%, Blatek, Inc., State College, PA) was used for both the transmitter and receiver due to its relatively high electro-mechanical coupling factor (k_t of 0.65) and low acoustic impedance (19.8 MRayl) [10,11]. The 1–3 composite has several advantages over the conventional PMN–PT single crystal design, especially for the low-frequency transmitter. Due to its relatively low stiffness (~70 GPa of effective Young's modulus), the aperture can be designed with a small thickness (~710 μm, 0.4λ of 2 MHz vibration) at the designed operating frequency (2 MHz). An additional advantage is the laterally isolated connectivity of 1–3 composites, can suppress the mode-coupling between the thickness and lateral resonance modes when a small aperture (width to thickness ratio of <3) is required. Therefore, a low aspect ratio (width to thickness, <3) active layer can be achieved by using 1–3 composites, which is advantageous for the design of small size transducers required for interventional applications [9].

The matching and isolation layers were designed by using the Krimholtz–Leedom–Matthaei (KLM) model and finite element analysis (FEA). The transmitting frequency was selected to be 2 MHz which is near the resonance frequency of polydispersed (0.9 ± 0.45 μm in diameter) microbubbles determined in previous work [1]. The microbubbles consisted of a decafluorobutane core with a stabilizing phospholipid monolayer shell, enriched with polyethylene glycol. Detailed procedures for microbubble preparation can be found in previous work [12]. Lindsey et al. demonstrated that 10 MHz and 15 MHz receiving frequencies exhibited higher CTR than other higher (20 MHz and 25 MHz) or lower (7.5 MHz) receiving frequencies using the same type of microbubble population [1]. Based on these results, we selected a receiving frequency range of 12–14 MHz that corresponds to 6th and 7th harmonics of the transmitter.

2.2. Acoustic characterization methods

Pulse-echo, wave-form, and output pressure tests were performed to characterize key acoustic parameters for the prototyped transducer prior to microbubble detection and superharmonic imaging tests. The key parameters were selected based on our previous studies [1,6]. A summary of the measured parameters obtained using each characterization method and their relevance are included in Table 1. Experimental setups for each characterization procedure are depicted in Fig. 2, and detailed information of the equipment including input conditions are summarized in Table 2.

During the pulse-echo test, illustrated in Fig. 2(a), a stainless steel block, positioned at approximately 10 mm away from the transducer, was used as a target. The 2 MHz-transmitter and the 14-MHz receiver were tested with two different pulser/receivers considering their different usable frequency ranges. The 5077PR and 5900PR pulser/receivers are typically used for the 0.5–20 MHz and 10–125 MHz frequency ranges, respectively.

For the transmission waveform test, illustrated in Fig. 2(b), a hydrophone was positioned approximately 10 mm away from the transducer and was connected to an oscilloscope through a 20 dB gain amplifier. For microbubble imaging, only one distinct negative peak (>6 dB greater than neighboring peaks) is preferable because increasing the number of excitation cycles results in the degradation of axial resolution due to a longer microbubble harmonic response. Thus, the relative peak values with a different number of cycles (1–4 cycles) and wave forms (sine or cosine) were compared to determine the best input conditions for imaging.

For the pressure output tests (illustrated in Fig. 2(c)), a 60 dB radio-frequency amplifier was used to measure peak negative pressure (PNP) values at different excitation voltages. The transmitting element was driven by one- and two-cycle sinusoidal inputs at 2 MHz with various peak-to-peak voltages (100, 150,

Table 1
Characterization methods for important acoustic parameters and their relevance to acoustic angiography. (TX, RX, FBW, PNP, MI, and SNR denote transmitter, receiver, fractional bandwidth, peak-negative- pressure, mechanical index, and signal-to-noise ratio, respectively.).

Methods	Acoustic parameters	Relevance to acoustic angiography
Pulse-echo test	• Center frequency of TX • −6 dB FBW of TX • Center frequency of RX • −6 dB FBW of RX • Pulse-echo sensitivity of RX	• TX center frequency affects MI and CTR; center frequency should be near the microbubble resonance (1–5 MHz) [5] • −6 dB FBW of TX affects rise time and ring down time for microbubble excitation [9] • RX center frequency determines detectable order of harmonic responses • −6 dB FBW of RX determines an axial resolution of vascular images • Pulse-echo sensitivity of RX affects SNR and CTR [6]
Wave form test	• Normalized PNP for various number of input cycles (TX)	• Input excitation function (sine or cosine) for acoustic angiography is determined by the measured wave form • Number of input cycle affects an axial resolution of vascular images
Pressure output test	• PNP (TX) • MI (TX)	• PNP determines MI; MI is required to be lower than 1.9 for diagnostic ultrasound (FDA stipulation) • Excitation of microbubbles with moderate PNP is required for nonlinear harmonic responses of microbubbles • MI affects CTR and SNR [1]

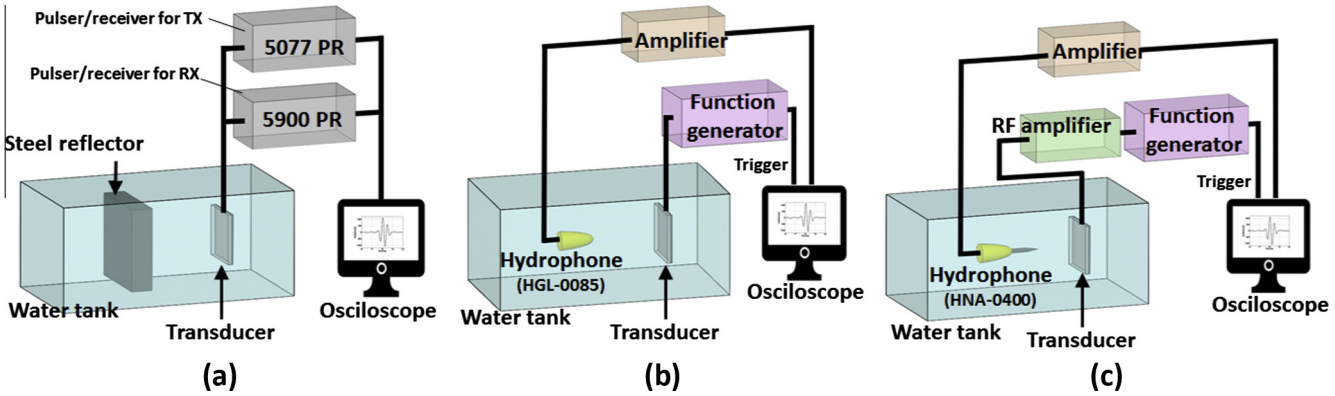

Fig. 2. Experimental setup for each characterization method; (a) pulse-echo test for both transmitter and receiver, (b) transmitting wave form test for the transmitter, (c) pressure output test for the transmitter.

Table 2
Equipment and input conditions for each characterization method.

Methods	Equipment	Input condition
Pulse-echo test	• Square wave pulser/receiver (Olympus 5077PR, Olympus NDT, Inc., Waltham, MA) for TX test • Olympus 5900PR (Panametrics Inc., Waltham, MA) for RX test • Digital oscilloscope (DSO7104B, Agilent Technologies Inc., Santa Clara, CA)	• 100 V_{pp} for TX test • 65 V_{pp} for RX test
Wave form test	• Arbitrary function generator (AFG3101, Tektronix Inc., Beaverton, OR) • Hydrophone (HGL-0085, Onda Corp., Sunnyvale, CA) • 20 dB gain preamplifier (AH-2010, Onda Corp., Sunnyvale, CA) • Digital oscilloscope (DSO7104B)	• 10 V_{pp} input voltage • 1, 2, 3 and 4 cycles of sine and cosine waveform at 2 MHz
Pressure output test	• Arbitrary function generator (AFG3101) • Needle hydrophone (HNA-0400, Onda Corp., Sunnyvale, CA) • 20 dB gain preamplifier (AH-1100, Onda Corp., Sunnyvale, CA) • 60 dB radio-frequency amplifier (Model 3200L, Electronic Navigation Industries Inc., Rochester, NY) • Digital oscilloscope (DSO7104B)	• 1 and 2 cycles of sinusoidal waveform at 2 MHz • 100, 150, 200, 250, and 300 mV_{pp} amplified by a 60 dB RF amplifier

200, 250, and 300 mV_{pp} with 60 dB gain). A needle hydrophone was used to measure the output PNP because it is durable to high-intensity ultrasound fields (15 MPa peak positive and 3.7 MPa negative pressure for 1.5 MHz source). The mechanical index (MI) corresponding to the measured PNP with each input condition was analyzed.

2.3. Tissue-mimicking phantom fabrication

A graphite–gelatin phantom was used for this study to validate the detection of higher harmonic microbubble signal within a scattering and attenuating environment. The phantom was composed of 92.5% de-ionized water, 5% n-propanol (to adjust for speed of sound), 2.5% Kodak Photo-Flo 200 (surfactant), 7.5 g/mL porcine gelatin, and 0.115 g/mL graphite. The concentration of graphite was chosen to match experimental attenuation data for normal human prostate tissue of 0.75 dB/cm/MHz [13]. The ingredients were mixed with a stir bar over a stir plate and simultaneously heated to 40–45 °C. Once the liquid phantom cooled down to 30 °C, it was poured into a custom mold and refrigerated for 24 h. The design of the mold consisted of two parallel cellulose tubes (200 μm diameter) suspended in a hollow rectangular cup. The cellulose tubes were bound to a larger diameter polyethylene tube, used for fluid input, using a water-proof adhesive. The

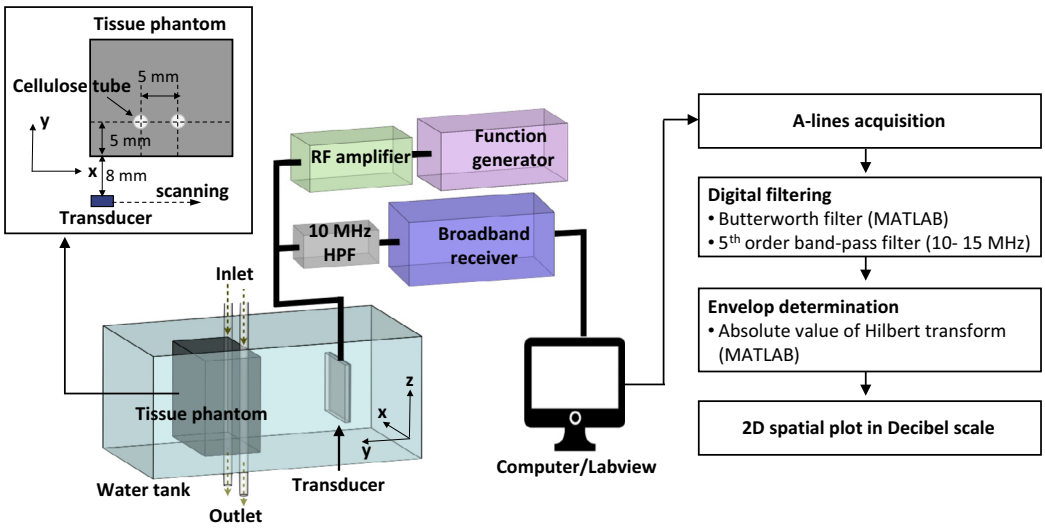

Fig. 3. Experimental setup and data processing steps for the microbubble detection test and superharmonic imaging with a tissue phantom.

distance from the cellulose tube to the surface of the phantom was approximately 5 mm, with a tube separation of 5 mm (Fig. 3).

2.4. Bubble signal detection and superharmonic imaging

The tissue-mimicking phantom previously described was used for both microbubble signal detection and phantom blood vessel imaging (Fig. 3). The transducer was positioned at 8 mm away from the tissue phantom surface (approximately 13 mm away from the tubes). The 8 mm distance was selected as approximately twice of the estimated far field distance of the transmitter (4 mm) to remove pressure fluctuation in the near field region. For microbubble signal detection, only one cellulose tube was used, using three different scenarios including the cellulose tube filled with air, de-ionized water, and microbubbles. The stock microbubble solution was 1×10^{10} microbubbles/ml, and the solution was diluted 1:100 in saline. In each case, the received signals were processed to obtain the frequency spectrum, and band-pass filtered with a frequency window of 10–15 MHz by using a 5th order Butterworth filter (MATLAB, Mathworks Inc., Natick, MA) to obtain the higher-harmonic content of the signals. When the cellulose tube was infused with microbubbles, SNR and CTR were calculated and compared using following equations [1]:

$$\mathrm{SNR} = 20 \cdot \log\left(\frac{V_{\mathrm{bubble}}}{V_{\mathrm{noise}}}\right) \tag{1}$$

$$\mathrm{CTR} = 20 \cdot \log\left(\frac{V_{\mathrm{bubble}}}{V_{\mathrm{tissue}}}\right) \tag{2}$$

where V_{bubble} denotes the detected peak voltage amplitude from microbubbles, and V_{tissue} and V_{noise} are the peak voltage amplitude detected from the tissue-phantom and water, respectively.

When performing superharmonic imaging tests, 2D images of the tissue-phantom with microbubbles flowing through the cellulose tubes (x–y plane in Fig. 3) were acquired. The transducer was 13 mm away from the tubes and scanned along the lateral axis (x-direction in Fig. 3) in 500 μm increments using a 3-axis linear motion stage. Both cellulose tubes were infused with microbubbles simultaneously during the linear scanning using a syringe pump set an infusion rate of 50 μL/min. The same function generator and RF power amplifier used for testing the pressure output were used for the superharmonic imaging tests (300 $\mathrm{mV_{pp}}$ and 60 dB gain). One- and two-cycle sinusoidal inputs at 2 MHz were applied, respectively, and SNR, CTR and −6 dB axial resolution under different input conditions were obtained and compared. The received microbubble signals were high-pass filtered at 10 MHz using a HC7 filter (TTE Filters, LLC., Los Angeles, CA) to eliminate the fundamental and lower-order harmonic responses (<5th harmonic) from the tissue phantom. 100 A-lines acquired using a broadband receiver (BR-640, RITEC Inc. Warwick, RI) with a 16 dB gain were individually stored using an analog-to-digital converter (National Instruments, Austin, TX) and converted to B-mode images offline.

3. Results and discussion

3.1. Design and fabrication results

The key design features of the prototype transducer are summarized as follows.

(1) 1–3 piezoelectric composites were used for both the transmitter and receiver due to their wideband (short pulse) characteristics and low-profile.
(2) The prototype was designed without a highly attenuative (~16 dB/mm loss at 2 MHz) and thick backing layer (>4 mm to remove reflected echoes from the back side) in order to reduce the total thickness of the transducer. Another reason for designing the transducer without a backing layer was to produce a PNP of >1.5 MPa for the generation of nonlinear harmonic echoes from microbubbles, otherwise difficult to achieve with a heavy backing layer (>10 MRayl, ~16 dB/mm loss at 2 MHz). The intrinsic wideband characteristics of the 1–3 composite compensate for the reduced bandwidth caused by the absence of the backing layer. KLM modeling results demonstrated that 1–3 composite with heavy backing (10 MRayl, 4 mm thick, 16 dB/mm loss at 2 MHz) results in 3% greater −6 dB fractional bandwidth than with air-backing.
(3) The high-frequency (14 MHz) receiver was included in the matching layer of the low-frequency (2 MHz) transmitter to share a coaxial beam profile for the dual-frequency mode.
(4) To account for the acoustic impedance mismatch (5.5 and 50 MRayl), a dual-isolation layer was used between the receiver and transmitter, which blocks the penetration of received signals from the transmitter and eliminates the aliasing echo reflected from the backside of the transmitter [14].

A detailed explanation of the design technique and procedures and the fabrication procedures are summarized in our previous work [9]. Based on the design parameters (Table 3), stacked-type dual-frequency transducer prototypes were fabricated (Fig. 4) and mounted on the tip of a 16-gauge needle (All-Spec Industries Inc., Wilmington, NC).

3.2. Pulse-echo response results

The pulse-echo response of the transmitter demonstrated a center frequency of 2.2 MHz, peak-to-peak echo amplitude of 2.65 V, and a −6 dB fractional bandwidth of 56.5% (Fig. 5(a)). An acceptable −6 dB fractional bandwidth of 56.5% was obtained without a backing layer. Although the backside of the transmitter is close to the free boundary, which cannot absorb backward travelling waves, the low acoustic impedance (19.8 MRayl) and low mechanical quality factor of 1–3 composites (<50) enable a short pulse-echo response (−6 dB pulse duration of 0.57 μs) from the low-frequency transmitter. The small-amplitude (−14 dB to the peak echo) ringing of the echo signal is likely due to the mounting condition of the transducer on the needle tip, which can cause a flexural (bending) vibration of the attached transmitting element. However, this vibration is negligible because its low echo amplitude (−14 dB) is unable to elicit a detectable nonlinear microbubble response during imaging.

The receiving element demonstrated a center frequency of 13.7 MHz, peak-to-peak echo amplitude of 325 mV, and the

Table 3
Material properties and dimensions of each constitutive component of the transducer. The active material volume fraction of 1–3 composite is 60%. ρ = density, v_l = longitudinal wave velocity, k_t = thickness mode electromechanical coupling factor, $\varepsilon^S_{33}/\varepsilon_0$ = dielectric constant. Material properties of E-solder 3022 and epoxy (EPO-TEK 301) are from the reference [15].

Components	Material	Dimension (mm^3)	ρ (kg/m^3)	v_l (m/s)	k_t	$\varepsilon^S_{33}/\varepsilon_0$
Transmitter	PZT-5H 1–3 composite	3.8 × 7.0 × 0.71	5300	3740	0.65	660
Matching layer (TX)	Al_2O_3/epoxy	3.8 × 6.5 × 0.29	2000	2800	–	–
Isolation layer 1	E-solder 3022	2.0 × 2.0 × 0.06	2590	2110	–	–
Isolation layer 2	Carbon steel	2.0 × 2.0 × 0.08	7700	6100	–	–
Receiver	PZT-5H 1–3 composite	2.0 × 2.0 × 0.09	5300	3740	0.65	660
Matching layer (RX)	Al_2O_3/epoxy	2.0 × 2.0 × 0.06	2000	2800	–	–

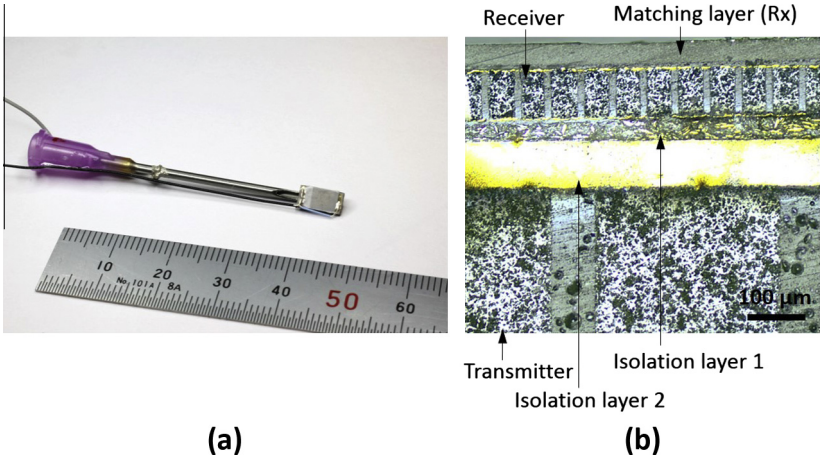

Fig. 4. The prototyped dual-frequency transducer; (a) prototype transducer housed on the tip of a 16-gauge needle, (b) cross sectional view of the center part of the prototyped transducer.

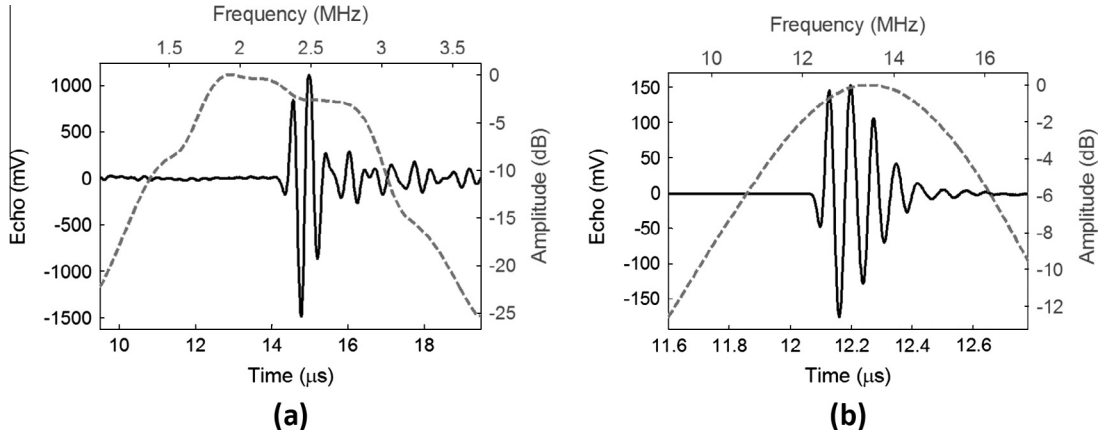

Fig. 5. Pulse-echo test results of the prototype dual-frequency transducer; (a) response of the transmitter, (b) response of the receiver.

−6 dB fractional bandwidth of 41.8% (Fig. 5(b)). It showed a relatively long ring down (−6 dB pulse duration of 16.4 ns, spatial pulse length of 2.2λ) due to the dual-isolation layer which is designed to reflect high-frequency waves [14]. Despite the fact that no perfect lossy backing layer exists for the receiving element, the measured response from the receiver showed a sufficient −6 dB bandwidth to cover the 6th and 7th harmonic frequencies (12–14 MHz).

3.3. Transmitting waveform test results

Testing different number of cycles (1–4 cycles of 10 V_{pp} sine-waveform-input at 2 MHz) for the transmitting waveform showed that PNP increased with the number of cycles (Fig. 6(a)). The measured data was normalized by the absolute peak value achieved with the 4-cycle excitation. The results show that there is significant difference in PNP between the 1-cycle and 2-cycle excitations (58 vs 88%), whereas the 2, 3, and 4-cycle excitations exhibited a relatively small difference in peak amplitudes (88, 93.5, and 100%, respectively). Although 3 and 4-cycle excitations or excitations with even higher number of cycles can generate higher peak pressures, a long excitation (e.g. 3–4 cycles) is accompanied with a decrease of axial resolution due to the respective increase in the length of microbubble response. The axial resolution was estimated to be 450 μm (4λ at 14 MHz), which is worse than achieved in our previous work (200 μm, 4λ at 30 MHz) [6]. This reduction in resolution is an inherent trade-off with the lowered frequency combination (from 6.5/30 MHz to 2/14 MHz), which was chosen to achieve a greater (>3 mm) penetration depth with comparable CTR (12 dB). Thus, 1 and 2-cycle excitations using a cosine-wave form were considered as the input condition for further acoustic characterization and superharmonic imaging.

3.4. Pressure output test results

The acoustic pressure produced at various voltage inputs were measured to determine the proper input conditions for acoustic angiography (Fig. 7). The maximum PNP measured at a distance of 13 mm was 1.97 MPa with a 1-cyle burst and 2.31 MPa with a 2-cycle burst, both with an input voltage of 300 V_{pp} (300 mV_{pp} with 60 dB gain). The corresponding MI values for the 1-cycle and 2-cycle input waveforms were 1.39 and 1.63 respectively. These values meet the estimated PNP requirement (>1.5 MPa) for CTR comparable with our previous work (>12 dB). 300 V_{pp} (106 V_{rms}) is about 38% of the AC depoling field of PZT-5H ceramics (4 kV_{rms}/cm or 280 V_{rms} for 710 μm thickness), which may be

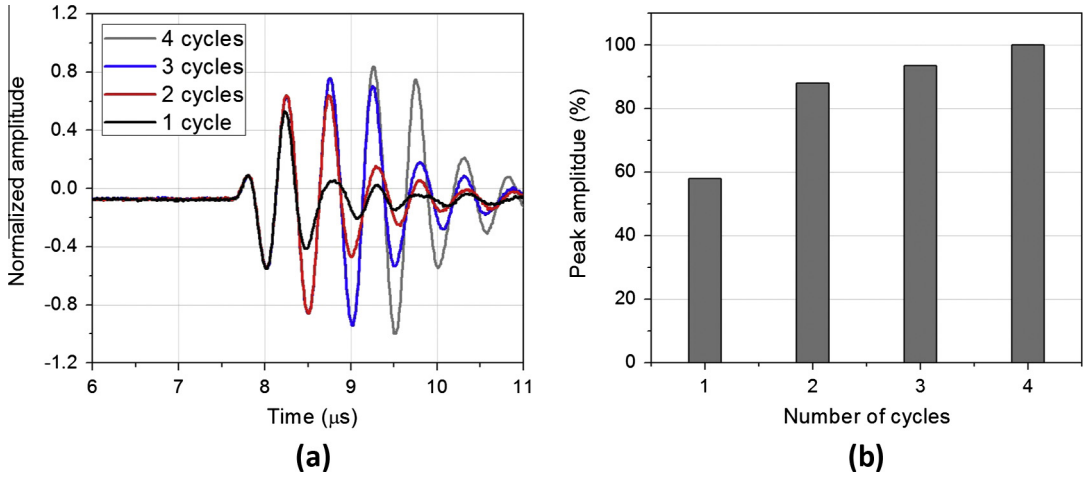

Fig. 6. Transmitting waveform test with 1–4 cycles of 2 MHz sine-wave excitation; (a) normalized waveform comparison for each case of excitation, (b) peak amplitude (either positive or negative peak) comparison for each case of excitation.

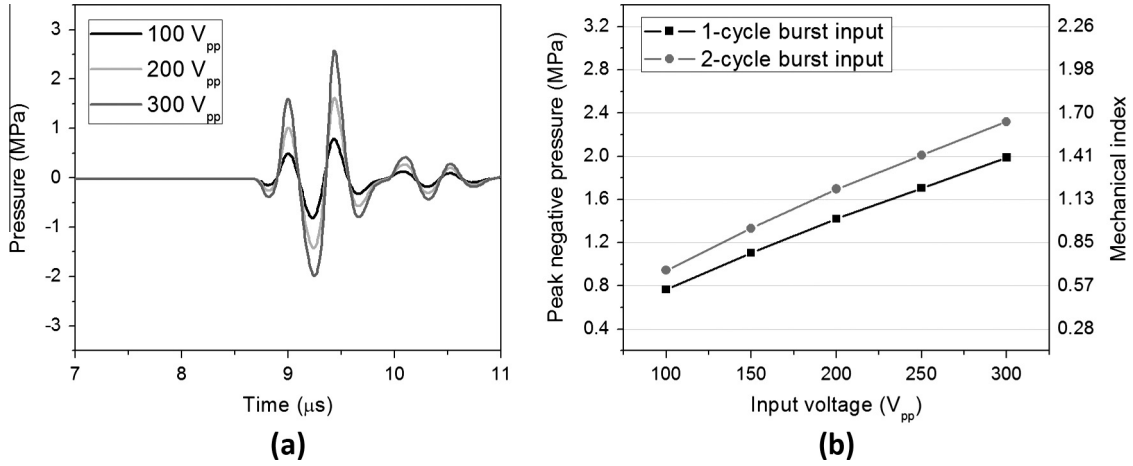

Fig. 7. Measurements for different transmitted pressures of 100–300 V_{pp} (100–300 mV_{pp} with 60 dB gain) cosine-wave form excitation at 2 MHz; (a) 1-cycle excitation, (b) relation of peak negative pressure (PNP) and input voltage; corresponding mechanical index values to PNP of 0.4–3.2 MPa are labeled at the right vertical axis.

slightly higher than the voltage recommended by some PZT manufacturers due to depoling concerns, (e.g., 30% of depoling voltage) [16]. In this work, the transmitter was excited with a low duty cycle (0.2–0.4% with a pulse-repetition rate of 4 kHz) at 300 V_{pp}. Although no degradation of output pressure was observed during acoustic tests and phantom evaluations, the input voltage required to produce a sufficient PNP (>1.5 MPa) needs to be lower than 300 V_{pp}. The input voltage can be reduced by using an impedance matching circuit or multi-layer design to decrease the electrical impedance at 2 MHz (~150 Ω) to close to 50 Ω.

3.5. Microbubble signal detection results

For the case of water injected into a microcellulose tube (200 μm diameter), the detected signal showed only acoustic reflections from the tissue-phantom boundary (Fig. 8(a)). No signal was reflected from the tube due to its negligible wall thickness (<1 μm, less than 0.001λ for 2 MHz waves) and its similar acoustic impedance to that of the tissue-mimicking phantom and water. For the case of air injected into the tube after water was drained out completely, the high-frequency receiver detected a 2 MHz fundamental response from the air-filled tube, followed by the phantom boundary reflection. Due to the large acoustic impedance difference between air (415 Rayl) and water (1.5 MRayl), the fundamental frequency dominated the frequency content of the response from air.

The signal detected from the tube infused with microbubbles showed a reduced peak-to-peak amplitude (87%) and a distorted waveform when compared with the linear signal from the tissue-phantom boundary (Fig. 8(b)). This is due to the nonlinear response of the microbubbles. However, the higher frequency (>2 MHz) components from the microbubble response were not explicit in the detected signal. Therefore, the frequency spectrum of the response from microbubbles and air were analyzed and compared (Fig. 8(c)). A time range of 19–21.5 μs was used as the window for the fast Fourier transform that contained the signal from the tube. In addition to a strong second-harmonic response (−10 dB), the microbubble frequency spectrum showed high amplitudes at the 4th through the 7th harmonics (−23 to −30 dB), whereas the air-filled tube showed these same harmonic components as less than −40 dB in amplitude. This comparison clearly demonstrates that the microbubble response contains 13–20 dB greater higher-harmonic-frequency (10–15 MHz) components.

The microbubble and air signals were filtered using a 5th order Butterworth band-pass filter (10–15 MHz) and compared (Fig. 8(d)). After the fundamental frequency component was completely removed from both the air and microbubble signals, only the filtered microbubble signal exhibited high-frequency harmonics with peak-to-peak amplitudes of 13.5 mV, without amplification. The filtered signal from air showed only noise level signals (<1.2 mV_{pp}). Overall, the superharmonic responses of the

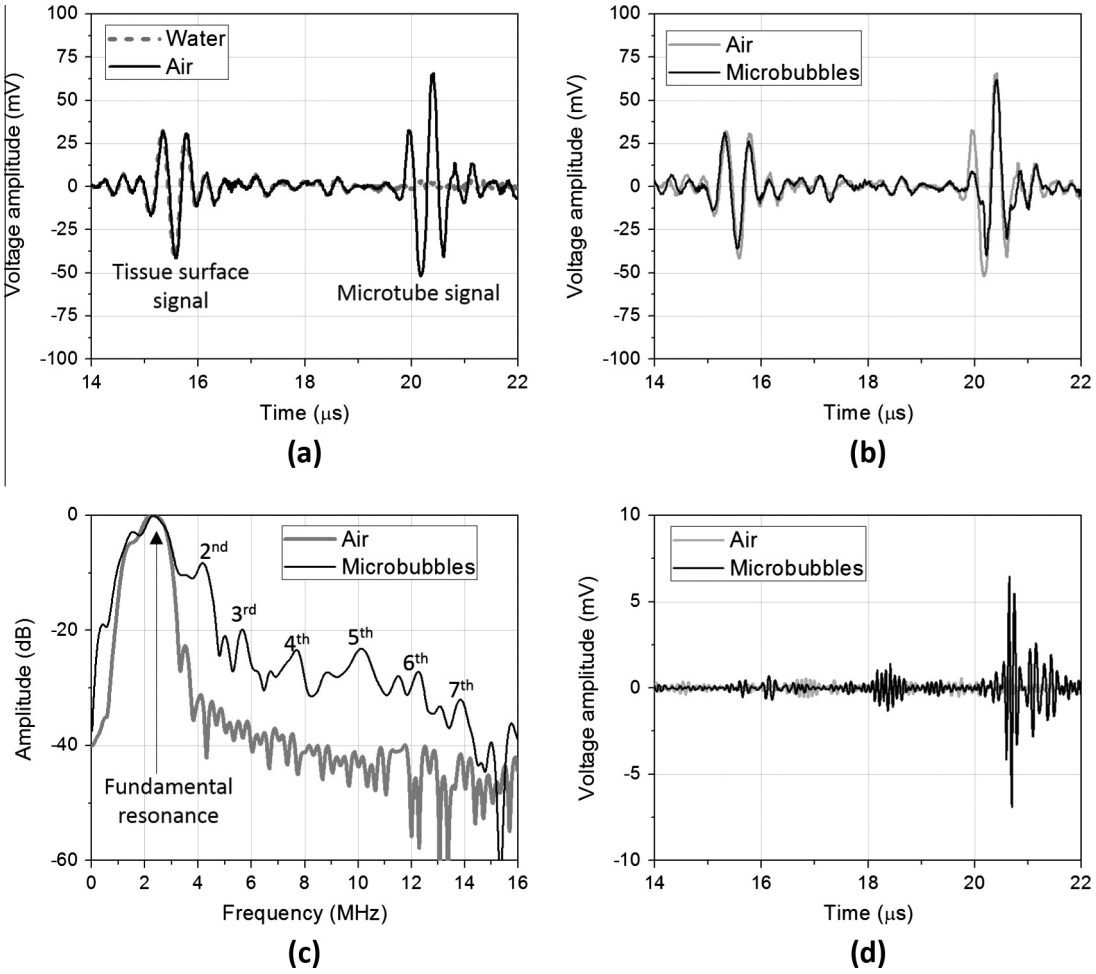

Fig. 8. Microbubble signal detection test results; voltage amplitude comparison between (a) air vs water, (b–d) microbubbles vs air; (c) frequency spectra transformed with the FFT window of 19–21.5 μs in (b), (d) amplitudes filtered by a 5th order Butterworth band-pass filter (10–15 MHz).

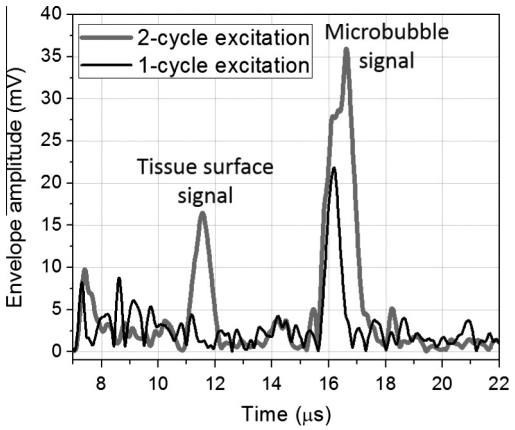

Fig. 9. Envelope amplitude comparison between 1-cycle and 2-cycle excitation.

microbubbles (5th through 7th harmonics) were successfully detected with a penetration depth of about 5 mm in a tissue phantom.

Fig. 9 shows the comparison between the detected microbubble signals from 1-cycle and 2-cycle excitations. The microbubble signals were band-pass filtered (10–15 MHz) and envelope was detected. The comparison showed that the 1-cycle excitation produced a microbubble SNR of 16 dB, CTR of 16 dB, and −6 dB pulse-length of 0.57 μs and the 2-cycle excitation produced a SNR of 20 dB, CTR of 7 dB, and −6 dB pulse-length of 1.09 μs. Microbubble SNR increased due to the higher MI (~1.63) produced by the 2-cycle excitation, but the additional pulse cycles degraded resolution. It should also be noted that CTR decreased with increasing number of cycle (16 dB to 7 dB). It was noted that with a 2-cycle excitation, there was a distinguishable high-frequency (10–15 MHz) signal from the tissue-phantom surface. This phenomenon was observed in previous work [6] as well, where harmonic signals were detected from a steel rod acting as a linear reflector. This may be due to the reverberation caused by the increased number of cycle as well as the direct reflection of harmonic components in 2 MHz-transmitting signal.

3.6. Superharmonic imaging results

The cellulose tubes in the tissue-mimicking phantom were scanned by the aforementioned dual frequency imaging procedure. The results show that the superharmonic images obtained by our dual-frequency transducer clearly visualize the cross-section of tubes filled with microbubbles (Fig. 10). In both images, a faint horizontal line is visible at approximately 6 mm in depth and it was generated by the electrical excitation from the function generator. The 1-cycle excitation waveform produced an averaged SNR and CTR of 16 dB (Fig. 10(a)), whereas the 2-cycle excitation waveform produced an average SNR and CTR of 19 dB and 5 dB, respectively (Fig. 10(b)). The 3 dB higher SNR produced by the 2-cycle excitation compared to the 1-cycle excitation is attributed to a 67% stronger microbubble harmonic response, which is caused by the increased MI (from 1.39 to 1.63). On the other hand, the 11 dB decrease in CTR with the 2-cycle excitation is due to the higher frequency harmonic response (10–15 MHz) from the tissue-phantom boundary. This tissue-response generates a distinguishable line at a distance of 8 mm in Fig. 10(b). The −6 dB axial resolution for the 1-cycle and 2-cycle excitations were measured to be 615 μm (5.5λ of 14 MHz waves) and 1.1 mm (10.2λ of 14 MHz waves), respectively. As predicted based on the enveloped amplitude results (Fig. 9), the extended pulse length of microbubbles due to the increased pulse length of the 2-cycle excitation, reduces the quality of microcellulose tube images.

4. Conclusion

In this work, we developed a stacked-type, small-size aperture (7.0×3.8 mm^2), dual-frequency (2/14 MHz) transducer for feasibility demonstration of intracavitary acoustic angiography. The acoustic characterization results indicate that our design concept and technique can achieve an acceptable −6 dB fractional bandwidth (57% for the transmitter and 42% for the receiver) and a sufficient MI (>1.0) for superharmonic microbubble imaging. We demonstrated that these imaging conditions are capable of inducing a nonlinear higher harmonic response of microbubble contrast agents with a penetration depth in a tissue-phantom of about 5 mm (total distance of 13 mm), and detecting higher-order harmonics (5th through 7th) from microbubbles with the suppression of linear tissue signal.

Multiple A-line images confirmed that a single-cycle excitation input is more advantageous for high-resolution and high-CTR acoustic angiography imaging when compared to a multiple-cycle excitation input. Although the 2-cycle excitation waveform resulted in a higher SNR (19 dB) compared to the single-cycle excitation (16 dB), the −11 dB decrease in CTR and

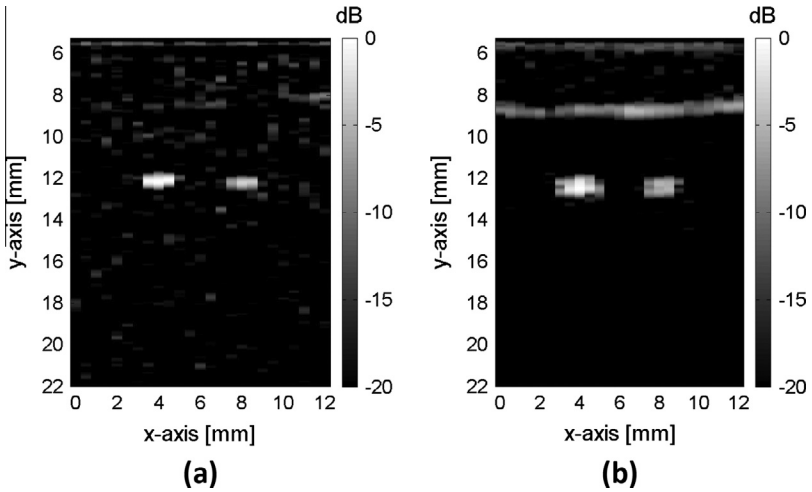

Fig. 10. Superharmonic B-mode images of microtubes in a tissue-mimicking phantom using the prototype dual-frequency transducer by applying sinusoidal excitation at 2 MHz and receiving harmonic responses in the frequency range of 10–15 MHz; (a) 1-cycle excitation, (b) 2-cycle excitation.

90% larger −6 dB resolution are not practical for intracavitary acoustic angiography. The comparison of the acquired acoustic angiography images using two different excitations concluded that it is desirable to use the minimum number of cycles to maintain resolution while achieving a sufficient MI for increasing the amplitude of the higher-harmonic microbubble response.

This feasibility study on intracavitary acoustic angiography of a single-element dual-frequency design, including phantom evaluation and detailed characterization techniques for key acoustic parameters, will be a useful guideline for further developing dual-frequency ultrasound imaging for specific clinical applications. This work will be adopted and expanded into the development of future dual-frequency array transducers for intracavitary acoustic angiography applications.

Acknowledgements

The authors would like to acknowledge the financial support from U.S. Army Medical Research and Materiel Command under the contract PC111309. The authors like to thank Jianguo Ma, Anthony Novell, K. Heath Martin and Wei-Yi Chang for providing instruction and assistance in transducer design, microbubble detection tests and manuscript preparation. The authors are also grateful to the editor and the reviewers for their exceptional contribution to improving the paper with valuable comments and suggestions.

References

[1] B.D. Lindsey, J.D. Rojas, K.H. Martin, S.E. Shelton, P.A. Dayton, Acoustic characterization of contrast-to-tissue ratio and axial resolution for dual-frequency contrast-specific acoustic angiography imaging, IEEE Trans. Ultrason. Ferroelectr. Freq. Control 61 (2014) 1668–1687.

[2] B.D. Lindsey, J.D. Rojas, P.A. Dayton, On the relationship between microbubble fragmentation, deflation and broadband superharmonic signal production, Ultrasound Med. Biol. 41 (2015) 1711–1725.

[3] P. Carmeliet, R.K. Jain, Angiogenesis in cancer and other diseases, Nature 407 (2000) 249–257.

[4] S.E. Shelton, Y.Z. Lee, M. Lee, E. Cherin, F.S. Foster, S.R. Aylward, P.A. Dayton, Quantification of microvascular tortuosity during tumor evolution using acoustic angiography, Ultrasound Med. Biol. 41 (2015) 1896–1904.

[5] K.H. Martin, B.D. Lindsey, J. Ma, M. Lee, S. Li, F.S. Foster, X. Jiang, P.A. Dayton, Dual-frequency piezoelectric transducers for contrast enhanced ultrasound imaging, Sensors 14 (2014) 20825–20842.

[6] J. Ma, K.H. Martin, P.A. Dayton, X. Jiang, A preliminary engineering design of intravascular dual-frequency transducers for contrast-enhanced acoustic angiography and molecular imaging, IEEE Trans. Ultrason. Ferroelectr. Freq. Control 61 (2014) 870–880.

[7] A. Bouakaz, F. ten Cate, N. de Jong, A new ultrasonic transducer for improved contrast nonlinear imaging, Phys. Med. Biol. 49 (2004) 3515.

[8] R. Gessner, M. Lukacs, M. Lee, E. Cherin, F. Foster, P.A. Dayton, High-resolution, high-contrast ultrasound imaging using a prototype dual-frequency transducer: in vitro and in vivo studies, IEEE Trans. Ultrason. Ferroelectr. Freq. Control 57 (2010) 1772–1781.

[9] J. Kim, S. Li, X. Jiang, S. Kasoji, P.A. Dayton, Development of transmitters in dual-frequency transducers for interventional contrast enhanced imaging and acoustic angiography, in: Proc. IEEE Ultrasonics Symp., IEEE, 2014, pp. 679–682.

[10] S. Zhang, F. Li, X. Jiang, J. Kim, J. Luo, X. Geng, Advantages and challenges of relaxor-$PbTiO_3$ ferroelectric crystals for electroacoustic transducers–A review, Prog. Mater Sci. 68 (2015) 1–66.

[11] J. Kim, Y. Roh, Homogenization of PMN–PT/epoxy 1–3 piezocomposites by resonator measurements and finite element analysis, Sens. Actuators, A 206 (2014) 97–106.

[12] J.E. Streeter, R. Gessner, I. Miles, P.A. Dayton, Improving sensitivity in ultrasound molecular imaging by tailoring contrast agent size distribution: in vivo studies, Mol. Imaging 9 (2010) 87.

[13] K. Parker, S. Huang, R. Lerner, F. Lee Jr, D. Rubens, D. Roach, Elastic and ultrasonic properties of the prostate, in: Proc. IEEE Ultrasonics Symp., IEEE, 1993, pp. 1035–1038.

[14] J. Ma, M.B. Steer, X. Jiang, An acoustic filter based on layered structure, Appl. Phys. Lett. 106 (2015) 111903.

[15] H. Wang, T. Ritter, W. Cao, K.K. Shung, High frequency properties of passive materials for ultrasonic transducers, IEEE Trans. Ultrason. Ferroelectr. Freq. Control 48 (2001) 78–84.

[16] I. Chopra, J. Sirohi, Smart Structures Theory, Cambridge University Press, New York, 2013.

The implementation of acoustic angiography for microvascular and angiogenesis imaging

Paul A. Dayton[1*] - *IEEE Member*, Ryan C. Gessner[1], Linsey Phillips[1], Sarah E. Shelton[1], K. Heath Martin[1], Mike Lee[2], and F. Stuart Foster[2] - *IEEE Member*

***Abstract*— Recently, it has been demonstrated that through the use of contrast agents and multi-frequency transducer technology, high resolution and high signal to noise ultrasound images can be obtained which illustrate microvascular structure in unprecedented detail for an ultrasound modality. The enabling technology is ultrasound transducers which are fabricated with elements which can excite microbubble contrast agents near resonance and detect their broadband harmonics at a much higher bandwidth (several times the fundamental frequency). The resulting images contain very little background from tissue scattering and thus provide high contrast, and can have a resolution on the order of 130 microns with an appropriate high frequency receiving element. Because microbubbles are strictly an intravascular agent, this approach enables visualization of microvascular morphology with unique clarity, providing insight into angiogenesis associated with tumor development.**

I. Introduction

Ultrasound imaging is already widely used in clinical and preclinical imaging, with several advantages over competing modalities such as low cost, safety, convenience, high frame rate, and soft tissue contrast. Microbubbles provide additional utility as contrast agents in ultrasound imaging by increasing backscatter from blood flow, which would be otherwise difficult to image in small vessels due to low signal to noise. To date, contrast enhanced ultrasound has shown unique utility in enhancing blood-tissue border definition, such as myocardial border delineation; perfusion imaging, where microbubble flow into an organ can provide quantifiable information about local blood flow; and molecular imaging, where targeted contrast agents can elucidate the presents of molecular markers expressed on the endothelium. However, until recently, contrast enhanced ultrasound could not clearly define microvessel structure without using "persistence" imaging approaches, which track contrast presence over a long (many seconds) time period.[1] This is largely due to the fact that contrast imaging has been primarily used at low frequencies, which have resulted in low resolution, and the fact that current contrast imaging techniques can still suffer from tissue nonlinearities contaminating the contrast signal. Although persistence imaging can provide some useful images depicting vascular morphology, the presence of any tissue motion quickly degrades the image even in 2-D, and thus persistence images are very challenging to acquire in 3-D, which is what is ultimately required for mapping microvascular structure.

In this paper, we describe an approach for using contrast ultrasound to image the microvasculature in 3-D with high resolution and contrast. This approach, which we refer to as "acoustic angiography" because of its similarity in appearance to x-ray angiography, is enabled through the use of ultrasound transducers fabricated with multiple elements to achieve a very broad bandwidth across transmit and receive, enabling detection of broadband superharmonic content from cavitating microbubbles.[2]

II. Methods

A. Transducer Design

The enabling technology for acoustic angiography is the dual-frequency transducer, which provides a low frequency bandwidth for transmitting and a high frequency bandwidth for receiving. The principle behind the imaging is that excited microbubbles produce very broad harmonic content as they oscillate aggressively in an acoustic field. Driving these microbubbles can be performed effectively with transmission frequencies which induce maximal oscillation, which are typically low frequencies (a few MHz). Kruse et al. demonstrated even with 2 MHz excitation, the resulting high frequency energy can be as high as 45 MHz.[3] To date, no commercial imaging transducers have been able to transmit and receive with such a broad bandwidth, so our team has fabricated transducers for this purpose.[4] Our prototypes consist of a modified Visualsonics RMV probe with a 30 MHz center frequency element. Confocally aligned with this element is a low frequency (4 MHz) annulus used as a transmitter. The high frequency element can be used for standard pulse-echo b-mode imaging to obtain anatomical information, or can be used as a receiver only to obtain contrast only information. The transmitter is driven by an RF amplifier and pulse generator synchronized with the Visualsonics Vevo 770 commercial ultrasound system. A 7th order 10 MHz butterworth high-pass filter on the receive line filters out any received tissue echoes.

Research supported by the National Institutes of Health through R01EB009066 and R01CA170665 (PAD), as well as the Terry Fox Foundation, The Ontario Research Fund, and VisualSonics (FSF)

[1]Joint Department of Biomedical Engineering, UNC at Chapel Hill and NC State University.

[2]Department of Medical Biophysics, University of Toronto at Sunnybrook

[*]corresponding author: phone 919-843-9521; e-mail: padayton@bme.unc.edu

978-1-4244-7929-0/14/$26.00 ©2014 IEEE

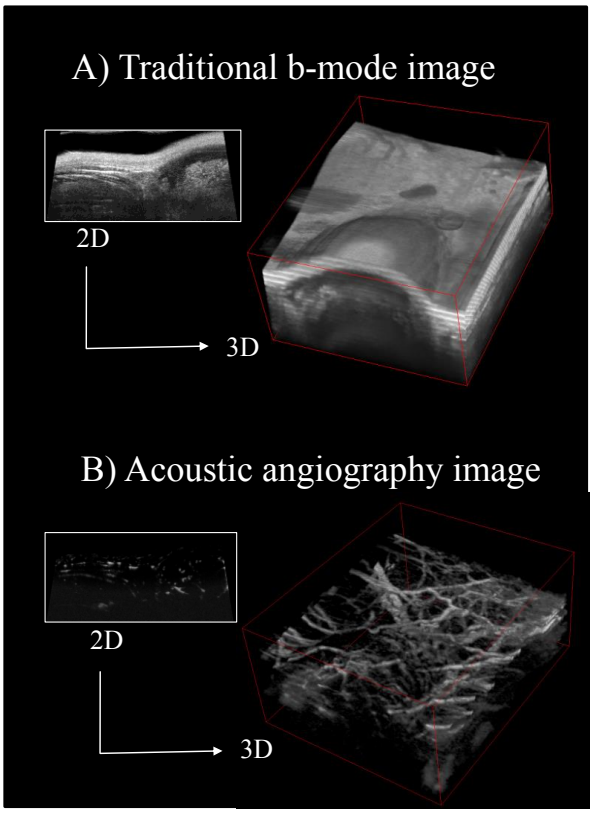

Figure 1. A) 30 MHz b-mode imaging of a subcutaneous FSA tumor in a rat in 2D and 3D. B) acoustic angiography of the same sample volume, illustrating microvasculature within the tissue and tumor region.

B. In Vivo Imaging

All imaging studies were approved by the IACUC at the University of North Carolina at Chapel Hill. In-vivo imaging was performed on healthy mice or rats bearing subcutaneous fibrosarcoma (FSA) tumors, as described previously.[5] Lipid-shelled perfluorocarbon-filled microbubble contrast agents, as previously described,[6] were administered via continuous infusion. A mechanical stage translated the custom transducer probe in the elevational direction to enable 3-D volume reconstruction during imaging.

III. RESULTS

A. Transducer Performance

The custom transmit 4 MHz/receive 30 MHz RMV probe demonstrated a -6dB focal beamwidth for the receiver of approximately 130 microns, suggesting a resolution on this order. Most imaging was performed at a mechanical index of approximately 0.6 (1.2 MPa at 4 MHz) which is less than the recommended energy for Definity imaging in patients,[7] but likely sufficient for contrast agent destruction, although our additional data (not shown here) suggests that some bubbles can survive multiple pulses before complete destruction at this frequency and pressure combination. We utilized low frame rate imaging (several Hertz), which enabled sufficient contrast wash in into the area of interest for imaging with the parameters utilized.

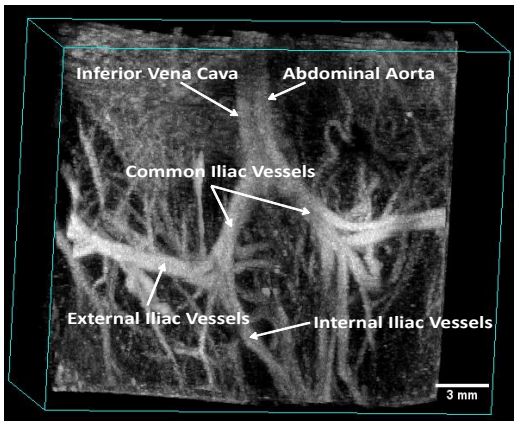

Figure 2. Acoustic angiography of mouse abdomen showing vascular structure.

The dual-frequency probe could be utilized in two separate imaging modes, standard pulse-echo imaging at 30 MHz, which would provide anatomical information (Figure 1A), or transmit 4 MHz/receive 30 MHz mode, which would provide contrast information (Figure 1B). Contrast imaging illustrated microvasculature with high resolution and high signal (acoustic angiography) to noise due to the detection of flowing contrast limited to within the vascular space, and low background from tissue due to the substantial bandwidth separation. Both images could be readily registered to provide simultaneous tissue and microvascular information (not shown). Acoustic angiography of the mouse abdomen provided clear delineation of major and minor vasculature (Figure 2).

B. Angiogenesis Imaging

When applied to subcutaneous tumors, angiogenesis was readily visualized. Figures 3(A-B) show acoustic angiography of subcutaneous tumors in a rat. The angiogenic growth of feeder vessels from left to right into the

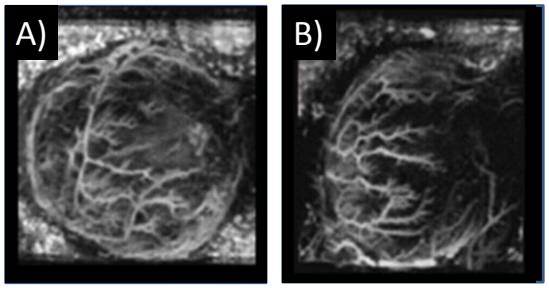

Figure 3. A) and B) exampes of acoustic angiography (maximum intensity projections from 3-D datasets) of angiogenic microvasculature present in subcutaneous FSA tumors in rats.

tumor tissue is readily visualized. Each image frame is approximately 15 mm square.

C. Derived Features of Microvascular Morphology

One of the exciting possibilities with acoustic angiography is the ability to quantify microvascular characteristics due to the high resolution and high contrast in the 3-D images. We have previously shown that these images can be segmented and analyzed. Features such as vessel size and vascular density can be measured,[8] as well as measures of microvascular tortuosity.[5] It is well believed that tortuosity is a characteristic abundantly present in angiogenic vessels and less present in healthy vessels. Our prior studies have demonstrated that through acoustic angiography analysis of rodents, we could distinguish healthy tissue from tumor-bearing tissue based on microvessel morphology alone using measurements of microvascular tortuosity. Similar techniques have been applied to magnetic resonance angiography data,[9-13] although it has not been until the development of acoustic angiography that microvascular morphology analysis has been feasible on ultrasound data.

IV. Conclusion

The development of dual-frequency transducers to take advantage of the high-frequency broadband energy from contrast agent microbubbles has enabled a new contrast imaging approach which produces ultrasound images with unprecedented resolution and contrast. Although this technique has some notable limitations, such as limited depth of penetration due to the high frequency received energy, and the likely need for bubble destruction to obtain the best signal, acoustic angiography will likely provide utility as a tool in serial imaging of angiogenesis and microvessel morphology. For this technique to become more widely useful, multi-frequency array transducers will need to be fabricated and integrated with commercial hardware. One alternate application also in development is micro-scale dual-frequency transducers for intravascular contrast ultrasound imaging, which may play a future role in vasa vasorum imaging.[14]

Acknowledgment

The authors thank Dr. James Tsuruta for assistance with contrast agent preparation, as well as Drs. Marc Lukacs and Emmanuel Cherin for their assistance with the development of the prototype dual-frequency RMV probe.

References

[1] M. A. Pysz, K. Foygel, C. M. Panje, A. Needles, L. Tian, and J. K. Willmann, "Assessment and monitoring tumor vascularity with contrast-enhanced ultrasound maximum intensity persistence imaging," *Invest Radiol,* vol. 46, pp. 187-95, Mar 2011.

[2] R. C. Gessner, C. B. Frederick, F. S. Foster, and P. A. Dayton, "Acoustic angiography: a new imaging modality for assessing microvasculature architecture," *Int J Biomed Imaging,* vol. 2013, p. 936593, 2013.

[3] D. E. Kruse and K. W. Ferrara, "A new imaging strategy using wideband transient response of ultrasound contrast agents," *IEEE Trans Ultrason Ferroelectr Freq Control,* vol. 52, pp. 1320-9, Aug 2005.

[4] R. Gessner, M. Lukacs, M. Lee, E. F. Cherin, S. Foster, and P. A. Dayton, "High-resolution, high-contrast ultrasound imaging using a prototype dual-frequency transducer: in-vitro and in-vivo studies," *Transactions on Ultrasonics, Ferroelectrics, and Frequency Control,* 2010.

[5] R. C. Gessner, S. R. Aylward, and P. A. Dayton, "Mapping microvasculature with acoustic angiography yields quantifiable differences between healthy and tumor-bearing tissue volumes in a rodent model," *Radiology,* vol. 264, pp. 733-40, Sep 2012.

[6] J. E. Streeter, R. Gessner, I. Miles, and P. A. Dayton, "Improving sensitivity in ultrasound molecular imaging by tailoring contrast agent size distribution: in vivo studies," *Mol Imaging,* vol. 9, pp. 87-95, Apr 2010.

[7] B.M.S., "Definity package insert," ed, 2008.

[8] R. C. Gessner, A. D. Hanson, S. Feingold, A. T. Cashion, A. Corcimaru, B. T. Wu*, et al.*, "Functional ultrasound imaging for assessment of extracellular matrix scaffolds used for liver organoid formation," *Biomaterials,* vol. 34, pp. 9341-51, Dec 2013.

[9] L. M. Brubaker, E. Bullitt, C. Yin, T. Van Dyke, and W. Lin, "Magnetic resonance angiography visualization of abnormal tumor vasculature in genetically engineered mice," *Cancer Res,* vol. 65, pp. 8218-23, Sep 15 2005.

[10] E. Bullitt, M. Ewend, J. Vredenburgh, A. Friedman, W. Lin, K. Wilber*, et al.*, "Computerized assessment of vessel morphological changes during treatment of glioblastoma multiforme: report of a case imaged serially by MRA over four years," *Neuroimage,* vol. 47 Suppl 2, pp. T143-51, Aug 2009.

[11] E. Bullitt, G. Gerig, S. M. Pizer, W. Lin, and S. R. Aylward, "Measuring tortuosity of the intracerebral vasculature from MRA images," *IEEE Trans Med Imaging,* vol. 22, pp. 1163-71, Sep 2003.

[12] E. Bullitt, N. U. Lin, M. G. Ewend, D. Zeng, E. P. Winer, L. A. Carey*, et al.*, "Tumor therapeutic response and vessel tortuosity: preliminary report in metastatic breast cancer," *Med Image Comput Comput Assist Interv,* vol. 9, pp. 561-8, 2006.

[13] E. Bullitt, K. E. Muller, I. Jung, W. Lin, and S. Aylward, "Analyzing attributes of vessel populations," *Med Image Anal,* vol. 9, pp. 39-49, Feb 2005.

[14] J. Ma, K. H. Martin, P. A. Dayton, and X. Jiang, "A preliminary engineering design of intravascular dual-frequency transducers for contrast enhanced acoustic angiography and molecular imaging," *IEEE Ultrasonics, Ferroelectrics, and Frequency Control,* 61(5):870-80, May 2014.

Sensors **2014**, *14*, 20825-20842; doi:10.3390/s141120825

OPEN ACCESS

sensors

ISSN 1424-8220

www.mdpi.com/journal/sensors

Review

Dual-Frequency Piezoelectric Transducers for Contrast Enhanced Ultrasound Imaging

K. Heath Martin [1], Brooks D. Lindsey [1], Jianguo Ma [2], Mike Lee [3], Sibo Li [2], F. Stuart Foster [3], Xiaoning Jiang [2] and Paul A. Dayton [1,*]

[1] Joint Department of Biomedical Engineering, University of North Carolina at Chapel Hill and North Carolina State University at Raleigh, Chapel Hill, NC 27599, USA; E-Mails: khmartin@ncsu.edu (K.H.M.); brooks.lindsey@unc.edu (B.D.L.)

[2] Department of Mechanical & Aero-Space Engineering, North Carolina State University, Raleigh, NC 27695, USA; E-Mails: jma9@ncsu.edu (J.M.); sli26@ncsu.edu (S.L.); xjiang5@ncsu.edu (X.J.)

[3] Sunnybrook Health Sciences Centre, Toronto, ON M4N 3M5, Canada; E-Mails: hlee@sri.utoronto.ca (M.L.); stuart@sri.utoronto.ca (F.S.F.)

* Author to whom correspondence should be addressed; E-Mail: padayton@email.unc.edu; Tel.: +1-919-966-1175; Fax: +1-919-966-2963.

External Editor: Vittorio M.N. Passaro

Received: 6 August 2014; in revised form: 3 October 2014 / Accepted: 16 October 2014 / Published: 4 November 2014

Abstract: For many years, ultrasound has provided clinicians with an affordable and effective imaging tool for applications ranging from cardiology to obstetrics. Development of microbubble contrast agents over the past several decades has enabled ultrasound to distinguish between blood flow and surrounding tissue. Current clinical practices using microbubble contrast agents rely heavily on user training to evaluate degree of localized perfusion. Advances in separating the signals produced from contrast agents *versus* surrounding tissue backscatter provide unique opportunities for specialized sensors designed to image microbubbles with higher signal to noise and resolution than previously possible. In this review article, we describe the background principles and recent developments of ultrasound transducer technology for receiving signals produced by contrast agents while rejecting signals arising from soft tissue. This approach relies on transmitting at a low-frequency and receiving microbubble harmonic signals at frequencies many times higher than the transmitted frequency. Design and fabrication of dual-frequency transducers

and the extension of recent developments in transducer technology for dual-frequency harmonic imaging are discussed.

Keywords: acoustics; acoustic angiography; dual-frequency; superharmonic; harmonic; broadband; microbubbles

1. Introduction

Fundamentally, ultrasound images are visual representations of the interaction between sound waves and the medium of wave propagation. In ultrasound imaging, an acoustic pulse is transmitted into the field using a transducer capable of producing a temporally short mechanical wave (1–4 cycles) in response to a voltage applied to the transducer. As the incident wave travels into tissue, some of the wave's energy is reflected back toward the transducer by scatterers in the tissue having different acoustic properties (*i.e.*, density and speed of sound) than the background medium. These backscattered acoustic waves are received by the same transducer, which converts mechanical waves into time-varying voltages. These signals are then amplified, digitized, and processed into an image by the ultrasound imaging system. In the most common mode of operation, called "brightness-mode" or "B-mode" ultrasound, grayscale images are formed in which pixel values are proportional to the brightness of scattered acoustic waves. In other system modes, B-mode images are overlaid with colorized maps of blood velocity (color Doppler) or integrated energy from moving scatterers (power Doppler). However, at frequencies typically used in transthoracic and transabdominal ultrasound imaging, blood is a poor ultrasound scatterer which produces echoes approximately a factor of 300 times weaker than surrounding soft tissues [1], making the detection of blood flow in small vessels challenging. For this reason, microbubbles are used as injectable contrast agents, which serve as strong scattering sources and thereby improve imaging of blood flow [2]. While contrast ultrasound is used primarily in cardiology in the United States, it is used more widely in Europe and Asia, and there are substantial ongoing research efforts aimed at evaluating microbubbles as a platform for additional diagnostic and therapeutic applications [3,4]. This review will primarily focus on development of dual-frequency piezoelectric transducers for imaging nonlinear harmonics produced by microbubbles under ultrasound excitation.

1.1. Theory of Operation

Microbubble contrast agents are micron-sized shelled gas bubbles that are injected into the vascular space in order to visualize blood flow. When excited by an external acoustic field, microbubbles oscillate non-linearly, producing waves with harmonic content in addition to the fundamental frequency. The degree of harmonic content produced by a single interaction between a microbubble and an acoustic wave increases as the amplitude of the acoustic wave increases, and also increases at frequencies near the resonance frequency of the microbubble [5–8]. Microbubble resonance frequency depends primarily on bubble diameter, though many other physical factors also play a role in determining resonance [9,10]. While microbubbles are strong scatterers that are visible on standard B-mode imaging at the fundamental imaging frequency, the energy arising from microbubbles cannot be separated from that arising from the

surrounding tissue. However, by isolating the harmonic signals resulting from microbubble nonlinear behavior it is possible to image microbubbles alone with high specificity.

An effective approach for minimizing tissue echoes in microbubble-specific imaging is to use higher order harmonics. An acoustic wave traveling through tissue generates harmonics due to nonlinear propagation effects, however, most of the energy received at the transducer remains confined to the transmitted frequency (f_0) and the second harmonic ($2f_0$) [11,12]. Alternatively, microbubble echoes contain higher order harmonics, or "superharmonics," at frequencies three to 10 times the transmitted frequency [13–16]. In this review paper, we describe transducer technology designed to transmit at low frequencies near microbubble resonance and receive only microbubble harmonics at much higher frequencies, thus spectrally separating microbubble-scattered waves from tissue-scattered waves.

1.2. Summary of Commercial Contrast Detection Methods

Currently, most commercial ultrasound systems form images of microbubbles using frequency content within the bandwidth of a single transducer, which is used for both transmitting and receiving. These systems typically reduce tissue echoes by transmitting multiple versions of similar pulses having varying phases and/or amplitudes, then summing received signals from these pulses. Using this process, linear signals originating from tissue cancel while nonlinear microbubble signals sum constructively. In the simplest of these techniques, pulse inversion, a pair of pulses are transmitted which are inverted replicas of one another (*i.e.*, 180° out of phase) [17]. Linear scatterers produce two sets of similarly inverted signals, thus when the received signals from each of the two pulses are added together, the net sum due to linear scattering is zero, assuming no motion has occurred. Because shelled microbubbles vibrate nonlinearly, waves scattered from the contrast agents contain nonlinear components, which do not sum to zero, producing an image of microbubbles alone. Various multi-pulse schemes exist in which the phases and amplitudes of transmitted pulses are altered in order to improve separation of microbubble and tissue signals or to isolate a specific range of harmonics [18–21]. These algorithms are found on commercial ultrasound scanners under names such as Cadence Contrast Pulse Sequencing (CPS) (Siemens) or Power Pulse Inversion (Philips) [22]. The ratio of microbubble to tissue amplitude in an image is known as contrast to tissue ratio (CTR) and is often expressed in dB as a quantitative metric of the effectiveness of a contrast imaging technique. Multi-pulse approaches achieve high CTR at the cost of reduced frame rate and increased susceptibility to motion artifacts. Alternatively, dual-frequency transducers alleviate these problems because their large effective bandwidths allow high CTR imaging using a single pulse.

1.3. Design and Fabrication of Piezoelectric Transducers in Diagnostic Ultrasound

1.3.1. Piezoceramic Dimensions

While design theory of piezoelectric transducers is well-covered elsewhere [23,24], basic principles will be reviewed briefly to elucidate challenges relating to dual-frequency transducer fabrication. Transducers used in medical ultrasound consist of a thickness mode resonator. Wave propagation velocity in lead zirconate titanate (PZT) is approximately 4350 m/s [25], resulting in a nominal thickness ($\lambda/2$) of 435 μm at 5 MHz, for example, though other factors also affect transducer resonance [26]. In

array transducers, grating lobes are avoided by maintaining inter-element separation less than or equal to λ/2. Element width-to-thickness ratio must also be considered, as element aspect ratios determine the acoustic resonance modes [27,28]. Fabrication challenges tend to intensify as feature sizes decrease in all dimensions with increasing frequency. Tradeoffs between desired resonance frequency and element dimensions represent a primary challenge in array design.

1.3.2. Element Boundary Condition Considerations

Matching and backing layers designed with desired acoustic properties are attached in series to the front and back faces of the piezoelectric material, respectively. By reducing the mismatch in acoustic impedance between the piezoelectric material ($Z_{PZT} \approx 34$ MRayl) and tissue ($Z_{water} = 1.5$ MRayl), matching layers increase acoustic transmission into and from the tissue and act as quarter wave transformers. Backing layers improve bandwidth by damping acoustic vibrations at the rear boundary of the piezoelectric material. The loading provided by matching and backing layers also modulates the resonant frequency of the transducer [26]. The primary challenge in design of matching and backing layers is the tradeoff between high sensitivity and broad bandwidth.

1.3.3. Fabrication, Dicing, and Composites

For piezoelectric transducers operating in thickness mode, a "dice-and-fill" approach is commonly used in array fabrication. A wafer-dicing saw cuts and isolates sensing elements, and kerfs resulting from saw cuts are then backfilled to minimize acoustic crosstalk. A dice-and-fill approach is also used to create low-frequency composite materials [29–31] from plates of either piezoelectric ceramics [32] or electrostrictive PMN-PT single crystals [33] by dicing the material and filling the gaps with a polymer [34], then further dicing into individual elements for fabrication of an array. Composite materials can produce better harmonic images than conventional materials because they yield transducers with broader bandwidths (>75%) and improved acoustic matching [35]. Fabrication challenges associated with physical dicing limit acoustic impedance matching in composites.

For harmonic imaging, it may be possible to design a transducer so that both transmission and receiving frequencies are within the bandwidth of a single composite transducer. These composites can be made with 1–3 connectivity, mechanically decoupling the thickness-mode vibration resonance from other undesirable resonances (lateral or elevational modes) [27]. Lateral modes are λ/2 resonances determined by the dimension of the transducer in the lateral direction, or the dimension of image formation. Designing with respect to lateral modes takes on added importance in environments such as intravascular ultrasound (IVUS) in which strict limitations on device size imposed by lumen diameter can create severe aspect ratios (width-to-thickness) that are normally avoided to preserve forward looking directional sensitivity. As an alternative to dice-and-fill methods at higher frequencies, Jiang *et al.*, have demonstrated fabrication of a 40 MHz, 1–3 composite transducer using a plasma etching-based micromachining technique [36]. A 60 MHz IVUS transducer using 1–3 composite has been fabricated and tested on a porcine animal model [35]. These high-frequency broadband transducer materials are promising for imaging microbubble harmonics. The development of high-frequency arrays was greatly facilitated by the introduction of laser micro-machining by Foster *et al.*, a process which has

become a standard for commercially-available high-frequency imaging systems [37]. Providing individual electrical interconnects also poses a significant fabrication challenge in high-frequency arrays.

While developments in materials and fabrication have led to diagnostic transducers having increased sensitivity and bandwidth, the use of two independent frequency bands having large separation (at least 3× to 5×) can maximize sensitivity while requiring lower transmit pressures for contrast-specific imaging applications. In the following sections, we describe recent developments in dual-frequency transducer technology.

2. Dual-Frequency Transducers

The goal of dual-frequency contrast imaging is to form images of only microbubble harmonics by transmitting acoustic waves at lower frequencies near microbubble resonance (approximately 1–6 MHz) and receiving only higher order harmonic vibrations produced by microbubbles (approximately 10–30 MHz). Researchers have recently demonstrated electrostatic transducers that are capable of encompassing both frequency ranges within a single, extremely broad bandwidth [38,39]. Details of the operation and fabrication of these transducers, commonly referred to as capacitive micromachined ultrasound transducers (CMUTs), are discussed elsewhere [40–42]. CMUTs exhibit inherent nonlinear behavior, which limits their ability to accurately distinguish nonlinear microbubble response, though ongoing investigations attempt to account for these nonlinearities so they may be used for contrast detection reliably [43]. Although CMUTs may eventually demonstrate superior performance to piezoceramics for contrast imaging, they have not yet been demonstrated for this use *in vivo*. While researchers continue to investigate ultra-wideband electrostatic transducers as well as approaches for increasing the bandwidth of piezoelectric transducers [35,36,44,45], this review will primarily focus on devices that use separate transducers for transmission and reception and thus allow for independent design of the two transducers to achieve desired characteristics.

2.1. Imaging Microbubble Contrast Agents

Bouakaz *et al.* first reported imaging of third and fourth harmonics of microbubbles in 2002 in experiments which used a 96-element array with interleaved 0.9 MHz transmission elements (50% bandwidth) and 2.8 MHz receiving elements (80% bandwidth) [46–48]. Using this probe with a commercial imaging system, the authors demonstrated the ability to image microbubbles while rejecting tissue signals *in vivo* [47] (Figure 1). While interleaving low and high-frequency elements yields dual-frequency transducer arrays with smaller form factors relative to arrays stacked in the elevation direction, grating lobes were introduced due to an increase in inter-element separation, and signal-to-noise ratio (SNR) was diminished due to reduction in receiving area and in the number of received signals contributing to the beamformed signal.

In 2005, Kruse and Ferrara demonstrated the use of two piston transducers with a wide bandwidth separation for imaging microbubbles using a transmission frequency of 2.25 MHz (70% bandwidth) and a receiving frequency of 15 MHz (66% bandwidth) [49]. Wide separation between the two frequencies ensured high CTR due to the low amplitude of higher order tissue harmonics, while a high receiving frequency produced high-resolution images. In more recent studies, Ferrara's group has designed transmit low/receive high (TLRH) arrays with two outer rows of 64 elements transmitting at 1.48 MHz,

and a central row of 128 elements receiving at 5.24 MHz [50]. In addition to harmonic imaging of microbubbles, the high-frequency row of this three-row array was used to deliver a long (100 cycle), low-amplitude (200 kPa peak negative pressure) "pushing" pulse for radiation-force enhanced adhesion of targeted microbubbles for molecular imaging [51,52]. This work has recently been extended to 3D molecular imaging [53]. Subsequent generations of this array featured low-frequency rows capable of delivering either broadband, high peak pressure waveforms for cavitation-mediated therapy or narrower band, high time-average power waveforms for thermal therapy [54,55]. A similar three-row array with a central row of 128 elements operating at 1 MHz (90% bandwidth) and elevationally-aligned outer rows of 128 elements operating at 10 MHz (90% bandwidth) was constructed by Vermon (Tours, France) [56].

Figure 1. Schematic of the first design incorporating dual-frequency transducers for the purpose of contrast detection (**top**). Odd numbered elements had a center frequency of 2.8 MHz with a fractional bandwidth of 80% while the even elements had a center frequency of 0.9 MHz with a fractional bandwidth of 50%. Odd numbered elements were used for imaging superharmonics generated by nonlinear vibrations of microbubbles excited with a low-frequency pulse provided by the even elements. A photograph of the actual transducer is shown after the elevational lens has been added (**bottom**). Figure reprinted with permission from [46].

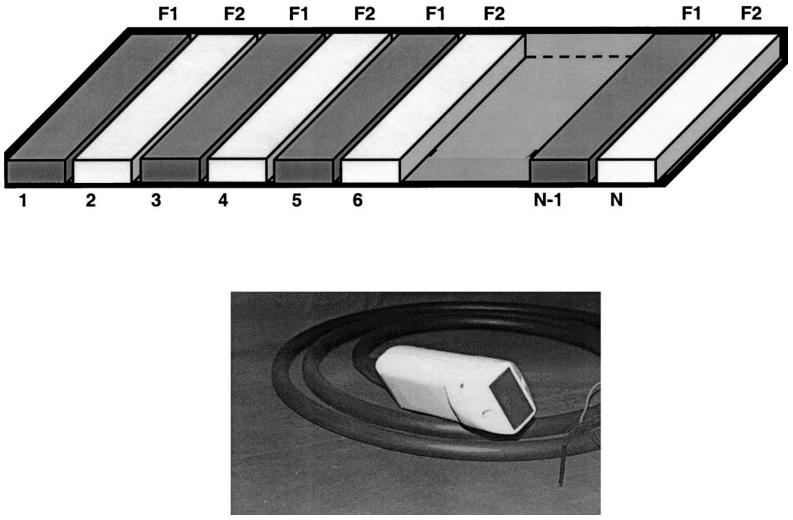

In 2010, van Neer *et al.* compared designs for interleaved and multi-row arrays [57,58]. Designs with interleaved elements having high ratios of receive to transmit elements (*i.e.*, at least three receive elements per transmit element) were capable of producing beams with reduced distortion artifacts and tighter −6 dB beam widths relative to two- or three-row arrays. By greatly increasing the number of receiving elements, grating lobes of interleaved designs were limited to −40 dB and high SNR was ensured. However, it should be noted that arrays with interleaved elements of different frequencies cannot be manufactured using standard dice-and-fill approaches from a single piezoelectric plate without significant alteration to manufacturing processes (see "Design and Fabrication" section).

In spite of the promise shown by several of these dual-frequency arrays, transition towards transducers with higher receiving frequencies has been accompanied by several fabrication challenges. Because standard array production techniques faces difficulties scaling to higher frequencies [59],

high-frequency transducers can utilize mechanical steering of a single focused element in lieu of an array. Many of these focused single-element transducers have been possible due to the use of flexible piezoelectric composites rather than inflexible piezoelectric ceramics [60,61]. An important advancement for high-frequency arrays has been the development of composites with large triangular pillars to suppress lateral modes while maintaining high sensitivity [62,63].

Figure 2. The mechanically steered dual-frequency transducer is composed of a central high-frequency (25 MHz) spherically focused piston transducer inserted into an annular, confocally aligned low-frequency transducer (4 MHz). (**A**, End-on view) Harmonic imaging is performed by mechanically sweeping the arm while transmitting on the outer element and receiving on the inner element. (**B**, Side view)

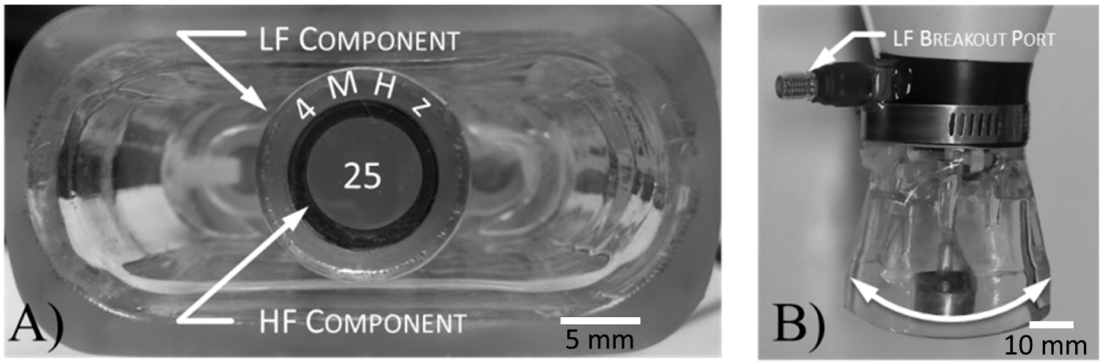

Using this technology, Foster's group working with Dayton has constructed several mechanically-steered transducers consisting of concentric low- (2.5–4 MHz) and high-frequency (25–30 MHz) elements [64,65]. These probes have been integrated with a commercial small animal imaging system (VisualSonics, Toronto, ON, Canada) (Figure 2). Imaging with these dual-frequency transducers has provided a high-resolution (~200 μm), high CTR (~25 dB) imaging technique, which the authors call "acoustic angiography" due to the resemblance between the vascular images acquired and those in x-ray, or magnetic resonance angiography [66]. This approach has demonstrated sensitivity to vessels containing contrast agents at frequencies higher than previously published (as high as 10 times the transmission frequency) (Figure 3) [67]. As a result, acquired images can be segmented by computational algorithms to analyze vessel morphology based on quantitative metrics such as vessel density and tortuosity [67–69].

Several similar transducers have recently been reported. A mechanically-scanned transducer with two concentric elements operating at 4 MHz and 14 MHz was demonstrated by Guiroy *et al.* [70]. Li *et al.* have alternatively demonstrated a micromachined PMN-PT 1–3 composite based dual-frequency (17.5/35 MHz) transducer (Figure 4) for harmonic imaging [71]. In this design, two active layers were mechanically bonded in series and poled in opposite directions. Composite piezoelectrics and electrostrictive materials such as PMN-PT have been increasingly utilized over traditional ceramics like PZT, which have limitations for use at higher frequencies due to manufacturing challenges and grain dimensions which become increasingly close to one wavelength as frequency increases [72].

Figure 3. Acoustic angiography amplitude spectrum (**top**) and example images (**bottom**). Wideband separation between tissue response and microbubble response produces images that are drastically different from conventional B-mode images and illustrate blood flow in the microvasculature with high-resolution and high-contrast to tissue ratio. Acoustic angiography images displayed using maximum intensity projections of volumetric scan volumes. Bounding boxes are approximately 0.75 × 1.25 × 1.5 cm (axial, lateral, and elevational). Figure adapted from [68].

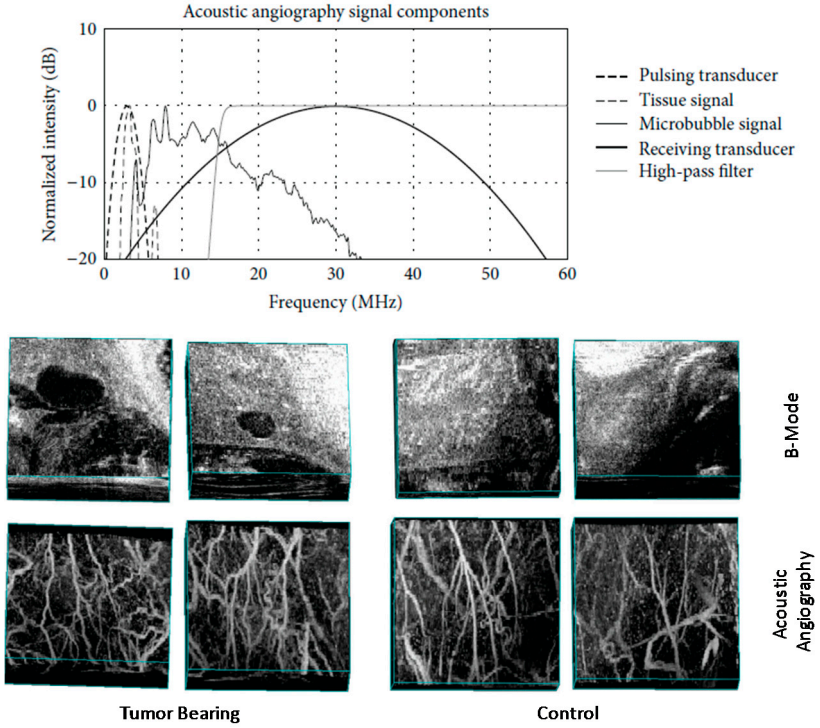

Figure 4. Schematic view of a dual-layer, dual-frequency transducer (**left**) and its operation for transmitting and receiving (**right**). When transmitting, both active layers are electrically connected in parallel and are excited by the same signal, effectively behaving as a single, active element at f_0. When receiving, the front layer records the majority of the signal with a resonance at twice the transmission frequency ($2f_0$) because the thickness of the active layer has effectively been halved. Figure reprinted with permission from [71].

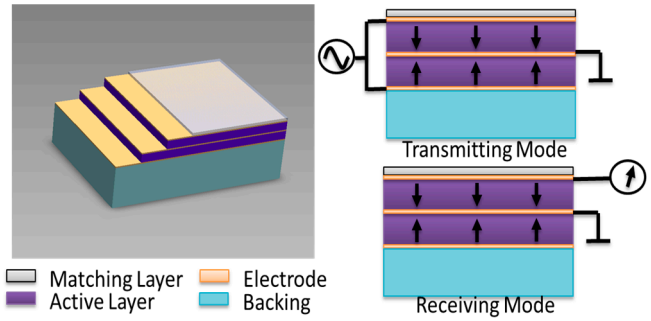

In recent years, researchers have developed several other dual-frequency transducers with high receiving frequencies (>10 MHz) for specific applications. One area of interest has been intravascular ultrasound, in which a small catheter-based transducer is introduced into the body to perform minimally

invasive imaging of occlusive plaques within the coronary arteries [73]. In particular, the presence of vessels known as *vasa vasorum* (70–180 μm in diameter [74]) in plaques has been hypothesized to be linked with decreased plaque stability and increased risk of future complications [75]. Because superharmonic imaging of microbubbles could enable direct visualization of *vasa vasorum*, several researchers have pursued dual-frequency transducer designs for this application. In 2005, Vos *et al.* developed single element transducers for second harmonic imaging designed with dual resonance peaks at 20 and 40 MHz and a 1 mm outer diameter [76,77]. This group has also used commercial IVUS catheters to demonstrate the benefits of pulse inversion detection methods for this application [78,79].

Recently, Jiang's group working with Dayton reported on the design and evaluation of dual-frequency IVUS transducers for superharmonic imaging (6.5 MHz/30 MHz) which were fabricated using stacked piezoelectric plates (Figure 5A) with co-aligned transmit and receive beams [80]. Transmitting and receiving elements were electrically separated by a frequency selective isolation layer (FSIL) [81] between the two active elements. This transducer had an aperture size of 0.6 mm × 3 mm and could be housed inside a commercial (Boston Scientific, Natick, MA) catheter (Figure 5B). Broadband emission and reception were performed by 6.5 and 30 MHz elements, respectively (Figure 5C). Superharmonic IVUS phantom imaging was acquired with a good CTR (12 dB) and high-resolution (200 μm) *in vitro* (Figure 5D).

Figure 5. Dual-frequency IVUS transducer designed for superharmonic imaging. (**A**) Structure of the transducer with stacked dual layers of piezoelectric plates; (**B**) The fabricated prototype mounted in an 8.5 F commercial catheter; (**C**) Use of two elements with separate bandwidths allows coverage of the transmitting and receiving frequencies needed for the superharmonic imaging; (**D**) Contrast enhanced IVUS imaging with microbubbles in phantom with fully-developed speckle. Figure reprinted with permission from [80], front cover.

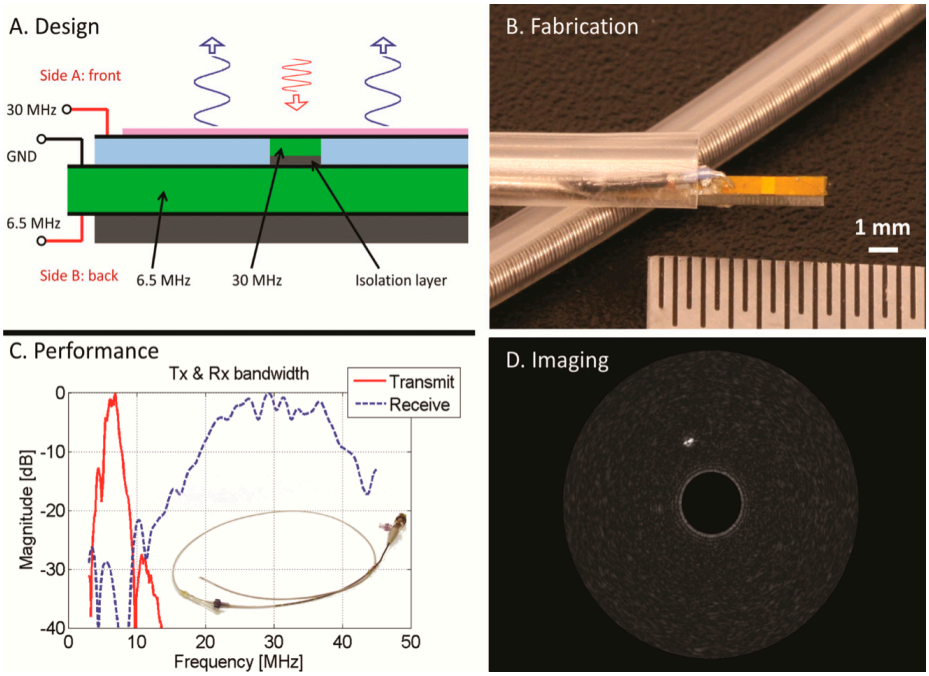

2.2. Other Applications

Researchers have developed dual-frequency ultrasound arrays for applications other than contrast agent imaging, which have provided useful insights into design or fabrication strategies. The earliest reported dual-frequency transducer was that of von Ramm and Smith in 1978, in which a phased array with adjacent rows of 1.5 and 2.5 MHz elements was designed to reduce off-axis contributions to the two-way point spread function by misaligning grating lobes from transmitting and receiving arrays [82]. In 1988, Bui *et al.* showed 1–3 composites can be designed to exhibit multiple frequency sensitivities by tailoring the dimensions for separate resonance modes [83]. De Fraguier *et al.* reported separate transducers for B-mode (4.6 MHz) and color Doppler mode (2.3 MHz) in order to improve Doppler sensitivity by reducing transmitted frequency and increasing pulse length [84]. Similarly, Saitoh *et al.* presented a transducer capable of operating at either 3.75 MHz or 7.5 MHz using two layers of PZT poled in opposite directions for increasing Doppler sensitivity [85].

In 2000, Hossack *et al.* reported a dual-frequency transducer to improve sensitivity for tissue harmonic imaging [86]. This transducer—based on earlier work by Hossack and Auld for increasing bandwidth [87]—used two piezoelectric layers having independent electrical contacts. The two layers were operated either in phase when transmitting at f_0, or 180° out of phase when receiving at $2f_0$. Several other authors developed similar transducers having two resonances at the fundamental and twice the fundamental [88,89]. Dual-frequency transducer design in tissue harmonic imaging has been studied extensively in the past and has aided in the development of recent transducer design in contrast specific imaging. For example, confocal annular elements operating at large frequency separations (20 and 40 MHz) produced by Kirk Shung's group were used in tissue harmonic imaging of excised porcine eyes before similar form factor transducers were used in acoustic angiography [90].

In addition, many other authors have demonstrated dual-frequency arrays for combined imaging-therapy applications. Recent devices of interest for imaging have included a three-row array with 128 elements per row for use in prostate cancer imaging and treatment [91], a small-form factor 32-element system for guidance of high-intensity focused ultrasound (HIFU) [92], and a three-row array for thermal strain imaging performing heating at 1.5 MHz and imaging at 5.5 MHz [93]. Smith *et al.* have also demonstrated dual-frequency combined imaging and therapeutic catheter-based devices [94,95]. While a comprehensive review of image guidance in therapeutic ultrasound is beyond the scope of this review, the interested reader is referred to recent reviews on image-guided therapy [96], HIFU [97,98] and thermal strain imaging [99].

Several recent design developments within other applications are of particular interest for imaging microbubble harmonics. Azuma *et al.* have described the design and fabrication of a 0.5/2.0 MHz dual-frequency array for sonothrombolysis and transcranial ultrasound imaging [81]. This paper presented the first dual-frequency array to use a unique design in which the low-frequency array is positioned directly below the high-frequency array within the transducer housing. Low- and high-frequency arrays were isolated by the aforementioned FSIL, an important design achievement. Dual-frequency transducers could also provide distinct advantages over single-frequency transducers in acoustic radiation force impulse (ARFI) imaging, which visualizes mechanical properties of tissue using a low-frequency pushing pulse and high-frequency tracking pulses [100]. Finally, Yen *et al.* have described several dual-layer 2D array transducers capable of performing 3D rectilinear imaging

at 5 and 7.5 MHz at a reduced cost relative to conventional 2D arrays with high channel counts [101,102]. Linear and 2D bilaminar arrays with frequency-selective layers could enable imaging of microbubble harmonics over a large field of view with greater image uniformity than that currently afforded by fixed-focus transducers.

3. Conclusions

Images formed from harmonic content scattered by ultrasound contrast agents have demonstrated increased image quality over fundamental mode images [103–107], making spectral separation of tissue and harmonic signals using dual-frequency transducers an attractive approach. Transducers having wide frequency separation between the transmission and reception bandwidths have allowed for efficient excitation of microbubbles near resonance and reception of broadband, transient harmonics without dependence on multi-pulse strategies. Single-pulse harmonic imaging has enabled higher frame rates and elimination of motion artifacts found in currently-available contrast imaging approaches requiring multiple pulses. Forming images from higher harmonics has also enabled high-resolution imaging with reduced attenuation, as high-frequency echoes are subject to attenuation in only a single direction. New technical developments have demonstrated the potential for dual-layer, dual-frequency arrays for both 2D and 3D imaging.

Acknowledgments

The authors acknowledge financial support from the National Institutes of Health under the grants 1R01EB015508 (XJ), R01EB009066 (PD), R01CA170665 (PD), Department of Defense PC111309 (PD), the Terry Fox Foundation (SF), The Ontario Research Fund (SF), and VisualSonics (SF).

Conflicts of Interest

Authors declare pending patents on dual-frequency transducers and applications detailed in this manuscript, as well as interest in companies (Visualsonics, Inc., Toronto, ON, Canada) and (SonoVol, LLC, Chapel Hill, NC, USA).

References

1. Shung, K.K. *In vitro* experimental results on ultrasonic scattering in biological tissues. In *Ultrasonic Scattering in Biological Tissues*; Shung, K.K., Thieme, G.A., Eds.; CRC Press: Boca Raton, FL, USA, 1992.
2. Gramiak, R.; Shah, P.M. Echocardiography of the aortic root. *Investig. Radiol.* **1968**, *3*, 356–366.
3. Ferrara, K.; Pollard, R.; Borden, M. Ultrasound microbubble contrast agents: Fundamentals and application to gene and drug delivery. *Annu. Rev. Biomed. Eng.* **2007**, *9*, 415–447.
4. Klibanov, A.L. Microbubble contrast agents: Targeted ultrasound imaging and ultrasound-assisted drug-delivery applications. *Investig. Radiol.* **2006**, *41*, 354–362.
5. Ainslie, M.A.; Leighton, T.G. Review of scattering and extinction cross-sections, damping factors, and resonance frequencies of a spherical gas bubble. *J. Acoust. Soc. Am.* **2011**, *130*, 3184–3208.

6. Lauterborn, W. Numerical investigation of nonlinear oscillations of gas bubbles in liquids. *J. Acoust. Soc. Am.* **1976**, *59*, 283–283.
7. Chen, Q.; Zagzebski, J.; Wilson, T.; Stiles, T. Pressure-dependent attenuation in ultrasound contrast agents. *Ultrasound Med. Biol.* **2002**, *28*, 1041–1051.
8. Sboros, V.; MacDonald, C.A.; Pye, S.D.; Moran, C.M.; Gomatam, J.; McDicken, W.N. The dependence of ultrasound contrast agents backscatter on acoustic pressure: Theory *versus* experiment. *Ultrasonics* **2002**, *40*, 579–583.
9. Talu, E.; Hettiarachchi, K.; Zhao, S.; Powell, R.L.; Lee, A.P.; Longo, M.L.; Dayton, P.A. Tailoring the size distribution of ultrasound contrast agents: Possible method for improving sensitivity in molecular imaging. *Mol. Imaging* **2008**, *6*, 384–392.
10. Streeter, J.E.; Gessner, R.; Miles, I.; Dayton, P.A. Improving sensitivity in ultrasound molecular imaging by tailoring contrast agent size distribution: *In vivo* studies. *Mol. Imaging* **2010**, *9*, 87–95.
11. Averkiou, M. Tissue harmonic imaging. In *IEEE International Ultrasonics Symposium*; IEEE: San Juan, PR, USA, 2000; Volume 2, pp. 1563–1572.
12. Christopher, P.T.; Parker, K.J. New approaches to nonlinear diffractive field propagation. *J. Acoust. Soc. Am.* **1991**, *90*, 488–499.
13. Flynn, H.G. Physics of acoustic cavitation in liquids. *Phys. Acoust.* **1964**, *1*, 57–172.
14. De Jong, N.; Cornet, R.; Lancée, C.T. Higher harmonics of vibrating gas-filled microspheres. Part one: Simulations. *Ultrasonics* **1994**, *32*, 447–453.
15. De Jong, N.; Cornet, R.; Lancée, C.T. Higher harmonics of vibrating gas-filled microspheres. Part two: Measurements. *Ultrasonics* **1994**, *32*, 455–459.
16. De Jong, N.; Bouakaz, A.; Frinking, P. Basic acoustic properties of microbubbles. *Echocardiography* **2002**, *19*, 229–240.
17. Simpson, D.H.; Chin, C.T.; Burns, P.N. Pulse inversion doppler: A new method for detecting nonlinear echoes from microbubble contrast agents. *IEEE Trans. Ultrason. Ferroelectr. Freq. Control* **1999**, *46*, 372–382.
18. Brock-Fisher, G.A.; Poland, M.D.; Rafter, P.G. Means for Increasing Sensitivity in Non-Linear Ultrasound Imaging Systems. U.S. Patent 5577505 A, 26 November 1996.
19. Eckersley, R.J.; Chin, C.T.; Burns, P.N. Optimising phase and amplitude modulation schemes for imaging microbubble contrast agents at low acoustic power. *Ultrasound Med. Biol.* **2005**, *31*, 213–219.
20. Haider, B.; Chiao, R.Y. Higher order nonlinear ultrasonic imaging. In Proceedings of the IEEE Ultrasonics Symposium, Caesars Tahoe, NV, USA, 17–20 October 1999; Volume 2, pp. 1527–1531.
21. Phillips, P. Contrast pulse sequences (CPS): Imaging nonlinear microbubbles. In Proceedings of the IEEE Ultrasonics Symposium, Atlanta, GA, USA, 7–10 October 2001; Volume 2, pp. 1739–1745.
22. Phillips, P.; Gardner, P.P.E. Contrast-agent detection and quantification. *Eur. Radiol. Suppl.* **2004**, *14*, P4–P10.
23. Hunt, J.W.; Arditi, M.; Foster, F.S. Ultrasound transducers for pulse-echo medical imaging. *IEEE Trans. Biomed. Eng.* **1983**, *30*, 453–481.

24. Desilets, C.S.; Fraser, J.D.; Kino, G.S. The design of efficient broad-band piezoelectric transducers. *IEEE Trans. Sonics Ultrason.* **1978**, *SU-25*, 115–125.
25. Kino, G.S. *Acoustic Waves: Devices, Imaging, and Analog Signal Processing*; Prentice Hall PTR: Englewood Cliffs, NJ, USA, 1987.
26. McKeighen, R.E. Design guidelines for medical ultrasonic arrays. In *Medical Imaging 1998: Ultrasonic Transducer Engineering*; The International Society for Optical Engineering: San Diego, CA, USA, 1998; Volume 3341, pp. 2–18.
27. Chan, H.L.W.; Unsworth, J.; Bui, T. Mode coupling in modified lead titanate/polymer 1–3 composites. *J. Appl. Phys.* **1989**, doi:10.1063/1.342926.
28. Lerch, R. Simulation of piezoelectric devices by two- and three-dimensional finite elements. *IEEE Trans. Ultrason. Ferroelectr. Freq. Control* **1990**, *37*, 233–247.
29. Safari, A.; Newnham, R.E.; Cross, L.E.; Schulze, W.A. Perforated pzt-polymer composites for piezoelectric transducer applications. *Ferroelectrics* **1982**, *41*, 197–205.
30. Smith, W.A.; Shaulov, A.; Auld, B.A. Tailoring the properties of composite piezoelectric materials for medical ultrasonic transducers. In Proceedings of the IEEE 1985 Ultrasonics Symposium, San Francisco, CA, USA, 16–18 October 1985; pp. 642–647.
31. Smith, W.A. The application of 1–3 piezocomposites in acoustic transducers. In Proceedings of the IEEE 7th International Symposium on the Applications of Ferroelectrics, Urbana-Champaign, IL, USA, 6–8 June 1990; pp. 145–152.
32. Lam, K.H.; Chan, H.L.W. Piezoelectric cement-based 1–3 composites. *Appl. Phys. A* **2005**, *81*, 1451–1454.
33. Cheng, K.C.; Chan, H.L.W.; Choy, C.L.; Yin, Q.; Luo, H.; Yin, J. Single crystal PMN-0.33PT/epoxy 1–3 composites for ultrasonic transducer applications. *IEEE Trans. Ultrason. Ferroelectr. Freq. Control* **2003**, *50*, 1177–1183.
34. Savakus, H.P.; Klicker, K.A.; Newnham, R.E. Pzt-epoxy piezoelectric transducers: A simplified fabrication procedure. *Mater. Res. Bull.* **1981**, *16*, 677–680.
35. Yuan, J.; Rhee, S.; Jiang, X.N. 60 MHz PMN-PT based 1–3 composite transducer for IVUS imaging. In Proceedings of the IEEE International Ultrasonics Symposium, Beijing, China, 2–5 November 2008; pp. 682–685.
36. Jiang, X.; Yuan, J.; Cheng, A.; Snook, K.; Cao, P.; Rehrig, P.; Hackenberger, W.; Lavalelle, G.; Geng, X.; Shrout, T. 5I-1 Microfabrication of piezoelectric composite ultrasound transducers (PC-MUT). In Proceedings of the IEEE International Ultrasonics Symposium, Vancouver, BC, Canada, 2–6 October 2006; pp. 922–925.
37. Foster, F.S.; Mehi, J.; Lukacs, M.; Hirson, D.; White, C.; Chaggares, C.; Needles, A. A new 15–50 MHz array-based micro-ultrasound scanner for preclinical imaging. *Ultrasound Med. Biol.* **2009**, *35*, 1700–1708.
38. Novell, A.; Legros, M.; Felix, N.; Bouakaz, A. Exploitation of capacitive micromachined transducers for nonlinear ultrasound imaging. *IEEE Trans. Ultrason. Ferroelectr. Freq. Control* **2009**, *56*, 2733–2743.
39. Novell, A.; Escoffre, J.M.; Bouakaz, A. Second harmonic and subharmonic for non-linear wideband contrast imaging using a capacitive micromachined ultrasonic transducer array. *Ultrasound Med. Biol.* **2013**, *39*, 1500–1512.

40. Oralkan, O.; Ergun, A.S.; Johnson, J.A.; Karaman, M.; Demirci, U.; Kaviani, K.; Lee, T.H.; Khuri-Yakub, B.T. Capacitive micromachined ultrasonic transducers: Next-generation arrays for acoustic imaging? *IEEE Trans. Ultrason. Ferroelectr. Freq. Control* **2002**, *49*, 1596–1610.
41. Ergun, A.S.; Yaralioglu, G.G.; Khuri-yakub, B.T. Capacitive micromachined ultrasonic transducers: Theory and technology. *J. Aerosp. Eng.* **2003**, *16*, 76–84.
42. Ergun, A.S.; Huang, Y.; Member, S. Capacitive micromachined ultrasonic transducers: Fabrication technology. *IEEE Trans. Ultrason. Ferroelectr. Freq. Control* **2005**, *52*, 2242–2258.
43. Novell, A.; Legros, M.; Grégoire, J.M.; Dayton, P.A.; Bouakaz, A. Evaluation of bias voltage modulation sequence for nonlinear contrast agent imaging using a capacitive micromachined ultrasonic transducer array. *Phys. Med. Biol.* **2014**, *59*, 4879–4896.
44. Frijlink, M.E.; Lovstakken, L.; Torp, H. Investigation of transmit and receive performance at the fundamental and third harmonic resonance frequency of a medical ultrasound transducer. *Ultrasonics* **2009**, *49*, 601–604.
45. Hackenberger, W.; Jiang, X.; Rehrig, P.; Xuecang, G.; Winder, A.; Forsberg, F. Broad band single crystal transducer for contrast agent harmonic imaging. In Proceedings of the 2003 IEEE International Ultrasonics Symposium, Honolulu, HI, USA, 5–8 October 2003; Volume 1, pp. 778–781.
46. Bouakaz, A.; Frigstad, S.; Ten Cate, F.J.; de Jong, N. Super harmonic imaging: A new imaging technique for improved contrast detection. *Ultrasound Med. Biol.* **2002**, *28*, 59–68.
47. Bouakaz, A.; Krenning, B.J.; Vletter, W.B.; ten Cate, F.J.; de Jong, N. Contrast superharmonic imaging: A feasibility study. *Ultrasound Med. Biol.* **2003**, *29*, 547–553.
48. Bouakaz, A.; Cate, F.; de Jong, N. A new ultrasonic transducer for improved contrast nonlinear imaging. *Phys. Med. Biol.* **2004**, *49*, 3515–3525.
49. Kruse, D.E.; Ferrara, K.W. A new imaging strategy using wideband transient response of ultrasound contrast agents. *IEEE Trans. Ultrason. Ferroelectr. Freq. Control* **2005**, *52*, 1320–1329.
50. Stephens, D.N.; Lu, X.M.; Proulx, T.; Walters, W.; Dayton, P.; Tartis, M.; Kruse, D.E.; Lum, A.F.H.; Kitano, T.; Stieger, S.M.; *et al.* Multi-frequency array development for drug delivery therapies: Characterization and first use of a triple row ultrasound probe. In Proceedings of the IEEE International Ultrasonics Symposium, Vancouver, BC, Canada, 2–6 October 2006; pp. 66–69.
51. Zheng, H.; Kruse, D.E.; Stephens, D.N.; Ferrara, K.; Sutcliffe, P.; Gardner, E. A sensitive ultrasonic imaging method for targeted contrast microbubble detection. In Proceedings of the 30th Annual International IEEE EMBS Conference, Vancouver, BC, Canada, 20–25 August 2008; pp. 5290–5293.
52. Hu, X.; Zheng, H.; Kruse, D.E.; Sutcliffe, P.; Stephens, D.N.; Ferrara, K.W. A sensitive TLRH targeted imaging technique for ultrasonic molecular imaging. *IEEE Trans. Ultrason. Ferroelectr. Freq. Control* **2010**, *57*, 305–316.
53. Hu, X.; Caskey, C.F.; Mahakian, L.M.; Kruse, D.E.; Beegle, J.R.; Decleves, A.E.; Rychak, J.J.; Sutcliffe, P.L.; Sharma, K.; Ferrara, K.W. *In vivo* validation and 3d visualization of broadband ultrasound molecular imaging. *Am. J. Nucl. Med. Mol. Imaging* **2013**, *3*, 336–349.

54. Stephens, D.N.; Kruse, D.E.; Ergun, A.S.; Barnes, S.; Lu, X.M.; Ferrara, K.W. Efficient array design for sonotherapy. *Phys. Med. Biol.* **2008**, *53*, 3943–3969.
55. Kruse, D.E.; Lai, C.Y.; Stephens, D.N.; Sutcliffe, P.; Paoli, E.E.; Barnes, S.H.; Ferrara, K.W. Spatial and temporal-controlled tissue heating on a modified clinical ultrasound scanner for generating mild hyperthermia in tumors. *IEEE Trans. Biomed. Eng.* **2010**, *57*, 155–166.
56. Ferin, G.; Legros, M.; Felix, N.; Notard, C.; Ratsimandresey, L. Ultra-wide bandwidth array for new imaging modalities. In Proceedings of the IEEE International Ultrasonics Symposium, New York, NY, USA, 28–31 October 2007; pp. 204–207.
57. Van Neer, P.L.M.J.; Matte, G.M.; Danilouchkine, M.G.; Verweij, M.D.; de Jong, N. A study of phased array transducer topology for superharmonic imaging. In Proceedings of the IEEE International Ultrasonics Symposium, San Diego, CA, USA, 11–14 October 2010; pp. 1222–1223.
58. Van Neer, P.L.; Matte, G.; Danilouchkine, M.G.; Prins, C.; van den Adel, F.; de Jong, N. Super-harmonic imaging: Development of an interleaved phased-array transducer. *IEEE Trans. Ultrason. Ferroelectr. Freq. Control.* **2010**, *57*, 455–468.
59. Shung, K.K. High frequency ultrasonic imaging. *J. Med. Ultrasound* **2009**, *17*, 25–30.
60. Zhao, J.-Z.; Alves, C.H.F.; Snook, K.A.; Cannata, J.A.; Chen, W.-H.; Meyer, R.J.; Ayyappan, S.; Ritter, T.A.; Shung, K.K. Performance of 50 MHz transducers incorporating fiber composite, PVDF, $PbTiO_3$, and $LiNbO_3$. In Proceedings of the IEEE International Ultrasonics Symposium, Caesars Tahoe, NV, USA, 17–20 October 1999; Volume 2, pp. 1185–1190.
61. Lous, G.M.; Cornejo, I.A.; McNulty, T.F.; Safari, A.; Danforth, S.A. Fabrication of curved ceramic/polymer composite transducer for ultrasonic imaging applications by fused deposition of ceramics. In Proceedings of the IEEE International Symposium on the Applications of Ferroelectrics, Montreaux, Switzerland, 24–27 August 1998; pp. 239–242.
62. Brown, J.A.; Foster, E.S.; Needles, A.; Cherin, E.; Lockwood, G.R. Fabrication and performance of a 40-MHz linear array based on a 1–3 composite with geometric elevation focusing. *IEEE Trans. Ultrason. Ferroelectr. Freq. Control* **2007**, *54*, 1888–1894.
63. Brown, J.A.; Cherin, E.; Jianhua, Y.; Foster, F.S. Fabrication and performance of high-frequency composite transducers with triangular-pillar geometry. *IEEE Trans. Ultrason. Ferroelectr. Freq. Control* **2009**, *56*, 827–836.
64. Lukacs, M.; Lee, M.; Cherin, E.; Yin, J.; Hirson, D.; Foster, F.S.; Gessner, R.; Dayton, P. Hybrid dual frequency transducer and scanhead for micro-ultrasound imaging. In Proceedings of the 2009 IEEE International Ultrasonics Symposium, Rome, Italy, 20–23 September 2009; pp. 1000–1003.
65. Gessner, R.; Lukacs, M.; Lee, M.; Cherin, E.; Foster, F.S.; Dayton, P.A. High-resolution, high-contrast ultrasound imaging using a prototype dual-frequency transducer: *In vitro* and *in vivo* studies. *IEEE Trans. Ultrason. Ferroelectr. Freq. Control* **2010**, *57*, 1772–1781.
66. Lindsey, B.D.; Rojas, J.D.; Shelton, S.E.; Martin, K.H.; Dayton, P.A. Acoustic characterization of contrast-to-tissue ratio and axial resolution for dual-frequency contrast-specific "acoustic angiography" imaging. *IEEE Trans. Ultrason. Ferroelectr. Freq. Control* **2014**, *61*, in press.
67. Gessner, R.C.; Aylward, S.R.; Dayton, P.A. Mapping microvasculature with acoustic angiography yields quantifiable differences between healthy and tumor-bearing tissue volumes in a rodent model. *Radiology* **2012**, *264*, 733–740.

68. Gessner, R.C.; Frederick, C.B.; Foster, F.S.; Dayton, P.A. Acoustic angiography: A new imaging modality for assessing microvasculature architecture. *Int. J. Biomed. Imaging* **2013**, doi:10.1155/2013/936593.
69. Shelton, S.E.; Lee, Y.Z.; Foster, F.S.; Lee, M.; Aylward, S.R.; Dayton, P.A. Quantification of microvascular tortuosity during tumor evolution utilizing acoustic angiography. Submitted for publication, 2014.
70. Guiroy, A.; Novell, A.; Ringgaard, E.; Lou-Moeller, R.; Gregoire, J.M.; Abellard, A.P.; Zawada, T.; Bouakaz, A.; Levassort, F. Dual-frequency transducer for nonlinear contrast agent imaging. *IEEE Trans. Ultrason. Ferroelectr. Freq. Control* **2013**, *60*, 2634–2644.
71. Li, S.; Huang, W.; Jiang, X.; Jian, X.; Cui, Y. A dual-layer micromachined PMN-PT 1–3 composite transducer for broadband ultrasound imaging. In Proceedings of the 2013 IEEE International Ultrasonics Symposium, Prague, Czech, 21–25 July 2013; Volume 10, pp. 781–784.
72. Shung, K.K.; Cannata, J.M.; Zhou, Q.F. Piezoelectric materials for high frequency medical imaging applications: A review. *J. Electroceram.* **2007**, *19*, 141–147.
73. Nissen, S.E.; Yock, P. Intravascular ultrasound: Novel pathophysiological insights and current clinical applications. *Circulation* **2001**, *103*, 604–616.
74. Kwon, H.M.; Sangiorgi, G.; Ritman, E.L.; Lerman, A.; McKenna, C.; Virmani, R.; Edwards, W.D.; Holmes, D.R.; Schwartz, R.S. Adventitial vasa vasorum in balloon-injured coronary arteries: Visualization and quantitation by a microscopic three-dimensional computed tomography technique. *J. Am. Coll. Cardiol.* **1998**, *32*, 2072–2079.
75. Naghavi, M.; Libby, P.; Falk, E.; Casscells, S.W.; Litovsky, S.; Rumberger, J.; Badimon, J.J.; Stefanadis, C.; Moreno, P.; Pasterkamp, G.; *et al.* From vulnerable plaque to vulnerable patient: A call for new definitions and risk assessment strategies: Part i. *Circulation* **2003**, *108*, 1664–1672.
76. Vos, H.J.; Frijlink, M.E.; Droog, E.; Goertz, D.E.; Blacquière, G.; Gisolf, A.; de Jong, N.; van der Steen, A.F.W. Transducer for harmonic intravascular ultrasound imaging. *IEEE Trans. Ultrason. Ferroelectr. Freq. Control* **2005**, *52*, 2418–2422.
77. Vos, H.J.; Frijlink, M.E.; Droog, E.; Goertz, D.E.; Blacquiere, G.; Gisolf, A.; de Jong, N.; van der Steen, A.F.W. A 20–40 MHz ultrasound transducer for intravascular harmonic imaging. In Proceedings of the 2004 IEEE International Ultrasonics Symposium, Montreal, QC, Canada, 23–27 August 2004; Volume 3, pp. 1966–1969.
78. Frijlink, M.E.; Goertz, D.E.; van Damme, L.C.A.; Krams, R.; van der Steen, A.F.W. Intravascular ultrasound tissue harmonic imaging *in vivo*. *IEEE Trans. Ultrason. Ferroelectr. Freq. Control* **2006**, *53*, 1844–1852.
79. Goertz, D.E.; Frijlink, M.E.; Tempel, D.; van Damme, L.C.; Krams, R.; Schaar, J.A.; ten Cate, F.J.; Serruys, P.W.; de Jong, N.; van der Steen, A.F. Contrast harmonic intravascular ultrasound: A feasibility study for vasa vasorum imaging. *Investig. Radiol.* **2006**, *41*, 631–638.
80. Ma, J.; Martin, K.; Dayton, P.A.; Jiang, X. A preliminary engineering design of intravascular dual-frequency transducers for contrast-enhanced acoustic angiography and molecular imaging. *IEEE Trans. Ultrason. Ferroelectr. Freq. Control* **2014**, *61*, 870–880.
81. Azuma, T.; Ogihara, M.; Kubota, J.; Sasaki, A.; Umemura, S.; Furuhata, H. Dual-frequency ultrasound imaging and therapeutic bilaminar array using frequency selective isolation layer. *IEEE Trans. Ultrason. Ferroelectr. Freq. Control* **2010**, *57*, 1211–1224.

82. Von Ramm, O.T.; Smith, S.W. A multiple frequency array for improved diagnostic imaging. *IEEE Trans. Sonics Ultrason.* **1978**, *25*, 340–345.
83. Bui, T.; Chan, H.L.W.; Unsworth, J. A multifrequency composite ultrasonic transducer system. In Proceedings of the IEEE International Ultrasonics Symposium, Chicago, IL, USA, 2–5 October 1988; Volume 2, pp. 627–630.
84. De Fraguier, S.; Gelly, J.F.; Wolnerman, L.; Lannuzel, O. Novel acoustic design for dual frequency transducers resulting in separate bandpass for color flow mapping. In Proceedings of the IEEE International Ultrasonics Symposium, Honolulu, HI, USA, 4–7 December 1990; Volume 2, pp. 799–803.
85. Saitoh, S.; Izumi, M.; Mine, Y. A dual-frequency ultrasonic probe for medical applications. *IEEE Trans. Ultrason. Ferroelectr. Freq. Control* **1995**, *42*, 294–300.
86. Hossack, J.A.; Mauchamp, P.; Ratsimandresy, L. A high bandwidth transducer optimized for harmonic imaging. In Proceedings of the 2000 IEEE International Ultrasonics Symposium, San Juan, Puerto Rico, 22–25 October 2000; Volume 2, pp. 1021–1024.
87. Hossack, J.A.; Auld, B.A. Improving the characteristics of a transducer using multiple piezoelectric layers. *IEEE Trans. Ultrason. Ferroelectr. Freq. Control* **1993**, *40*, 131–139.
88. Gururaja, T.R.; Shurland, A.; Chen, J. Medical ultrasonic transducers with switchable frequency bands centered about f_0 and $2f_0$. In Proceedings of the IEEE International Ultrasonics Symposium, Toronto, ON, Canada, 5–8 October 1997; Volume 2, pp. 1659–1662.
89. Takeuchi, S.; Al Zaabi, M.R.A.; Sato, T.; Kawashima, N. Development of ultrasound transducer with double-peak-type frequency characteristics for harmonic imaging and subharmonic imaging. *Jpn. J. Appl. Phys.* **2002**, *41*, 3619–3623.
90. Kim, H.H.; Cannata, J.M.; Liu, R.; Chang, J.H.; Silverman, R.H.; Shung, K.K. 20 MHz/40 MHz dual element transducers for high frequency harmonic imaging. *IEEE Trans. Ultrason. Ferroelectr. Freq. Control* **2008**, *55*, 2683–2691.
91. Jeong, J.S.; Chang, J.H.; Shung, K.K. Ultrasound transducer and system for real-time simultaneous therapy and diagnosis for noninvasive surgery of prostate tissue. *IEEE Trans. Ultrason. Ferroelectr. Freq. Control* **2009**, *56*, 1913–1922.
92. Casper, A.J.; Liu, D.; Ballard, J.R.; Ebbini, E.S. Real-time implementation of a dual-mode ultrasound array system: *In vivo* results. *IEEE Trans. Biomed. Eng.* **2013**, *60*, 2751–2759.
93. Lai, C.Y.; Kruse, D.E.; Caskey, C.F.; Stephens, D.N.; Sutcliffe, P.L.; Ferrara, K.W. Noninvasive thermometry assisted by a dual-function ultrasound transducer for mild hyperthermia. *IEEE Trans. Ultrason. Ferroelectr. Freq. Control* **2010**, *57*, 2671–2684.
94. Herickhoff, C.D.; Light, E.D.; Bing, K.F.; Mukundan, S.; Grant, G.A.; Wolf, P.D.; Smith, S.W. Dual-mode intracranial catheter integrating 3d ultrasound imaging and hyperthermia for neuro-oncology: Feasibility study. *Ultrason. Imaging* **2009**, *31*, 81–100.
95. Herickhoff, C.D.; Wilson, C.M.; Grant, G.A.; Britz, G.W.; Light, E.D.; Palmeri, M.L.; Wolf, P.D.; Smith, S.W. Dual-mode ivus transducer for image-guided brain therapy: Preliminary experiments. *Ultrasound Med. Biol.* **2011**, *37*, 1667–1676.
96. Martin, K.H.; Dayton, P.A. Current status and prospects for microbubbles in ultrasound theranostics. *Wiley Interdiscip. Rev. Nanomed. Nanobiotechnol.* **2013**, *5*, 329–345.

97. Kennedy, J.E. High-intensity focused ultrasound in the treatment of solid tumours. *Nat. Rev. Cancer* **2005**, *5*, 321–327.
98. Ter Haar, G.; Coussios, C. High intensity focused ultrasound: Physical principles and devices. *Int. J. Hyperth.* **2007**, *23*, 89–104.
99. Seo, C.H.; Shi, Y.; Huang, S.W.; Kim, K.; O'Donnell, M. Thermal strain imaging: A review. *Interface Focus* **2011**, *1*, 649–664.
100. Shih, C.-C.; Huang, C.-C.; Zhou, Q.; Shung, K.K. High-resolution acoustic-radiation-force-impulse imaging for assessing corneal sclerosis. *IEEE Trans. Med. Imaging* **2013**, *32*, 1316–1324.
101. Chen, Y.; Nguyen, M.; Yen, J.T. 7.5 MHz dual-layer transducer array for 3-d rectilinear imaging. *Ultrason. Imaging* **2011**, *33*, 205–216.
102. Yen, J.T.; Seo, C.H.; Awad, S.I.; Jeong, J.S. A dual-layer transducer array for 3-d rectilinear imaging. *IEEE Trans. Ultrason. Ferroelectr. Freq. Control* **2009**, *56*, 204–212.
103. Basude, R.; Wheatley, M.A. Generation of ultraharmonics in surfactant based ultrasound contrast agents: Use and advantages. *Ultrasonics* **2001**, *39*, 437–444.
104. Shi, W.T.; Forsberg, F.; Hall, A.L.; Chiao, R.Y.; Liu, J.-B.; Miller, S.; Thomenius, K.E.; Wheatley, M.A.; Goldberg, B.B. Subharmonic imaging with microbubble contrast agents: Initial results. *Ultrason. Imaging* **1999**, *21*, 79–94.
105. Schrope, B.A.; Newhouse, V.L. Second harmonic ultrasonic blood perfusion measurement. *Ultrasound Med. Biol.* **1993**, *19*, 567–579.
106. Chang, P.H.; Shun, K.K.; Wu, S.-J.; Levene, H.B. Second harmonic imaging and harmonic doppler measurements with albunex. *IEEE Trans. Ultrason. Ferroelectr. Freq. Control* **1995**, *42*, 1020–1027.
107. Goertz, D.E.; Cherin, E.; Needles, A.; Karshafian, R.; Brown, A.S.; Burns, P.N.; Foster, F.S. High frequency nonlinear b-scan imaging of microbubble contrast agents. *IEEE Trans. Ultrason. Ferroelectr. Freq. Control* **2005**, *52*, 65–79.

A Dual-frequency Co-Linear Array for Prostate Acoustic Angiography

Sibo Li[1], Jinwook Kim[1],
Zhuochen Wang[1], Xiaoning Jiang[1,3]
[1]Department of Mechanical and Aerospace Engineering
North Carolina State Univ., Raleigh, NC, 27606, USA
[3]Department of Mechanical and Biomedical Engineering,
City Univ. of Hong Kong, Hong Kong 999077, China
xjiang5@ncsu.edu

Sunny Kasoji[2], Brooks Lindsey[2], Paul A. Dayton[2]
[2]Joint Department of Biomedical Engineering
University of North Carolina and NC State University
Chapel Hill, NC, 27599, USA
padayton@email.unc.edu

***Abstract*—Approximately 80% of men who reach 80-years of age will have some form of prostate cancer. The challenge remains to differentiate indolent from aggressive disease. Based on recent research, acoustic angiography, a novel contrast enhanced ultrasound imaging technique, can provide high-resolution visualization of tissue microvasculature and has demonstrated the ability to differentiate vascular characteristics between healthy and tumor tissue. We hypothesize that transrectal acoustic angiography may enhance assessment of prostate cancer. In this paper, we describe the development of a dual layer co-linear array ultrasound transducer for transrectal acoustic angiography. The KLM model and Field II were used for the element design and acoustic field simulation, respectively. The probe consists of 64 transmit elements with a center frequency of 3 MHz and 128 receive elements with a center frequency of 15 MHz. The dimensions of the array are 18 mm in azimuth and 8 mm in elevation. The pitch is 280 μm for transmitting (TX) elements and 140 μm for receiving (RX) elements. Pulse-echo test of TX/RX elements were conducted and compared with the simulation results. Real-time contrast imaging was tested using a Verasonics system. Non-linear responses from microbubble contrast agents at a depth of 18 mm were clearly observed. The axial beam width (-6 dB) and CTR were calculated from the measured signals to be 400 μm and 20 dB, respectively. These results suggest that the prototype co-linear array is capable of performing dual-frequency superharmonic imaging of microbubbles for prostate cancer assessment.**

Keywords—acoustic angiography; dual frequency; ultrasound contrast agent; transrectal ultrasound; prostate cancer

I. INTRODUCTION

Prostate cancer is the most common non-skin cancer and the second leading cause of cancer-related death in men in the United States; however, it still lacks a definitive, non-invasive diagnostic test [1]. Routine diagnostic tests, such as prostate-specific antigen level measurements and manual digital rectal examination are limited by poor sensitivity and high-false positive rates [2]. Core biopsies are painful, increase risk of hemorrhage, and provide little confidence that clinically-relevant regions are sampled. Traditionally, transrectal ultrasound (TRUS) has played a substantial role in the diagnosis of prostate cancer due to its ability to provide real-time imaging and biopsy guidance [3]. While TRUS is commonly used for biopsy guidance, B-mode ultrasound exhibits low sensitivity for locating cancerous regions for biopsy[4].

Recent research has indicated that contrast-enhanced ultrasound (CEUS) may potentially provide more accurate prostate cancer assessment [4-6]. Compared to conventional ultrasound, a contrast-enhanced approach can provide estimation of microvascular perfusion. Recently, our group has investigated an alternative approach to contrast-enhanced ultrasound imaging which relies on the superharmonic echoes produced by microbubble contrast agents, "acoustic angiography" [7]. Studies on contrast-enhanced dual-frequency ultrasound imaging indicate that microbubbles can be excited in the 2-4 MHz range and the superharmonic echoes from microbubbles can be detected at frequencies above 15 MHz, producing images having high contrast-to-tissue ratio (CTR) and high-resolution [8]. These images reveal unique information on tumor microvessel structure [7]. Because increased microvessel density is associated with progression of tumor growth [9], the ability to image the microvasculature enhances the accuracy during the biopsy evaluation.

The primary challenge to implementing this imaging technique is presented by transducer design and fabrication. In superharmonic imaging, separation of transmission and receiving bandwidths is required to ensure high contrast-to-tissue ratio, and thus the conventional transducer arrays with single center frequencies are not suitable. Compared with the mechanical scanning technique used with previous single-element systems for superharmonic imaging [7], dual-frequency imaging with an array provides increased frame rate, increased depth of field, more precise control over the acoustic pressure field, and also provides opportunities for different imaging modalities [10].

To extend our previous work with single-element, dual-frequency transducers [5, 11, 12] and a 3MHz/18MHz sub-aperture array [13], a 3 MHz/15 MHz ultrasound array was developed for transrectal dual-frequency acoustic angiography imaging. An array with 64 transmit and 128 receive elements was designed, fabricated and characterized. Pulse-echo tests were conducted for both low and high frequency elements. The transmitting array was also evaluated by measuring the acoustic pressure profile of a single element with a hydrophone. The array transducer's ability to perform superharmonic imaging was tested by exciting microbubbles flowing through a micro-cellulose tube using the 3 MHz transmitting array and detecting the super harmonic responses from microbubbles using the 15 MHz receiving array. Finally, contrast imaging was performed with a multi-channel imaging system in a tissue-mimicking phantom.

978-1-4673-9897-8/16/$31.00 ©2016 IEEE

II. Materials and Methods

A. Transducer Design and Fabrication

In transducer array design, the number of active elements is limited by the imaging system electronics, thus the element pitch and total aperture size were designed comprehensively. The prostate is located within 1 cm of the rectum, and is approximately ~30 mm in longitudinal dimension and ~25 mm in transverse dimension [14]. In order to meet these considerations, KLM model simulations were used to determine the geometry of the low and high frequency arrays. Field II was used to assess a series of designs with varying parameters, and a design with 19 low frequency elements in each transmit event (active sub-aperture of 5 mm in the azimuth direction) was ultimately adopted [15, 16]. The details of this configuration are summarized in Table 1.

Table 1 Design parameters of the co-linear array

Property	Value	
Aperture	8 mm by 18 mm	
Working mode	Transmitting (3 MHz)	Receiving (15 MHz)
Pitch	280 μm (0.5 λ)	140 μm (1.33 λ)
Element number	64	128

Because the TX and RX elements need to be physically separated while also having overlapping foci, the array transducer was designed using a stacked configuration (Figure 1). The RX and TX arrays were coupled with isolation layers (nickel and alumina/epoxy), which also served as common ground. To improve the transmission sensitivity, air backing was used for the low frequency array.

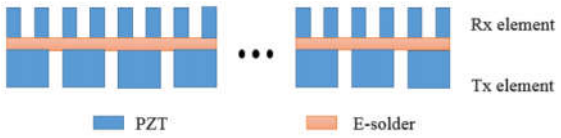

Figure 1 Schematic of array transducer

PZT ceramic (CTS 3203HD, CTS Corporation, Elkhart, Indiana, USA) and 2-2 composites were selected as the TX and RX material respectively. Due to the selected element pitch and aperture design, the piezoelectric layers were operated in sliver mode for the low frequency (TX) elements and in sliver composites mode for the high frequency (RX) elements. To minimize interference between TX and RX elements, a λ/4 layer (in 15 MHz) of E-solder was added [17]. The apertures and matching layers for both TX and RX, as well as the isolation layers were designed using the Krimholtz-Leedom-Matthaei (KLM) model [18]. Material properties of each constitutive component are summarized in Table 2.

A prototype of the dual-frequency array was then fabricated. First, a PZT plate with thickness of 500 μm (for low frequency TX) was cleaned and deposited with Ti/Au on both sides. The top electrode was then attached with a layer of conductive epoxy (E-solder 3022, Von Roll Isola, Inc. New Haven, CT), which was cured at room temperature for 24 hours. After curing, E-solder layer was carefully lapped to 30 μm thick, the RX material, 2-2 composites, was bonded to the TX layer using Epo-Tek 301 (Epoxy Technologies, Billerica, MA), and then lapped to the thickness of 100 μm for 15 MHZ resonance. Finally, the conductive layer, Ti/Au, was sputtered to the top receiving layer. The flex circuits for TX and RX were then bonded to both sides of the stack. After the epoxy was fully cured, the dicing process was performed according to the pitch design. Finally, the array was interconnected with a printed circuit board for further testing.

Table 2 Material properties of each component of the array

Materials	composition	Properties	
PZT	TX	Impedance Longitudinal Velocity Density	30 MRayl 3850 m/s 7700 kg/m^3
PZT 2-2 composites	RX	Impedance Longitudinal Velocity Density	20 MRayl 3800 m/s 5500kg/m^3
E-Solder 3022	Isolation layer	Impedance Longitudinal Velocity Density	5.5 MRayl 2110 m/s 2590 kg/m^3

B. Transducer Characterization

The electrical impedance magnitude and phase spectra for each TX and RX element were measured (HP 4194, Palo Alto, CA). For this test, the array was placed in a water tank, and the electrical impedance and phase spectra were measured. The element capacitance and dielectric loss at 1 KHz were characterized as well. Next, pulse-echo testing was conducted to measure sensitivity, center frequency, and bandwidth for each element. A Panametrics 5077PR and a 5900PR pulser/receiver (Panametrics, Inc., Waltham, MA) were used for the TX and RX pulse excitations, respectively. The array was positioned in a degassed/deionized water bath in front of a polished stainless steel plate reflector. The echo response was observed and recorded on an oscilloscope (DSO7104B, Agilent Technologies Inc., Santa Clara, CA). The fast Fourier transform (FFT) function on the oscilloscope was used to determine the frequency response of the acquired RF data. Low frequency elements were excited with 100V, and high frequency elements were excited separately with 1 μJ.

For dual-frequency imaging, the sensitivity of TX elements is important. The transmission pressure of TX elements was measured using a calibrated hydrophone (Onda HNA-0400, Onda Co., Sunnyvale, CA, USA) while focusing the array at a depth of 35 mm. The peak negative pressure was measured to determine the transmission sensitivity.

C. Contrast Imaging

Contrast imaging with the array transducer was conducted in a tissue-mimicking phantom. A 200 μm-diameter cellulose tube with flowing microbubbles (10^8 units/mL) was positioned 30 mm away from the ultrasound probe in the phantom. A multi-channel research imaging system (Verasonics Vantage, Kirkland, WA) was used to drive the array and acquire echoes. For this work, 19 TX elements were fired in each group, and the single RX element at the center of the sub-aperture captured the high frequency superharmonic echoes. Each low

frequency TX element was excited with a one-cycle, 35 V pulse. High frequency echoes were filtered with a bandpass filter (9-27 MHz) and time-gain compensation was applied.

III. Results and Discussion

A co-linear array prototype was fabricated to evaluate the performance for super-harmonic imaging (Figure 2). The active aperture was 8 mm by 18 mm. The total thickness (including flex circuit) was approximately 1 mm.

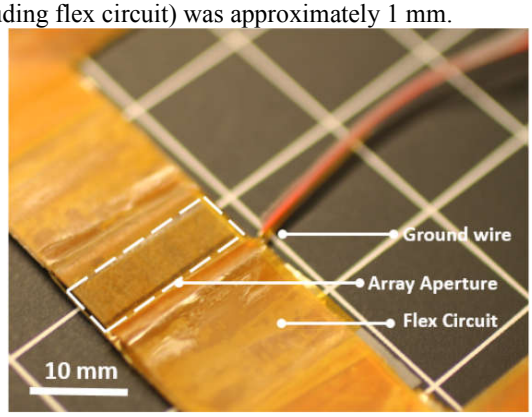

Figure 2 Photograph of the co-linear array

Based on the pulse/echo tests for all of the individual elements (Figure 3), the TX element exhibited a mean center frequency of 3.4±0.2MHz and -6 dB bandwidth of 45±5%, and the RX elements showed a mean center frequency of 14.8 ±0.4 MHz and -6 dB bandwidth of 40±8%. The measured results corresponded well with the KLM model simulation.

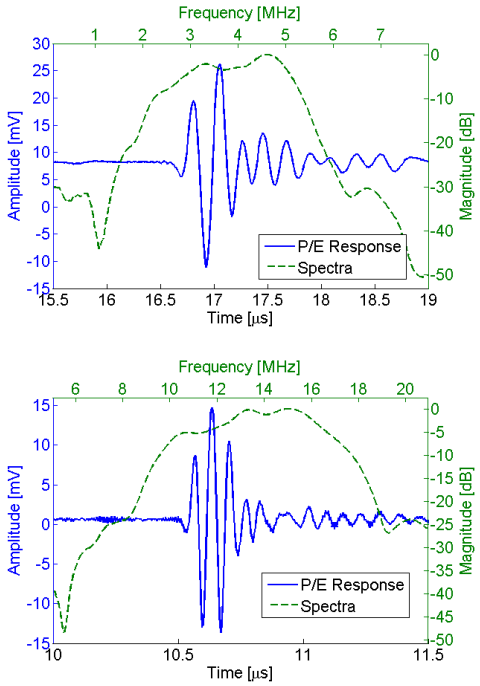

Figure 3. Pulse/echo test of typical TX (top) and RX (bottom) element and their FFT spectra

We characterized singular TX elements with the hydrophone test and measured a transmission sensitivity of 8 kPa/V (peak negative pressure). After correcting for attenuation in water and diffraction in the azimuth direction, an insertion loss of -30 dB was estimated. Crosstalk measurements indicated satisfactory but not ideal element-to-element isolation. The crosstalk near the center frequency of the array was measured to be 32 dB for TX elements and 28 dB for RX elements between adjacent elements. The second adjacent element showed ~35 and ~30 dB crosstalk for TX and RX elements, respectively. This crosstalk arises from the uncut isolation layers: because both TX and RX elements were interconnected at the middle common ground, acoustic surface and bulk waves could travel underneath. The results of individual element testing for the completed array are summarized in Table 3.

Table 3 Measured properties for the collinear array

Property	Value	
Aperture	8 mm by 18 mm	
Working mode	Transmitting (3 MHz)	Receiving (15 MHz)
Pitch size	280 μm (0.5 λ)	140 μm (1.33 λ)
Element number	64	128
Center frequency	3.4 MHz	14.8 MHz
-6 dB fractional bandwidth	36%	45%
Pulse width (-20 dB)	2.7 μs	0.3 μs
Capacitance@1 kHz	149±12pF	183± 36 pf
loss@1 kHz	52±9 mU	116±38 mU

The phantom image (Figure 4) shows that the co-linear array was able to capture the microbubble signal flowing in the cellulose tube. By analyzing the echo beam, the width in the axial and lateral dimensions were measured to be 400 μm and 200 μm, respectively. The contrast to tissue ratio was calculated to be ~20 dB.

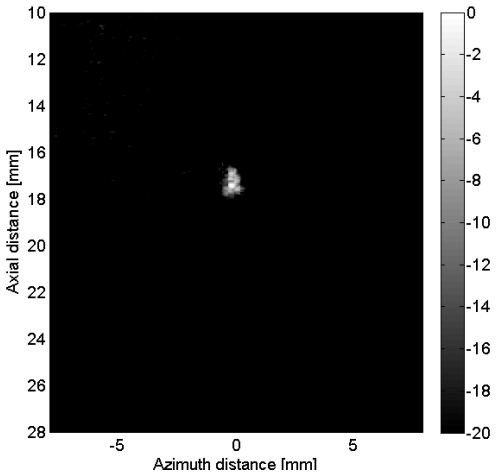

Figure 4 Superharmonic image of a cellulose tube filled with microbubbles in the tissue-mimic phantom.

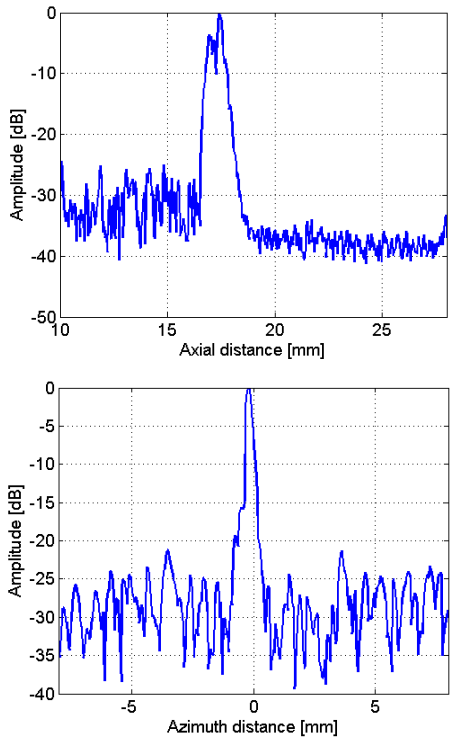

Figure 5 The target width in axial (middle) and azimuth (right) direction.

IV. CONCLUSION

In this work, we developed a co-linear, dual-frequency (3/15 MHz) transducer for demonstrating the feasibility of transrectal acoustic angiography. The acoustic characterization results indicate that our design concept and technique can achieve fractional bandwidths and transmission/receiving sensitivities which are sufficient for superharmonic microbubble imaging. We also used a multi-channel imaging system to demonstrate that the array was capable of inducing a higher harmonic response from microbubble contrast agents at a depth of 30 mm. With a 1-cycle burst excitation, the target widths in axial and lateral directions were 200 μm and 400 μm, respectively, and CTR was ~20 dB. These results indicate that the co-linear array can be used for acoustic angiography imaging for prostate tumor characterization and identification of regions of neovascularization for guidance of prostate biopsies.

ACKNOWLEDGMENT

The authors would like to acknowledge the financial support from U.S. Army Medical Research and Materiel Command under the grant PC111309. The authors would like to thank Jianguo Ma, Anthony Novell, K. Heath Martin and Wei-Yi Chang for providing instruction and assistance in transducer design, microbubble detection tests, and manuscript preparation.

REFERENCES

[1] R. Siegel, J. Ma, Z. Zou, and A. Jemal, "Cancer statistics, 2014," *CA: a cancer journal for clinicians,* vol. 64, pp. 9-29, 2014.

[2] W. Catalona, J. Richie, F. Ahmann, M. Hudson, P. Scardino, R. Flanigan, *et al.*, "Comparison of digital rectal examination and serum prostate specific antigen in the early detection of prostate cancer: results of a multicenter clinical trial of 6,630 men," *The Journal of urology,* vol. 151, pp. 1283-1290, 1994.

[3] M. A. Levine, M. Ittman, J. Melamed, and H. Lepor, "Two consecutive sets of transrectal ultrasound guided sextant biopsies of the prostate for the detection of prostate cancer," *The Journal of urology,* vol. 159, pp. 471-476, 1998.

[4] M. Wink, F. Frauscher, D. Cosgrove, J.-Y. Chapelon, L. Palwein, M. Mitterberger, *et al.*, "Contrast-enhanced ultrasound and prostate cancer; a multicentre European research coordination project," *European urology,* vol. 54, pp. 982-993, 2008.

[5] J. Kim, S. Li, S. Kasoji, P. A. Dayton, and X. Jiang, "Phantom evaluation of stacked-type dual-frequency 1–3 composite transducers: A feasibility study on intracavitary acoustic angiography," *Ultrasonics,* vol. 63, pp. 7-15, 2015.

[6] K. H. Martin, B. D. Lindsey, J. Ma, M. Lee, S. Li, F. S. Foster, *et al.*, "Dual-frequency piezoelectric transducers for contrast enhanced ultrasound imaging," *Sensors,* vol. 14, pp. 20825-20842, 2014.

[7] R. C. Gessner, C. B. Frederick, F. S. Foster, and P. A. Dayton, "Acoustic angiography: a new imaging modality for assessing microvasculature architecture," *Journal of Biomedical Imaging,* vol. 2013, p. 14, 2013.

[8] B. D. Lindsey, J. D. Rojas, K. Heath Martin, S. E. Shelton, and P. Dayton, "Acoustic characterization of contrast-to-tissue ratio and axial resolution for dual-frequency contrast-specific acoustic angiography imaging," *Ultrasonics, Ferroelectrics, and Frequency Control, IEEE Transactions on,* vol. 61, pp. 1668-1687, 2014.

[9] M. Borre, B. V. Offersen, B. Nerstrøm, and J. Overgaard, "Microvessel density predicts survival in prostate cancer patients subjected to watchful waiting," *British journal of cancer,* vol. 78, p. 940, 1998.

[10] T. Ritter, T. R. Shrout, R. Tutwiler, and K. K. Shung, "A 30-MHz piezo-composite ultrasound array for medical imaging applications," *Ultrasonics, Ferroelectrics, and Frequency Control, IEEE Transactions on,* vol. 49, pp. 217-230, 2002.

[11] J. Ma, K. H. Martin, Y. Li, P. A. Dayton, K. K. Shung, Q. Zhou, *et al.*, "Design factors of intravascular dual frequency transducers for super-harmonic contrast imaging and acoustic angiography," *Physics in medicine and biology,* vol. 60, p. 3441, 2015.

[12] J. Kim, S. Li, X. Jiang, S. Kasoji, and P. A. Dayton, "Development of transmitters in dual-frequency transducers for interventional contrast enhanced imaging and acoustic angiography," in *2014 IEEE International Ultrasonics Symposium*, 2014, pp. 679-682.

[13] S. Li, J. Kim, Z. Wang, X. Jiang, S. Kasoji, B. Lindsey, *et al.*, "A 3 MHz/18 MHz dual-layer co-linear array for transrectal acoustic angiography," in *Ultrasonics Symposium (IUS), 2015 IEEE International*, 2015, pp. 1-4.

[14] S.-J. Zhang, H.-N. Qian, Y. Zhao, K. Sun, H.-Q. Wang, G.-Q. Liang, *et al.*, "Relationship between age and prostate size," *Asian journal of andrology,* vol. 15, p. 116, 2013.

[15] J. A. Jensen, "Field: A program for simulating ultrasound systems," in *10TH NORDICBALTIC CONFERENCE ON BIOMEDICAL IMAGING, VOL. 4, SUPPLEMENT 1, PART 1: 351--353*, 1996.

[16] J. A. Jensen and N. B. Svendsen, "Calculation of pressure fields from arbitrarily shaped, apodized, and excited ultrasound transducers," *Ultrasonics, Ferroelectrics, and Frequency Control, IEEE Transactions on,* vol. 39, pp. 262-267, 1992.

[17] T. Azuma, M. Ogihara, J. Kubota, A. Sasaki, S.-i. Umemura, and H. Furuhata, "Dual-frequency ultrasound imaging and therapeutic bilaminar array using frequency selective isolation layer," *IEEE transactions on ultrasonics, ferroelectrics, and frequency control,* vol. 57, pp. 1211-1224, 2010.

[18] R. Krimholtz, D. A. Leedom, and G. L. Matthaei, "New equivalent circuits for elementary piezoelectric transducers," *Electronics Letters,* vol. 6, pp. 398-399, 1970.

10.1109/ULTSYM.2015.0030

A 3 MHz/18 MHz Dual-layer Co-Linear Array for Transrectal Acoustic Angiography

Sibo Li, Jinwook Kim,
Zhuochen Wang, Xiaoning Jiang
Department of Mechanical and Aerospace Engineering
North Carolina State University
Raleigh, NC, 27606, USA
xjiang5@ncsu.edu

Sunny Kasoji, Brooks Lindsey, Paul A. Dayton
Joint Department of Biomedical Engineering
University of North Carolina and NC State University
Chapel Hill, NC, 27599, USA
padayton@email.unc.edu

Abstract— **In this paper, a novel dual layer co-linear array ultrasound transducer was developed for transrectal dual-frequency superharmonic imaging. The KLM model and Field II were used for the acoustic stack design and simulation of the acoustic field of the array, respectively. The newly designed and fabricated probe consists of 50 transmit elements with a center frequency of 3 MHz and 100 receive elements with a center frequency of 18 MHz. The dimensions of the array are 15 mm in azimuth and 9 mm in elevation. The pitch is 270 μm for the transmitting elements and 135 μm for the receiving element. Pulse-echo testing of TX/RX elements corresponded with the simulation results. Real-time contrast imaging was tested using a multi-channel imaging system. The non-linear responses from microbubble contrast agents flowing through a 200 μm cellulose tube at a distance of 30 mm from the probe were clearly observed and displayed in the image. The axial beam width and CNR were calculated to be 200 μm and 18 dB, respectively. These results suggest that the prototyped co-linear array is capable of performing dual-frequency superharmonic imaging of microbubbles ("acoustic angiography") for prostate cancer assessment.**

Keywords—acoustic angiography; dual frequency; ultrasound contrast agent; transrectal ultrasound; prostate cancer

I. INTRODUCTION

In 2014, prostate cancer accounted for 27% of all cancer cases in men, and still lacks a definitive, non-invasive diagnostic test [1]. Routine diagnostic tests, such as prostate-specific antigen levels and manual digital rectal examination are limited by poor sensitivity and high-false positive rates [2]. Core biopsies are painful, increase risk of hemorrhage, and provide little confidence that clinically-relevant regions are sampled. In recent years, transrectal ultrasound (TRUS) has played a substantial role in the diagnosis of prostate cancer due to its ability to provide real-time imaging and biopsy guidance [3]. While TRUS is commonly used for biopsy guidance, B-mode ultrasound exhibits low sensitivity for locating cancerous regions for biopsy[4].

Recent research has shown that contrast-enhanced ultrasound (CEUS) may potentially provide more accurate prostate cancer assessment [5, 6]. Compared to conventional ultrasound, a contrast-enhanced approach can provide estimation of microvascular perfusion in organs and tissues. Recently, our group has investigated an alternative approach to contrast-enhanced ultrasound imaging which relies on the superharmonic echoes produced by microbubble contrast agents, "acoustic angiography". Because increased microvessel density is associated with progression of prostate cancer [7], the ability to image microvasculature during biopsy ensures that regions of neovascularization are sampled. Recent studies on contrast-enhanced dual-frequency ultrasound imaging suggest that microbubbles can be excited in the 2-4 MHz range and the superharmonic echoes from microbubbles can be detected at frequencies above 18 MHz, producing images having high contrast-to-tissue ratio and high-resolution [8]. These images reveal unique information of tumor microvessel structure [9].

The primary challenge to implementing this imaging technique is presented by transducer design and fabrication. In superharmonic imaging, separation of transmission and the receiving bandwidths is required to ensure high contrast-to-tissue ratio, and thus the conventional transducer arrays with single center frequencies are not suitable. Compared with the mechanical scanning technique used with previous single-element systems for superharmonic imaging [9], dual-frequency imaging with an array provides increased frame rate, increased depth of field, more precise control over the acoustic pressure field, and also provides opportunities for designing probes with alternative form factors [10].

To extend our previous work with single-element, dual-frequency transducers [5, 11], a 3 MHz/18 MHz ultrasound array was developed for transrectal dual-frequency imaging acoustic angiography. A 3 MHz/18 MHz co-linear array with 50 transmit and 100 receive elements was designed, fabricated and characterized. Pulse-echo tests were conducted for both low and high frequency elements. The transmitting array was also evaluated by measuring the acoustic pressure profile of single element with a hydrophone. The array transducer's ability to perform microbubble superharmonic imaging was tested by exciting microbubbles flowing through a micro-cellulose tube using the 3 MHz transmitting array and detecting the super harmonic responses from microbubbles using the 18

978-1-4799-8182-3/15/$31.00 ©2015 IEEE

MHz receiving array. Finally, contrast imaging was performed with a multi-channel imaging system.

II. Materials and Methods

A. Transducer Design and Fabrication

In array design, the number of active elements is limited by the imaging system electronics, thus the element pitch and total aperture size was designed considering imaging system limitations and the maximum acceptable probe dimensions for transrectal ultrasound. The prostate is within 2 cm of the rectum, and its size is approximately ~40 mm in longitudinal direction and ~25 mm in transverse direction [12](Figure 1).

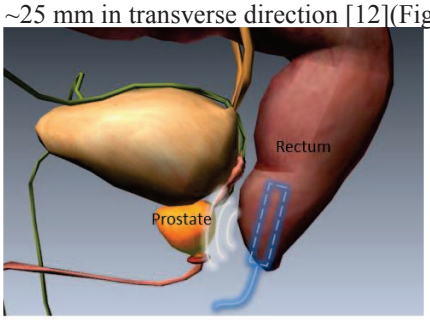

Figure 1 Schematic view of anatomy in prostate imaging

In order to meet these considerations, acoustic field simulations were used to determine the geometry of the low and high frequency arrays. Field II was used to assess a series of designs with varying parameters, and a design with 19 low frequency elements in each transmit event (active sub-aperture of 2.4 mm in the azimuth direction) was ultimately adopted [13, 14]. The details of this configuration are summarized in Table 1.

Table 1 Design parameters of co-linear array

Property	Value	
Aperture	9 mm by 14 mm	
Working mode	Transmitting (3 MHz)	Receiving (18 MHz)
Pitch	270 μm (0.5 λ)	135 μm (1.33 λ)
Element number	50	100

Because the TX and RX elements need to be physically separated while also sharing the same aperture, the array transducer was designed using a stacked configuration (Figure 2). The RX and TX were coupled with isolation layers (nickel and alumina/epoxy), which also served as common ground. To improve the transmission sensitivity, air backing was used for the low frequency array.

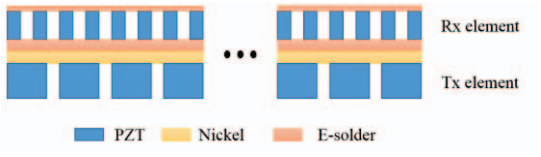

Figure 2 Schematic of array transducer

PZT ceramic (CTS 3203HD, CTS Corporation, Elkhart, Indiana, USA) was selected as the active material for array transducer. Due to the selected element pitch and aperture design, the piezoelectric layers were operated in sliver mode for the low frequency (TX) elements and in coupling mode (between thickness mode and bar mode) for the high frequency (RX) elements. To minimize interference between TX and RX elements, a λ/4 layer of nickel and a λ/4 layer of E-solder were added [15]. The apertures and matching layers for both TX and RX, as well as the isolation layers were designed using the Krimholtz-Leedom-Matthaei (KLM) model [16]. Material properties of each constitutive component are summarized in Table 2.

Table 2 Material properties of each component of the array

Materials	composition	Properties	
PZT	TX and RX	Impedance Longitudinal Velocity Density	30 MRayl 3850 m/s 7700 kg/m^3
Nickel	Isolation layer	Impedance Logitudinal Velocity Density	50 MRayl 5630 m/s 8800 kg/m^3
Backing Layer (E-solder)	Matching	Impedance Longitudinal Velocity Density	5.5 MRayl 2110 m/s 2590 kg/m^3

In fabricating the dual-frequency array, first a PZT plate of 650 μm (for low frequency TX) was cleaned and 1500 Å layers of Ti/Au were deposited on both sides. The top electrode was then plated with nickel and lapped to 90 μm to serve as the first isolation layer. For the second isolation layer, conductive epoxy (E-solder 3022, Von Roll Isola, Inc. New Haven, CT) was cast on the nickel. The material was cured at room temperature for 24 hours. After E-solder was carefully lapped to 30 μm thick, the RX plate was bonded to the TX layer using Epo-Tek 301 (Epoxy Technologies, Billerica, MA), and then lapped to the thickness of 110 μm for 18 MHZ resonance. Another layer of E-solder was added to the RX layer as matching material. The flex circuits for TX and RX were then bonded to both sides of the stack. After the epoxy was fully cured, the dicing process was performed according to the pitch design. Finally, the array was inserted in a custom acrylic housing for characterization and testing.

B. Transducer Characterization

The electrical impedance magnitude and phase spectra for each TX and RX element were measured (HP 4194, Palo Alto, CA). For this test, the array was placed in a water bath, and the electrical impedance magnitude and phase angle were measured over the passband. Next, the pulse-echo response was tested to measure sensitivity, center frequency, and bandwidth for each element. A Panametrics 5077PR and 5900PR pulser/receiver (Panametrics, Inc., Waltham, MA) were used for the TX and RX pulse excitations, respectively. The array was positioned in a degassed/deionized water bath in front of a polished stainless steel plate reflector. With 200V applied to each low frequency element and 1 μJ applied to each high frequency element, the echo response was observed and recorded on an oscilloscope (DSO7104B, Agilent Technologies Inc., Santa Clara, CA). The fast Fourier transform (FFT) function on the oscilloscope was used to determine the frequency response of the acquired RF data.

For dual-frequency imaging, sensitivity of both TX and RX elements are important. The pressure level of TX elements and insertion loss of RX elements were characterized. The transmission pressure of a TX element was measured with a calibrated hydrophone (Onda HNA-0400, Onda Co., Sunnyvale, CA, USA). The element was excited with a one-cycle, 3 MHz sinusoidal signal from a function generator (AFG3101, Tektronix Inc., Beaverton, OR). The relative position between transducer and hydrophone was controlled by a 3-axis motion stage in a water tank. The peak negative pressure was measured to determine the transmission sensitivity. Receive insertion loss was measured by exciting a representative array element with an 18-MHz burst and receiving the reflected echo from a polished steel reflector placed at the elevation focus. The measured value was then corrected for loss due to diffraction in the azimuth direction attenuation in the water bath (2.2×10^{-4} dB/mm-MHz) and reflection from the steel target (0.6 dB).

Cross talk was measured using a 5 V_{pp} 5-cycle burst to excite a single element. The same oscilloscope was used to acquire the responses from the first, second and the third adjacent elements.

C. Contrast Imaging

Contrast imaging with the array transducer was conducted in a water tank. A 200 μm-diameter cellulose tube with flowing microbubbles (10^8 units/mL) was positioned 30 mm away from the ultrasound probe. A multi-channel research imaging system (Verasonics Vantage, Kirkland, WA) was used to drive the array and acquire echoes. For this work, 19 TX elements were fired in each group, and the single RX element at the center of the sub-aperture captured the high frequency superharmonic echoes. Each low frequency TX element was excited with a one-cycle, 55 V pulse. High frequency echoes were filtered with a bandpass filter (9-27 MHz) and time-gain compensation was applied.

III. Results and Discussion

A prototyped co-linear array was fabricated to evaluate the performance for super-harmonic imaging (Figure 3). The active aperture was 9 mm by 15 mm. The total thickness (including flex circuit) was approximately 1 mm.

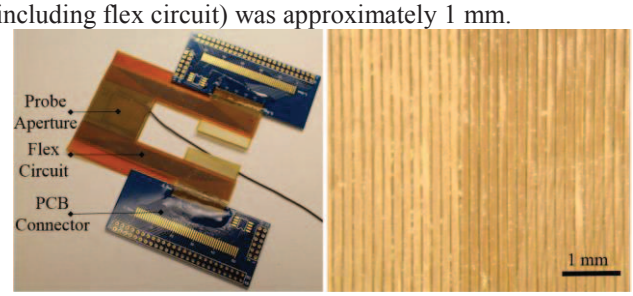

Figure 3 Photograph of co-linear array (left) and top view of element array under microscope (right)

Based on the pulse/echo test for all of the individual elements (Figure 4), the TX element exhibited a mean center frequency of 2.9 MHz and -6 dB bandwidth of 36%, and the RX elements showed a mean center frequency of 18.3 MHz and -6 dB bandwidth of 45%. The measured results corresponded well with the KLM model simulation.

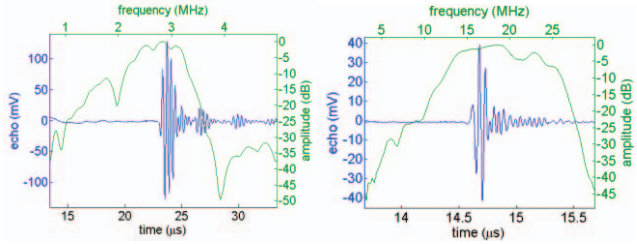

Figure 4 Pulse/echo test of typical TX (upper) and RX (downside) element and their FFT spectra

We characterized singular TX elements with the hydrophone test and measured a transmission sensitivity of 8 kPa/V (peak negative pressure). Based on this test result and Field II simulation (Figure 5), the focal zone of interest would reach a peak-negative pressure of 770 kPa with a 19-element group firing under 55 V excitation (the scenario of contrast imaging setup). The mechanical index was calculated to be 0.46.

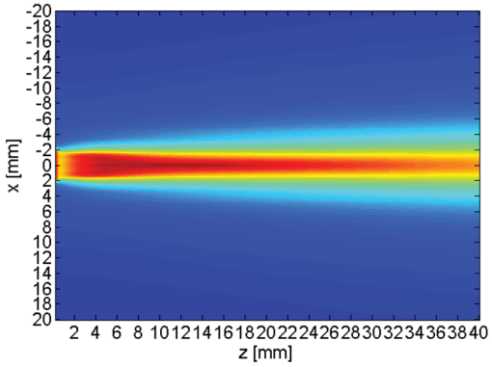

Figure 5 The beam profile of 19 TX-element group firing in Field II simulation

After correcting for attenuation in water and diffraction in the azimuth direction, an insertion loss of -30 dB was estimated. Crosstalk measurements indicated satisfactory but not ideal element-to-element isolation. The crosstalk near the center frequency of the array was measured to be 32 dB for TX elements and 28 dB for RX elements between the adjacent element. The second adjacent element showed ~35 and ~30 dB crosstalk for TX and RX elements, respectively. This crosstalk arises from the uncut isolation layers: because both TX and RX elements were interconnected at the middle common ground, acoustic surface and bulk waves could travel underneath. The results of individual element testing for the completed array are summarized in Table 3.

Table 3 Measured properties for the collinear array

Property	Value	
Aperture	9 mm by 14 mm	
Working mode	Transmitting (3 MHz)	Receiving (18 MHz)
Pitch size	270 μm (0.5 λ)	135 μm (1.33 λ)
Element number	50	100
Malfunctioned #	4	12

Center frequency	2.9 MHz	18.3 MHz
-6 dB fractional bandwidth	36%	45%
Pulse width (-20 dB)	2.7 μs	0.3 μs
Transmission sensitivity	8 kPa(PNP)/V	-
Insertion loss	-	-30 dB
Cross talk (1st adjacent element)	-32 dB	-28 dB

The acquired image (Figure 6) shows that the co-linear array was able to capture the microbubble signal flowing in the cellulose tube. There are two observable targets displayed in the image because of the ring-down of TX element. This might be avoided in the future by adding a backing layer to improve ring-down at the expense of peak negative pressure. The received echo beam width in the axial and lateral dimensions were measured to be 200 μm and 400 μm, respectively. The contrast to noise ratio was calculated to be ~18 dB.

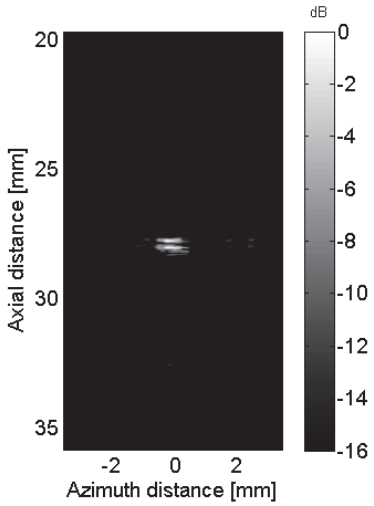

Figure 6 Superharmonic images of a microtube filled with microbubble contrast agent using the prototype dual-frequency array.

IV. CONCLUSION

In this work, we developed a co-linear, dual-frequency (3/18 MHz) transducer for demonstrating the feasibility of transrectal acoustic angiography. The acoustic characterization results indicate that our design concept and technique can achieve fractional bandwidths and transmission/receiving sensitivities which are sufficient for superharmonic microbubble imaging. We also used a multi-channel imaging system to demonstrate that the array was capable of inducing a higher harmonic response from microbubble contrast agents at a depth of 30 mm. These imaging results indicate that with a 1-cycle burst excitation, the beam width in axial and lateral was 200 μm and 400 μm, and CNR was ~20 dB. These results demonstrate that the co-linear array is capable of acoustic angiography imaging, which can be used for prostate tumor characterization and identify regions of neovascularization for guidance of prostate biopsies.

ACKNOWLEDGMENT

The authors would like to acknowledge the financial support from U.S. Army Medical Research and Materiel Command under the grant PC111309. The authors would like to thank Jianguo Ma, Anthony Novell, K. Heath Martin and Wei-Yi Chang for providing instruction and assistance in transducer design, microbubble detection tests, and manuscript preparation.

REFERENCES

[1] R. Siegel, J. Ma, Z. Zou, and A. Jemal, "Cancer statistics, 2014," *CA: a cancer journal for clinicians,* vol. 64, pp. 9-29, 2014.

[2] W. Catalona, J. Richie, F. Ahmann, M. Hudson, P. Scardino, R. Flanigan, *et al.*, "Comparison of digital rectal examination and serum prostate specific antigen in the early detection of prostate cancer: results of a multicenter clinical trial of 6,630 men," *The Journal of urology,* vol. 151, pp. 1283-1290, 1994.

[3] M. A. Levine, M. Ittman, J. Melamed, and H. Lepor, "Two consecutive sets of transrectal ultrasound guided sextant biopsies of the prostate for the detection of prostate cancer," *The Journal of urology,* vol. 159, pp. 471-476, 1998.

[4] M. Wink, F. Frauscher, D. Cosgrove, J.-Y. Chapelon, L. Palwein, M. Mitterberger, *et al.*, "Contrast-enhanced ultrasound and prostate cancer; a multicentre European research coordination project," *European urology,* vol. 54, pp. 982-993, 2008.

[5] J. Kim, S. Li, S. Kasoji, P. A. Dayton, and X. Jiang, "Phantom evaluation of stacked-type dual-frequency 1–3 composite transducers: A feasibility study on intracavitary acoustic angiography," *Ultrasonics,* vol. 63, pp. 7-15, 2015.

[6] K. H. Martin, B. D. Lindsey, J. Ma, M. Lee, S. Li, F. S. Foster, *et al.*, "Dual-frequency piezoelectric transducers for contrast enhanced ultrasound imaging," *Sensors,* vol. 14, pp. 20825-20842, 2014.

[7] M. Borre, B. V. Offersen, B. Nerstrøm, and J. Overgaard, "Microvessel density predicts survival in prostate cancer patients subjected to watchful waiting," *British journal of cancer,* vol. 78, p. 940, 1998.

[8] B. D. Lindsey, J. D. Rojas, K. Heath Martin, S. E. Shelton, and P. Dayton, "Acoustic characterization of contrast-to-tissue ratio and axial resolution for dual-frequency contrast-specific acoustic angiography imaging," *Ultrasonics, Ferroelectrics, and Frequency Control, IEEE Transactions on,* vol. 61, pp. 1668-1687, 2014.

[9] R. C. Gessner, C. B. Frederick, F. S. Foster, and P. A. Dayton, "Acoustic angiography: a new imaging modality for assessing microvasculature architecture," *Journal of Biomedical Imaging,* vol. 2013, p. 14, 2013.

[10] T. Ritter, T. R. Shrout, R. Tutwiler, and K. K. Shung, "A 30-MHz piezo-composite ultrasound array for medical imaging applications," *Ultrasonics, Ferroelectrics, and Frequency Control, IEEE Transactions on,* vol. 49, pp. 217-230, 2002.

[11] J. Ma, K. H. Martin, Y. Li, P. A. Dayton, K. K. Shung, Q. Zhou, *et al.*, "Design factors of intravascular dual frequency transducers for super-harmonic contrast imaging and acoustic angiography," *Physics in medicine and biology,* vol. 60, p. 3441, 2015.

[12] S.-J. Zhang, H.-N. Qian, Y. Zhao, K. Sun, H.-Q. Wang, G.-Q. Liang, *et al.*, "Relationship between age and prostate size," *Asian journal of andrology,* vol. 15, p. 116, 2013.

[13] J. A. Jensen, "Field: A program for simulating ultrasound systems," in *10TH NORDICBALTIC CONFERENCE ON BIOMEDICAL IMAGING, VOL. 4, SUPPLEMENT 1, PART 1: 351--353*, 1996.

[14] J. A. Jensen and N. B. Svendsen, "Calculation of pressure fields from arbitrarily shaped, apodized, and excited ultrasound transducers," *Ultrasonics, Ferroelectrics, and Frequency Control, IEEE Transactions on,* vol. 39, pp. 262-267, 1992.

[15] J. Ma, K. H. Martin, P. Dayton, and X. Jiang, "A preliminary engineering design of intravascular dual-frequency transducers for contrast-enhanced acoustic angiography and molecular imaging," *Ultrasonics, Ferroelectrics, and Frequency Control, IEEE Transactions on,* vol. 61, pp. 870-880, 2014.

[16] R. Krimholtz, D. A. Leedom, and G. L. Matthaei, "New equivalent circuits for elementary piezoelectric transducers," *Electronics Letters,* vol. 6, pp. 398-399, 1970.

Dual-frequency Super Harmonic Imaging Piezoelectric Transducers for Transrectal Ultrasound

Jinwook Kim[a], Sibo Li[a], Sandeep Kasoji[b], Paul A. Dayton[b], Xiaoning Jiang[*a]

[a]Department of Mechanical and Aerospace Engineering, North Carolina State University, Raleigh, NC 27695, USA
[b]Joint Department of Biomedical Engineering, University of North Carolina and North Carolina State University, Chapel Hill, NC, 27599, USA

ABSTRACT

In this paper, a 2/14 MHz dual-frequency single-element transducer and a 2/22 MHz sub-array (16/48-elements linear array) transducer were developed for contrast enhanced super-harmonic ultrasound imaging of prostate cancer with the low frequency ultrasound transducer as a transmitter for contrast agent (microbubble) excitation and the high frequency transducer as a receiver for detection of nonlinear responses from microbubbles. The 1-3 piezoelectric composite was used as active materials of the single-element transducers due to its low acoustic impedance and high coupling factor. A high dielectric constant PZT ceramic was used for the sub-array transducer due to its high dielectric property induced relatively low electrical impedance. The possible resonance modes of the active elements were estimated using finite element analysis (FEA). The pulse-echo response, peak-negative pressure and bubble response were tested, followed by in vitro contrast imaging tests using a graphite-gelatin tissue-mimicking phantom. The single-element dual frequency transducer ($8 \times 4 \times 2$ mm^3) showed a -6 dB fractional bandwidth of 56.5 % for the transmitter, and 41.8 % for the receiver. A 2 MHz-transmitter (730 μm pitch and 6.5 mm elevation aperture) and a 22 MHz-receiver (240 μm pitch and 1.5 mm aperture) of the sub-array transducer exhibited -6 dB fractional bandwidth of 51.0 % and 40.2 %, respectively. The peak negative pressure at the far field was about -1.3 MPa with 200 V_{pp}, 1-cycle 2 MHz burst, which is high enough to excite microbubbles for nonlinear responses. The 7th harmonic responses from micro bubbles were successfully detected in the phantom imaging test showing a contrast-to-tissue ratio (CTR) of 16 dB.

Keywords: Dual-frequency transducer, transrectal ultrasound, prostate probe, super-harmonic imaging, contrast imaging, mode coupling

1. INTRODUCTION

Prostate cancer is the second leading cause of cancer death of American men, with an estimated 29,720 deaths in 2013 in the USA.[1] In recent years, health monitoring for the prostate cancer by means of transrectal ultrasound (TRUS) has been considered as the standard diagnostic method. One of the key indicators of prostate cancer is pathological angiogenesis because tumor vessel networks are tortuous, leaky, and have unpredictable relationships between size and flow rate, whereas normal tissue has ordered and hierarchical branching networks.[2] For tumor imaging, piezoelectric ultrasound has been widely adopted due to its non-invasive real time imaging capability, relatively low cost, portability, and substantially improved image quality with high frequency ultrasound. In comparison with conventional ultrasound, contrast-enhanced

* xjiang5@ncsu.edu; www.mae.ncsu.edu/jiang

Health Monitoring of Structural and Biological Systems 2015, edited by Tribikram Kundu, Proc. of SPIE Vol. 9438, 943823
 · doi: 10.1117/12.2084459

ultrasound (CEUS) enables higher imaging sensitivity of blood vessels because the injected microbubble contrast agent (MCA) amplifies scattering from the blood.[3] A contrast enhanced super-harmonic imaging of microvasculature with suppression of tissue background is called acoustic angiography.[4] In acoustic angiography, microbubbles are excited by relatively low frequency waves (1-7 MHz), which is close to the resonant frequency of microbubbles. The high frequency (> 15 MHz) super-harmonic echoes from microbubbles are detected by a high frequency receiver.[5] In previous work, it was confirmed that this technique can achieve high contrast-to-tissue ratio (CTR) and high resolution in-vivo microvascular imaging.[6] However, the main challenge of acoustic angiography to date has been the lack of dual-frequency transducers that can efficiently transmit energy at a selected low frequency and simultaneously detect the high frequency harmonic echoes in a confocal fashion. To date, no dual-frequency transducer design has been optimized for transrectal ultrasound imaging applications. Several dual-frequency contrast enhanced imaging piezoelectric transducers with low frequency transmission (< 5 MHz) have been reported: 0.9/2.8 MHz interleaved (alternative arrangement of low-frequency transmitting and high-frequency receiving elements) array,[7] 0.9/7.5 MHz dual-band annular array transducer for second-order ultrasound field (SURF) imaging,[8] 1/3.7 MHz interleaved phase-array transducer,[9] 2.5/30 and 4/30 MHz transducers for in-vivo 3-D contrast imaging of tissue microvasculature,[10] and 4/14 MHz transducer composed of a pad-printed high-frequency element and a curved ring shape low-frequency element.[11] Unfortunately, the size of these single-element and array transducers are not suitable for TRUS applications. On the other hand, for the application of contrast enhance intravascular ultrasound (CE-IVUS), a 6.5/30 MHz sandwich-type dual-frequency transducer was developed.[12] This transducer showed the capability of high-resolution acoustic angiography with its compact structure (0.6 × 3 mm aperture and < 600 μm thickness), but the transducer size, frequency combination, and penetration depth were optimized only for IVUS applications.

We recently developed a small size (8 × 4 × 2 mm), sandwich-type dual-frequency piezoelectric transducer with a 2 MHz transmitter (TX) and a 12-14 MHz receiver (RX) using 1-3 piezoelectric composites for transrectal acoustic angiography (Figure 1). The design technique was briefly introduced in our previous work.[13] In this work, microbubble detection capability and multiple A-line super-harmonic imaging results were obtained using the 2/14 MHz single-element transducer. In addition, a preliminary design of 2/22 MHz dual-frequency sub-array transducer (16-element TX and 48-element RX array) was studied and discussed toward transrectal acoustic angiography.

2. MATERIALS AND METHODS

Among many smart materials, the PZT-5H 1-3 piezoelectric composite (volume fraction of 60 %, Blatek, Inc., State College, PA) and high-dielectric soft PZT ceramic (HK1-HD, TRS Technologies, Inc., State College, PA) were used. A single-element transducer was designed for operating at thickness extensional mode. Thus, 1-3 composite plates were used for both the TX and RX due to its high electro-mechanical coupling factor and low acoustic impedance.[14] On the other hand, due to the spatial limitation for sub-array elements, the designed operating modes were sliver mode for TX elements and a coupled mode (between width extensional and thickness extensional) for RX elements. Hence, HK1-HD ceramics (free dielectric constant ε_{33}^{T} of 6500) were used for relatively low aspect ratio (width/thickness < 3) elements. The apertures and matching layers for both a TX and a RX as well as an isolation layer were designed by using the Krimholtz–Leedom–Matthaei (KLM) model. Material properties of each constitutive component of transducers are shown in Table 1. Besides the conventional thickness mode which can be analyzed by 1-D model, the mode coupling of sliver, width extensional, and thickness modes were studied by finite element analysis (FEA) using ANSYS software (ANSYS Mechanical APDL®, ANSYS® Academic Research, Release 15.0.7, ANSYS, Inc., Canonsburg, USA). After a fabrication process, electrical impedance spectra of the prototype transducers were measured by Agilent 4294A impedance analyzer (Agilent Technologies Inc., Santa Clara, CA). The pulse-echo responses of the TX and RX were measured individually by using two different pulser/receivers: a square wave pulser/receiver (Olympus 5077PR, Olympus NDT, Inc., Waltham, MA) for

the TXs and an Olympus 5900PR (Panametrics Inc., Waltham, MA) for the RXs. The pulse-echo signals were recorded using a digital oscilloscope (DSO7104B, Agilent Technologies Inc., Santa Clara, CA).

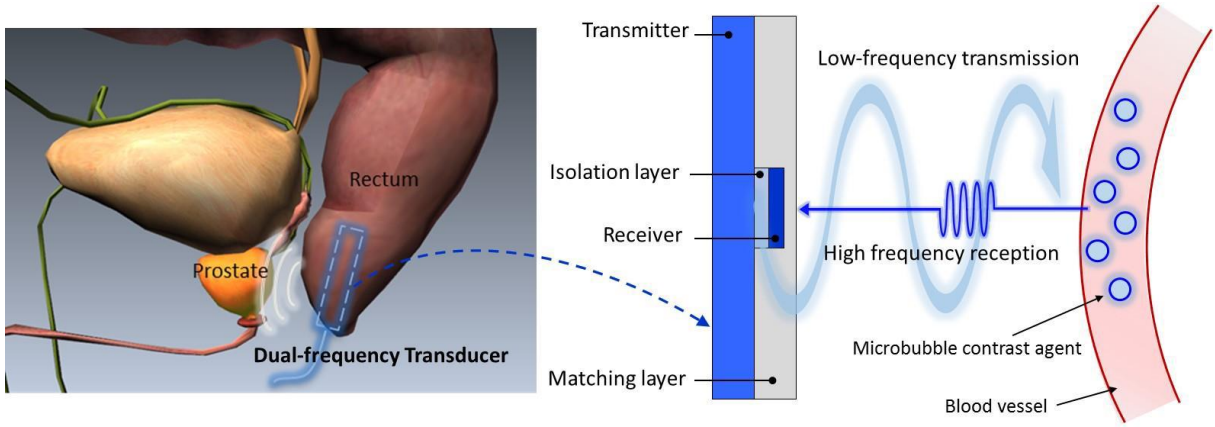

Figure 1. Schematic of the dual-frequency transducer for transrectal super-harmonic ultrasound imaging and acoustic angiography.

Table 1. Material properties of each constitutive component of the transducer.

Materials	Parts	ρ (kg/m^3)	v_l (m/s)	k_t	ε_{33}^S
1-3 composite	Single-element transducer TX & RX	5300	3740	0.65	660
TRS-HK1-HD PZT	Sub-array transducer TX & RX	8000	4180	0.50	2500
E-solder 3022	Isolation layer 2	2590	2110	.	.
Carbon steel	Isolation layer 1	7700	6100	.	.
Al2O3/epoxy	Matching layer of TX & RX	2700	1600	.	.

For the single-element prototype transducer, further acoustic and imaging tests were conducted. We measured the peak-negative-pressure (PNP) produced by the single-element prototype transducer at different voltage inputs to confirm that it was suitable for microbubble excitation. The transmitting element was driven by one-cycle sinusoidal input at 2 MHz with various peak-to-peak voltages (100, 150, and 200 V_{pp}). The mechanical index (MI) of each input condition was analyzed. A tissue-mimicking (graphite-gelatin) phantom was used for both bubble signal detection and phantom blood vessel imaging. The phantom design consisted of two parallel cellulose tubes (200 µm in diameter) suspended in the graphite-gelatin (Figure 2). The received signals were processed to obtain the frequency spectrum, and were further band-pass filtered to obtain the higher-harmonic content of the signals. When the cellulose tube was infused with microbubbles, CTR was calculated and compared using a following equation:

$$CTR = 20 \cdot \log\left(\frac{V_{bubble}}{V_{tissue}}\right) \quad (1)$$

where V_{bubble} denotes the detected peak voltage amplitude from microbubbles, and V_{tissue} is the peak voltage amplitude detected from the tissue-phantom. When performing the super-harmonic imaging test, 2D images of the tissue-phantom

with microbubbles flowing through the cellulose tubes (x-y plane in Figure 2) were acquired by collecting A-lines. The excitation pulse was a sinusoidal 1-cycle burst at 2 MHz generated from a function generator (AFG3101, Tektronix Inc., Beaverton, OR). The driving signal (300 mV_{pp}) generated by the function generator was amplified using a 60 dB radio-frequency amplifier (Model 3200L, Electronic Navigation Industries Inc., Rochester, NY). The received signals from microbubbles were high-pass filtered at 10 MHz to eliminate the fundamental and lower-order harmonic responses (< 6th harmonic) from the tissue phantom. The average and envelope of the 100 acquired A-lines with 16 dB gain were stored individually and converted to the B-mode images offline.

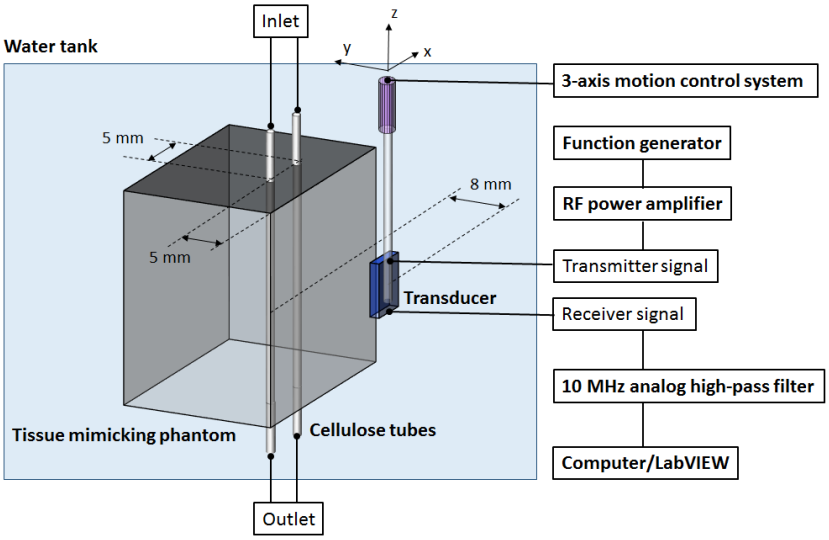

Figure 2. Experimental setup for the bubble detection test and super-harmonic imaging with a tissue phantom.

3. RESULTS AND DISCUSSION

3.1 Design and fabrication results

For the single-element transducer, an aperture of a 2 MHz-TX was designed as 3.8 × 7.0 mm^2 aiming for PNP of > 1 MPa at 10 mm away, -6 dB beam diameter of ~3 mm, and electrical impedance matching of ~ 50 Ω. The 14 MHz RX is required to share the same focal axis with the TX by positioning itself in front of the TX. Thus, the RX with a thickness of 90 μm is allowed to have a large enough aperture (> 0.9 × 0.9 mm^2) for the pure thickness vibration mode. On the other hand, resonance of other active components (TX of the single-element transducer, TX and RX of the sub-array transducer) were estimated by FEA (Figure 3) considering mode coupling effects caused by the element dimensions. Material properties, dimensions, and vibration modes of each active component are shown in Table 2. Although the thickness (710 μm) and the lateral dimension of the single-element transducer TX (3.8 × 7.0 mm^2) is not perfectly suitable for a pure thickness mode resonance (> 7.0 × 7.0 mm^2), a calculated impedance spectrum exhibited an isolated thickness mode resonance at 2 MHz from the lateral vibration (width extensional) mode at 292 kHz (Figure 3 (a)). This result shows that the 1-3 composite has several advantages for the low-frequency transmitter design, including 1) a thin active layer (~710 μm) for the designed frequency (2 MHz) due to its relatively low stiffness, 2) the suppressed mode-coupling between the thickness and lateral resonant modes due to the laterally isolated connectivity of 1-3 composites . Therefore, a low aspect ratio (width to thickness,

< 3) active layer is possible by using 1-3 composite, which is advantageous for single-element, small-size dual frequency transducers for interventional applications.

For the sub-array transducer, 1-3 composite is not an optimal candidate for an TX array element with an aspect ratio of 0.5 due to its low dielectric constants (ε_{33}^{S} of 660), which causes unacceptable electrical impedance at the resonance (> 1 kΩ). On the other hand, HK1-HD PZT ceramic with a high dielectric constant ε_{33}^{S} of 2500 showed 130 Ω at the 2 MHz sliver resonance (Figure 3 (b)). The width extensional resonance occurred at 3.3 MHz, which is 37 % higher than the anti-resonance frequency of the sliver mode (2.4 MHz). The RX elements of the sub-array had an aspect ratio of 3, and this structure exhibited a coupled mode at 22 MHz which is coupling between 5th harmonic width extensional resonance and the thickness resonance (Figure 3 (c)). Although this is not an optimal design of the RX for harmonic signal receiving, the electrical impedance amplitude at the resonance of 45 Ω is an acceptable value for RX array elements. The mode coupling at the designed frequency range can be removed by sub-dicing of elements.

Table 2. Configuration of each transducer component.

Components	Single-element TX	Single-element RX	Sub-array TX	Sub-array RX
Dimension (mm^3)	3.8 × 7.0 × 0.71	2.0 × 2.0 × 0.09	6.5 × 0.4 × 0.64	1.5 × 0.21 × 0.075
Vibration mode	Thickness extensional	Thickness extensional	Sliver	Coupled mode (width extensional + thickness extensional)
Material	PZT-5H 1-3 composite	PZT-5H 1-3 composite	HK1-HD PZT	HK1-HD PZT

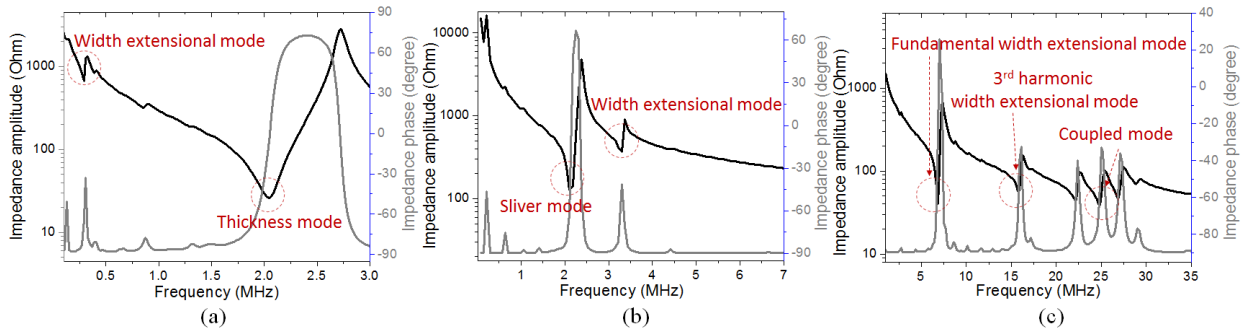

Figure 3. Calculated impedance spectra of active components: (a) Single element transducer TX; (b) Sub-array transducer TX; (c) Sub-array transducer RX. The coupled mode in (c) shows a mode coupling between 5th harmonic width extensional mode and thickness mode.

Based on the designed parameters, prototype transducers were fabricated. The fabrication procedures were presented in detail in our previous work for intravascular ultrasound transducers.[12] The key features of the prototype transducers (Figure 4) are summarized as follows; 1) 1-3 piezoelectric composite was used for single-element transducer due to its wideband (short pulse) characteristics and the low aspect ratio capabilities, whereas the sub-array transducer was made of high-dielectric soft PZT ceramic considering the aspect ratio limitation and electrical impedance of array elements, 2) The single-element prototype was designed without a highly attenuating and thick backing layer in order to reduce the total thickness

of the transducer. The intrinsic wideband characteristics of the 1-3 composite redeem the slightly declined bandwidth caused by the absence of the backing layer. In contrast, sub-array TX elements have a tungsten backing for a short-pulse excitation performance, 3) The high-frequency RX was included in the matching layer of the low-frequency TX to share a coaxial beam profile for the two frequencies, 4) The dual-isolation layer was used between the RX and TX for the acoustic impedance mismatch (5.5 and 50 MRayl), which blocks the received high frequency echo signals from entering into the transmitter and eliminates the aliasing echo reflected from the backside of the transmitter.

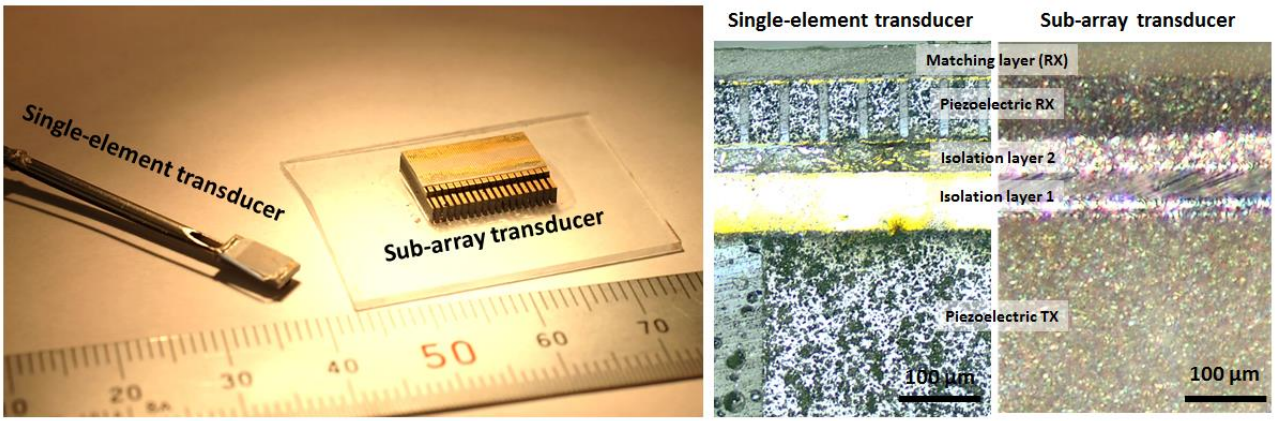

Figure 4. Fabrication results: (a) the prototype dual-frequency single-element and sub-array transducer; (b) cross sectional view of the center part of each transducer.

3.2 Impedance measurement results

Electrical impedance amplitude and phase angle spectra of each components were measured after a poling process. Figure 5 shows measured spectra of each component. The measured data denote that targeted resonance modes such as 2/14 MHz for the single-element transducer and 2/22 MHz for the sub-array transducer are clearly shown in each impedance spectrum. The anticipated width extensional mode of sub-array transducer's TX element at 3.3 MHz (Figure 5 (b)) was suppressed due to the thick (1 mm) and heavy backing of the prototype transducer.

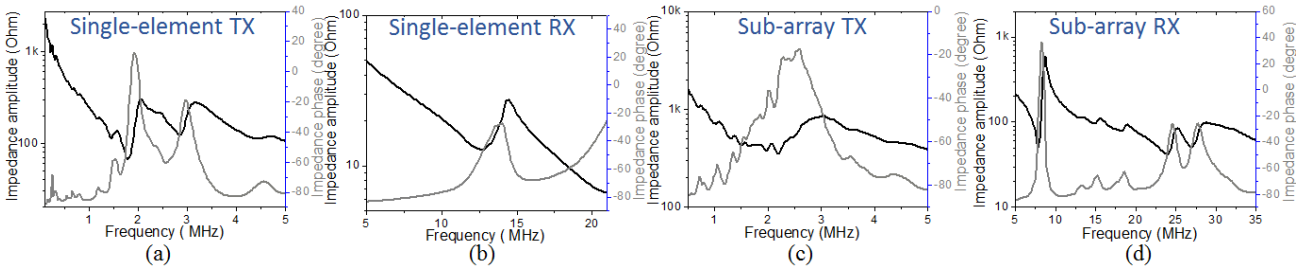

Figure 5. Measured impedance spectra of prototype transducers; top legend of each figure indicate the name of transducer components.

3.3 Pulse-echo and pressure output test results

The pulse-echo response of the single-element TX demonstrates a center frequency of 2.2 MHz and the -6 dB fractional bandwidth of 56.5 % (Figure 6 (a)). Though the backside of the TX is close to the free boundary, which cannot absorb backward travelling waves, the low acoustic impedance and low mechanical quality factor of 1-3 composites are capable of emitting a short pulse-echo response. The single-element RX demonstrates a center frequency of 13.7 MHz and the -6 dB fractional bandwidth of 41.8 % (Figure 6 (b)). It showed a relatively long ring down due to the dual-isolation layer which is designed to reflect high-frequency waves. The measured response from the receiver showed a sufficient -6 dB bandwidth to cover the 6th and 7th harmonic frequencies (12 to 14 MHz).

An element of sub-array TX showed the center frequency of 2.2 MHz and -6 dB fractional bandwidth of 51.0 % (Figure 6 (c)). Although peak-to-peak echo amplitude of a single channel TX is not sufficient for bubble excitation due to the heavy backing, it can be expected that group firing of multi-channel TX can excite micro bubbles for harmonic responses. A sub-array RX element showed the center frequency of 25.8 MHz and the -6 dB fractional bandwidth of 40.2 % (Figure 6 (d)). The width extensional mode at 8 MHz might cause ringing after 2.3 μs because the matching layer of RX was designed based on a quarter wavelength of 22 MHz waves. This aliasing echo at lower frequency than the target frequency of 22 MHz can be filtered out during super-harmonic imaging process.

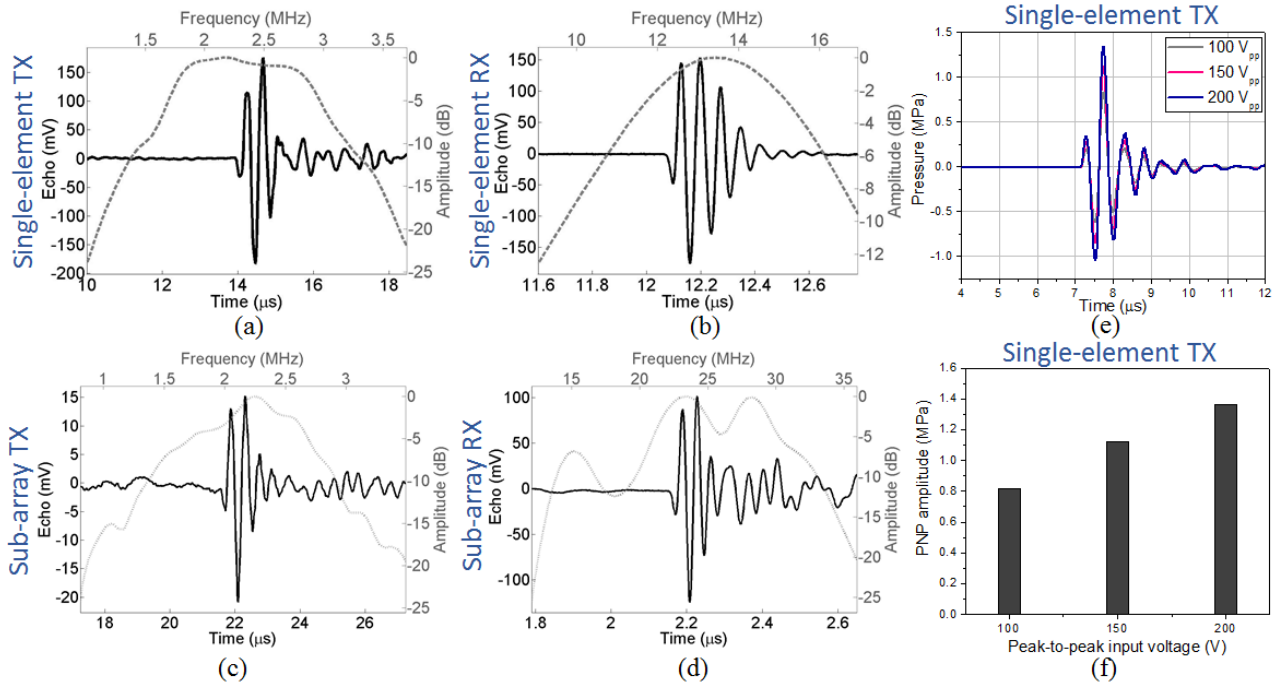

Figure 6. Acoustic test results of each transducer component; (a-d) pulse-echo response of each component shown at the left legend of each figure; (e-f) measured pressure waves and PNP with 1-cycle of 100, 150, and 200 V_{pp} excitation at 2 MHz.

Acoustic pressures produced by the single-element prototype transducer at various voltage inputs were measured to determine the proper input conditions for acoustic angiography (Figure 6 (e)). Using the 1-cycle excitation at 2 MHz, and

peak-to-peak voltage inputs of 100 V, 150 V, and 200 V, PNPs were measured to be 0.82, 1.12, and 1.36 MPa, respectively (Figure 6 (f)). Previous work confirmed that if the MI is as high as approximately 1.0 using a low-frequency (1.5-2.5 MHz) to excite microbubbles, a 15 MHz receiver can detect clear super-harmonic signals from the microbubbles. Therefore, transmission excitation pulses of 1-cycle and higher than 200 V_{pp} with associated MIs of > 0.96 may be appropriate excitation conditions for microbubble detection tests and super-harmonic imaging.

3.4 Bubble signal detection and super harmonic imaging results

Bubble signal detection and super harmonic imaging tests were conducted with the aforementioned experiment set-up shown in Figure 2. Figure 7 (a) shows the case of water injected into a microcellulose tube (200 µm in diameter). The received signal showed only acoustic reflections from the tissue-phantom boundary. In the case of injecting air into the tube 14 MHz RX detected the 2 MHz fundamental response from the air, followed by the phantom boundary reflection (Figure 7 (b)). Due to the large acoustic impedance difference between air and water, the frequency content of the response from air is dominantly around the fundamental frequency.

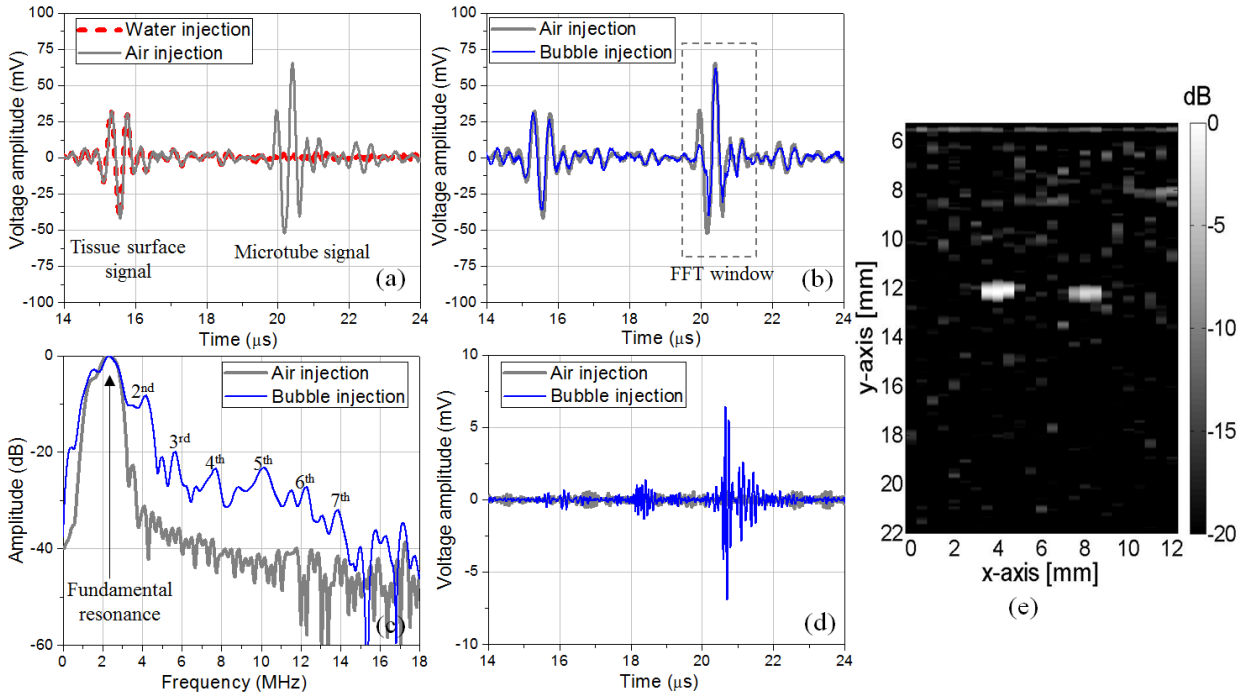

Figure 7. Bubble detection test and imaging results; (a) detected voltage amplitude comparison between water and air injection cases; (b-d) compassion between air and microbubble injection cases; (b) detected waveforms, (c) frequency spectra transformed with the designated FFT window in (b), (d) detected amplitudes filtered by a digital band-pass filter (8-15 MHz); (e) super-harmonic B-mode images of microtubes in a tissue-mimicking phantom.

In comparison with the linear signal from the tissue-phantom boundary, the signal from the tube filled with microbubbles showed a slightly reduced peak-to-peak amplitude and distorted waveform. This distortion of the signal is caused by the nonlinear response of the microbubbles. Time range of 19-21.5 µs was used as the window for the fast Fourier transform.

The frequency spectrum for the case with air was also analyzed to compare with the frequency spectrum for the microbubbles (Figure 7 (c)). In addition to a strong second-harmonic response (-10 dB), the microbubble frequency spectrum showed high amplitude at the 4th through the 7th harmonics (-23 to -30 dB), whereas the air-filled tube showed these same harmonic components as less than -40 dB in amplitude. This comparison clearly demonstrates that the microbubble response contains larger higher-harmonic components. By considering the measured higher harmonic components, the received bubble signal was processed with a digital band-pass filter which had cut-off frequencies between 8 and 15 MHz. The filtered microbubble signal was compared with filtered air signal (Figure 7 (d)). The fundamental frequency component was completely removed in both the air and microbubble signals, and only the filtered microbubble signal exhibited high-frequency harmonics with 13.5 mV_{pp}, whereas the filtered signal from air showed noise level signals (< 1.2 mV_{pp}). Overall, the super-harmonic responses of the microbubbles (5th through 7th harmonics) were successfully detected with a penetration depth in tissue of about 5 mm. The cellulose tubes in the tissue-mimicking phantom were scanned by the aforementioned acoustic angiography imaging procedure using the single-element transducer. The results showed that the super-harmonic images obtained by our single-element dual-frequency transducer clearly visualize the cross-section of tubes filled with microbubbles (Figure 7 (e)) suppressing tissue images. In Figure 7 (e), the averaged CTR is 16 dB. The slight error of tube position in acquired images (~12.2 mm along the y-axis)) was likely resulted from the pressure-dependent speed of sound in tissue-phantom for harmonic signals. The distortion of the imaged tube diameter (~615 μm) in comparison with an actual diameter (~200 μm) can be reduced by increasing the bandwidth and center frequency of the RX.

4. CONCLUSION

In this work, we developed a single-element and sub-array dual-frequency transducers for transrectal acoustic angiography. The possible resonance modes for 1-3 composite and TRS-HK1-HD ceramic drive sections in a sandwich design were analyzed considering spatial limitation of transrectal ultrasound probes. Our study on the dual-frequency design indicates that 1-3 composite is suitable for the single-element transducers due to its wideband and laterally isolated characteristics, whereas it is not proper for the array transducer design due to its low dielectric property. With a small-size aperture and total thickness (8 × 4 × 2 mm), our single-element prototype is capable of inducing the nonlinear higher harmonic response of MCA with a penetration depth in a tissue-phantom of about 5 mm. Moreover, it is capable of detecting higher-order harmonics (5th through 7th) from microbubbles with the suppression of linear tissue signal. The 2/12-14 MHz single-element 1-3 composite transducer can produce a vascular image with CTR of 16 dB and -6 dB resolution of 615 μm for 200 μm micro-blood vessels. This resolution can be improved by increasing the bandwidth and center frequency of the receiver. The bubble detection and imaging by using the developed 2/22 MHz sub-array transducer are currently underway, and this work on new dual frequency piezoelectric ultrasound transducer design is promising for transrectal acoustic angiography applications.

ACKNOWLEDGMENTS

The authors would like to acknowledge the financial support from U.S. Army Medical Research and Materiel Command under the contract PC111309.

REFERENCES

[1] Bard, R. L., Fütterer, J. J., and Sperling, D., [Image Guided Prostate Cancer Treatments], Springer, Berlin Heidelberg(2014).

[2] Carmeliet, P., "Angiogenesis in life, disease and medicine," Nature 438(7070), 932-936 (2005).

[3] Frinking, P. J., Bouakaz, A., Kirkhorn, J., Ten Cate, F. J., and De Jong, N., "Ultrasound contrast imaging: current and new potential methods," Ultrasound Med. Biol. 26(6), 965-975 (2000).

[4] Gessner, R. C., Frederick, C. B., Foster, F. S., and Dayton, P. A., "Acoustic angiography: a new imaging modality for assessing microvasculature architecture," Int. J. Biomed. Imaging 2013(936593), 14 (2013).

[5] Lindsey, B. D., Rojas, J. D., Martin, K. H., Shelton, S. E., and Dayton, P. A., "Acoustic characterization of contrast-to-tissue ratio and axial resolution for dual-rrequency contrast-specific acoustic angiography imaging," IEEE Trans. Ultrason. Ferroelectr. Freq. Control 61(10), 1668-1687 (2014).

[6] Martin, K. H., Lindsey, B. D., Ma, J., Lee, M., Li, S., Foster, F. S., Jiang, X., and Dayton, P. A., "Dual-Frequency Piezoelectric Transducers for Contrast Enhanced Ultrasound Imaging," Sensors 14(11), 20825-20842 (2014).

[7] Bouakaz, A., ten Cate, F., and de Jong, N., "A new ultrasonic transducer for improved contrast nonlinear imaging," Phys. Med. Biol. 49(16), 3515 (2004).

[8] Masoy, S.-E., Standal, O., Nasholm, P., Johansen, T. F., Angelsen, B., and Hansen, R., "SURF imaging: In vivo demonstration of an ultrasound contrast agent detection technique," IEEE Trans. Ultrason. Ferroelectr. Freq. Control 55(5), 1112-1121 (2008).

[9] Van Neer, P. L., Matte, G., Danilouchkine, M. G., Prins, C., Van Den Adel, F., and De Jong, N., "Super-harmonic imaging: development of an interleaved phased-array transducer," IEEE Trans. Ultrason. Ferroelectr. Freq. Control 57(2), 455-468 (2010).

[10] Gessner, R., Lukacs, M., Lee, M., Cherin, E., Foster, F., and Dayton, P. A., "High-resolution, high-contrast ultrasound imaging using a prototype dual-frequency transducer: in vitro and in vivo studies," IEEE Trans. Ultrason. Ferroelectr. Freq. Control 57(8), 1772-1781 (2010).

[11] Guiroy, A., Novell, A., Ringgaard, E., Lou-Moeller, R., Gregoire, J.-M., Abellard, A.-P., Zawada, T., Bouakaz, A., and Levassort, F., "Dual-frequency transducer for nonlinear contrast agent imaging," IEEE Trans. Ultrason. Ferroelectr. Freq. Control 60(12), 2634-2644 (2013).

[12] Ma, J., Martin, K. H., Dayton, P. A., and Jiang, X., "A preliminary engineering design of intravascular dual-frequency transducers for contrast-enhanced acoustic angiography and molecular imaging," IEEE Trans. Ultrason. Ferroelectr. Freq. Control 61(5), 870-880 (2014).

[13] Kim, J., Li, S., Jiang, X., Kasoji, S., and Dayton, P. A., "Development of transmitters in dual-frequency transducers for interventional contrast enhanced imaging and acoustic angiography," Proc. IEEE Ultrasonics Symp., 679-682 (2014).

[14] Kim, J., and Roh, Y., "Homogenization of PMN-PT/epoxy 1–3 piezocomposites by resonator measurements and finite element analysis," Sensors and Actuators A: Physical 206, 97-106 (2014).

10.1109/ULTSYM.2014.0167

Development of Transmitters in Dual-Frequency Transducers for Interventional Contrast Enhanced Imaging and Acoustic Angiography

Jinwook Kim, Sibo Li, Xiaoning Jiang
Department of Mechanical and Aerospace Engineering
North Carolina State University
Raleigh, NC 27695, USA
xjiang5@ncsu.edu

Sandeep Kasoji, Paul A. Dayton
Joint Department of Biomedical Engineering
University of North Carolina and NC State University
Chapel Hill, NC 27599, USA
padayton@email.unc.edu

***Abstract*—Spatial limitation can be a challenge to interventional ultrasound transducers for dual-frequency contrast-enhanced ultrasound imaging, or acoustic angiography. A low frequency (< 3 MHz) transmission with moderate peak negative pressure (PNP) and short pulse length is not easily attainable within limited dimensions. In this paper, a new design of the low frequency transmitter of dual-frequency transducers is presented. 1-3 composites for interventional transmitter design were analyzed by the Krimholtz–Leedom–Matthaei (KLM) model and finite element analysis (FEA). The dual frequency transducer prototype with a 2 MHz 1-3 composite transmitter and a 14 MHz receiver was fabricated and characterized, followed by microbubble detection tests. The transmitter showed the peak negative pressure (PNP) of -1.5 MPa. The -6 dB pulse echo fractional bandwidth for the transmitter and receiver were 61 % and 45 %, respectively. The prototyped dual frequency transducer was used to successfully excite microbubbles and to detect super harmonic responses from microbubbles. The measured harmonic signal showed a 12 dB contrast-to-noise ratio (CNR).**

Keywords—interventional ultrasound; contrast enhanced imaging; dual frequency transducers; super-harmonic imaging;

I. INTRODUCTION

Using conventional ultrasound for imaging blood flow in micro vessels is challenging due to weak ultrasound scattering from blood [1]. Thus, superharmonic imaging, also referred to as acoustic angiography when using a high frequency receiver, was developed because of its capability of producing high resolution images of blood vessels [1, 2]. In this technique, microbubbles are usually excited by low frequency acoustic waves (1-4 MHz) with moderate peak negative pressure and short pulse length near the resonant frequency of microbubbles; the high frequency (> 15 MHz) nonlinear echoes from microbubbles are received by a high frequency receiver [3, 4]. Proper frequency combinations that produces high contrast-to-tissue ratio in super harmonic imaging, and high resolution have been reported [2, 3, 5, 6]. However, the main challenge of this imaging method to date has been the lack of dual-frequency transducers that can transmit energy at a selected low frequency and simultaneous confocal detection of high frequency scattered echoes [1]. Dual-frequency transducers for interventional ultrasound imaging applications such as transrectal ultrasound and intravascular ultrasound (IVUS) need to be designed considering the spatial limitation. However, the design concept and important design parameters for dual-frequency super-harmonic imaging transducers have not been extensively reported so far. The 4/30 MHz dual frequency transducer design was introduced with high-frequency 3-D contrast imaging of *in vivo* microvasculature [1, 5], but the transducer size was not practical for interventional applications. Recently, the sandwich design of a small-aperture 6.5/30 MHz transducer made of PMN-PT crystals for the application of the contrast enhanced intravascular ultrasound (CE-IVUS) has been reported [7]. The simple design of this dual-frequency transducer showed promising performance with a small size aperture (0.6 × 3 mm^2 aperture and < 600 μm thickness).

Therefore, the sandwich design (Fig. 1) was adopted in this work and improved for general interventional acoustic angiography. By considering microbubble size and a penetration depth in other interventional applications such as transrectal ultrasound, transmission frequency was lowered to 2 MHz. Such a low frequency transmitter presents a serious challenge to the small aperture dual frequency transducer design. PZT-5H 1-3 composite was used for the transmitter instead of PMN-PT single crystal plate aiming to obtaining a broadband transmitter without a conventional thick and lossy backing. The design, fabrication, characterization, and microbubble test results for small aperture dual-frequency transducers are presented in detail in the following sections.

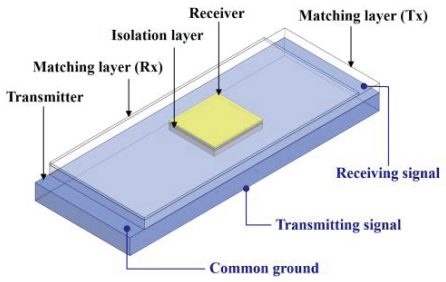

Fig. 1. Schematic design of the sandwich-type dual frequency transducer.

U.S. Army Medical Research and Materiel Command (PC111309)

978-1-4799-7049-0/14/$31.00 ©2014 IEEE

II. Materials and Methods

A. Design Methods and Material Properties

Key design parameters were analyzed by the Krimholtz–Leedom–Matthaei (KLM) model and finite element analysis (FEA). The low transmitting frequency element was designed at 2 MHz considering the resonant frequency of microbubbles and prior testing [6]. Thus, proper thickness, aperture, and material were then determined. Among conventional piezoelectric materials such as PZT-5H, PMN-PT single crystal, and PZT-5H 1-3 composite (Table I), suitability of each material for the transmitter element were compared by using ANSYS FEA software. In the case of 2 MHz transmission and 13-15 MHz receiving, appropriate apertures for both transmitter and receiver were determined by analyzing beam patterns. One particular design issue for the dual-frequency transducer is that the whole high-frequency receiving element should be placed at the center of the matching layer of the low-frequency transmitter as shown in Fig. 1. Therefore, the matching layer thickness was adjusted in accordance with the total thickness of the receiving element including a dual isolation layer based on the analyzed results from the KLM model and FEA. To simplify the calculation, homogenized single-phase 1-3 composite material was used [8], and a symmetric condition was applied to a quarter model. The matching layer material was selected as Al_2O_3/epoxy mixture due to its proper acoustic impedance (5.8 MRayl). A steel shim and silver epoxy (E-solder 3022) were used as a dual-isolation layer due to its large acoustic impedance difference of 50 MRayl and 5.5 MRayl, respectively. The large difference between acoustic impedance of isolation layers 1 and 2 can provide a strong reflection of received high frequency waves at the boundary. Although this reflection may slightly reduce the receiving bandwidth, the isolation layers would block the wave transmission to the transmitter and backscattered waves from the backside of the transmitter.

B. Fabrication, Characterization, Test Methods

The fabrication process for the dual-frequency transducer is similar to that reported previously [7]. The pulse-echo signals of both transmitters and the receivers were measured individually. A pulser/receiver (5900PR, Panametrics Inc., Waltham, MA) was used in a pulse-echo test and energies of 1 μJ and 2 μJ were used to excite the receiver and transmitter, respectively. The peak negative pressure of the prototypes was measured using a needle hydrophone (HNA-0400, Onda Corp., Sunnyvale, CA), which was positioned in front of the prototype transducer. The transmitter of the prototype was excited with a two-cycle sinusoidal input at 2 MHz and 300 mV_{pp} generated from a function generator (AFG3101, Tektronix Inc., Beaverton, OR). The driving signal was amplified by 60 dB using a radio-frequency amplifier (Model 3200L, Electronic Navigation Industries Inc., Rochester, NY). For the contrast test, the harmonic signals from microbubbles were measured. The cellulose tube (200 μm diameter) was positioned at about 8 mm away from the transducer. The transmission condition was same as the one used in the pressure mapping condition. The cellulose tube was filled with water, air, and micro bubbles, respectively, and then the received signals in each case were processed to obtain a frequency spectrum and filtered signals. The cut-off frequencies of the high and low pass filters were 10 MHz and 20 MHz, respectively.

III. Results

A. Design specifications

Based on the elastic material properties of conventional piezoelectric materials, the thickness of active materials for the 2 MHz-resonance was determined (Table I). The PZT-5H 1-3 composite (volume fraction of 60 %) exhibited the smallest thickness (~710 μm) for the designed operating frequency, which is preferred in interventional transducer designs. In addition, FEA on feasible minimum aperture without any mode coupling showed another merit of the 1-3 composite. In the case of 2 MHz resonance with an area of 3×3 mm^2, only the 1-3 composite showed a pure thickness resonance at the designed frequency (Fig. 2). Thus, the 1-3 composite plate was adopted as the transmitter due to its laterally isolated characteristics at smaller dimensions, which is a great merit to make smaller transducers for the interventional ultrasound applications. The designed transmitter showed a pulse-echo amplitude of 15.1 mV_{pp}/V and the -6dB fractional bandwidth of 61.2 %. The high-frequency receiver exhibited the sensitivity and bandwidth of 21.7 mV_{pp}/V and 49.3 %, respectively.

TABLE I. Properties of Piezoelectric Materials.

Parameters	PZT-5H	PMN-PT	PZT-5H 1-3 composite
ρ (kg/m^3)	7500	8040	5300
c_{33}^D (×10^9 N/m)	157	173	74.3
V_L (m/s)	4560	4640	3740
Z_L (MRayl)	34.2	37.3	19.7
k_t	0.51	0.64	0.65
t_{2MHz} (mm)	0.990	0.950	0.710

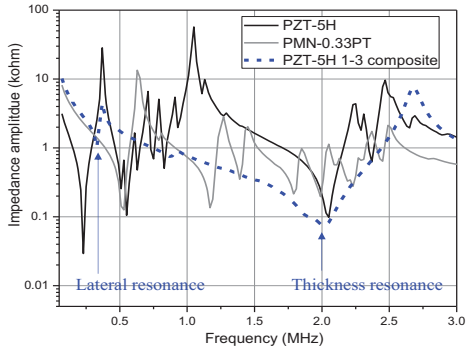

Fig. 2. Calculated impedance spectra of piezoelectric plates with 3×3 mm^2 and 2 MHz thickness resonance.

To check the receiver's effects on transmitting performance, the single-frequency design which has only Al_2O_3/epoxy mixture matching layer without a receiver part was also analyzed and compared with the dual-frequency model by FEA (Fig. 3). With a cycle of 100 V_{pp} sinusoidal excitation, the generated waveform and peak values of both cases are almost same, suggesting that the designed high frequency receiver layer will not affect transmitting performance significantly.

Table II presents key design specifications for the dual frequency transducer, and the prototypes were fabricated based on these parameters (Fig. 4). The difference between prototypes 1 and 2 is the aperture size of the receiver. The receiving aperture of prototype 1 was modified to 3.8 × 2.0 mm^2 from the designed dimension in Table II to compare receiving performance.

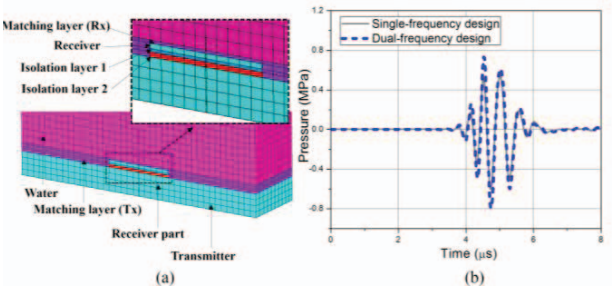

Fig. 3. 3D FEA for transmitting performance; (a) 3-D half finite element model of a dual-frequency transducer, (b) Comparison of transmitted wave forms with the 2 cycles of 100 V_{pp} sinusoidal excitation for both single frequency and dual frequency designs.

TABLE II. MATERIALS AND DIMENSIONS OF THE FINAL MODEL.

Part	Material	Dimension (mm^3)
Transmitter	1-3 composite	3.8 × 8.0 × 0.71
Matching layer (Tx)	Al_2O_3/epoxy	3.8 × 8.0 × 0.29
Isolation layer 1	E-solder 3022	2.0 × 2.0 × 0.06
Isolation layer 2	Carbon steel	2.0 × 2.0 × 0.08
Receiver	1-3 composite	2.0 × 2.0 × 0.09
Matching layer (Rx)	Al_2O_3/epoxy	2.0 × 2.0 × 0.06

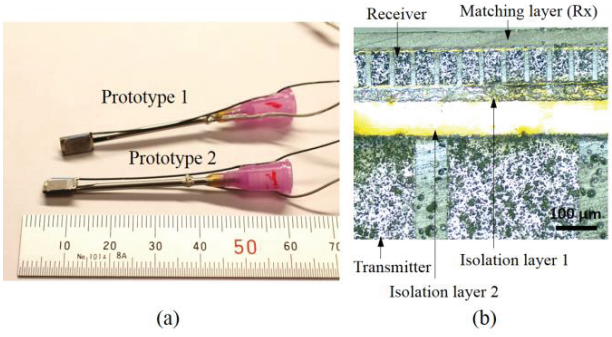

Fig. 4. The transducer prototypes; (a) Prototype transducer housed on the tip of a 16-gauge needle, (b) Cross sectional view of the center part of the transducer.

B. Acoustic Characterization Results

The transmitter of prototype 1 showed a peak-to-peak voltage of 210 mV and -6 dB fractional bandwidth of 61.1 %, and the receiver showed 430 mV_{pp} and 45.1 % (Fig. 5). For prototype 2, the measured echo peak voltages for the transmitter and receiver are 430 mV_{pp} and 410 mV_{pp}, respectively. The measured -6 dB fractional bandwidth for the transmitter and receiver were 55.2 % and 35.6 %, respectively. The measured performances of transmitters were in agreement with the simulation results. Aliasing echoes were not measured at the echoed signal of receivers, which means the dual-isolation layers were properly designed and fabricated. During the pressure mapping test, the peak negative pressure at the far field was about -1.5 MPa (Fig. 6), which is similar to the estimated pressure (6.1 kPa with a 2-cycle of 1 V_{pp} sinusoidal excitation). This is high enough to excite microbubbles for nonlinear responses due to a relatively high mechanical index (MI) of 1.01 [3]. In addition, the pressure mapping result showed that there is almost negligible disturbance by the receiver in the acoustic field.

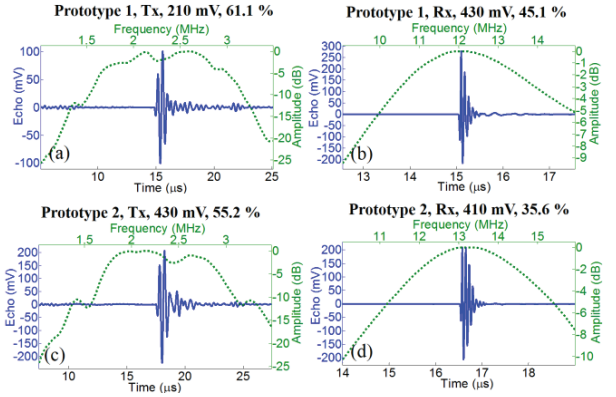

Fig. 5. Pulse echo test results of prototype 1 and 2 with an impulse excitation of 1 and 2 μJ for the receiver and transmitter, respectively; (a-d) the peak-to-peak echo amplitude and -6dB fractional bandwidth of each part were shown in the title of subfigures.

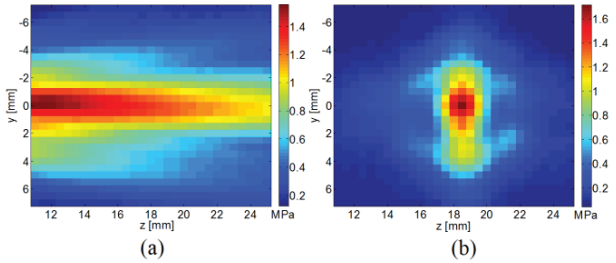

Fig. 6. Pressure mapping results; (a) along axial direction, (b) along lateral direction.

C. Contrast Test Results

The case of water in a micro-cellulose-tube was tested first. When water was injected into the micro-cellulose-tube, no signal reflected from the tube was measured (Fig. 7 (a)), since almost all the waves are transmitted through the tube filled with water. A 2 MHz frequency component in a spectrum (Fig. 7(b)) was attributed to the initial excitation signal. For the case of air injected into the micro-cellulose tube, the reflected waves from the tube due to the large acoustic impedance difference between water and air were detected by the high frequency receiver (Fig. 7 (d)). The frequency spectrum showed that the received signal has no harmonic components but scattered only the fundamental transmitting frequency. When the diluted microbubbles were pumped through the tube, the receiver successfully detected the fundamental reflection and super harmonic responses from the tube filled with microbubbles (Fig. 8). The peak amplitude in the raw signal was slightly reduced in the case with microbubbles, but the frequency spectrum showed distinctive harmonic components. The intended receiving frequency components (~14 MHz) were present in the frequency spectrum (Fig. 8 (b)). The filtered signal has a discernable peak but the amplitude was not high (5 mV) in comparison with the noise signal (Fig. 8 (c)). Thus, the bubble response was measured with a 16 dB gain and analog high-pass filter which had a cut-off frequency of 10 MHz (Fig. 8 (d)). With the 16 dB gain the harmonic bubble signal showed higher signal-to-noise ratio (~12 dB, Fig. 8 (f)).

IV. Conclusion

2/14 MHz dual-frequency transducers were designed, fabricated, and tested. 1-3 piezoelectric composite is a promising active material for the transmitter of interventional dual-frequency ultrasound transducers due to its low acoustic impedance and high coupling factor. With the merits of the 1-3 composite material, 7th order super harmonic responses from the micro-bubbles can be detected during 2 MHz excitation, within 1 mm total thickness of the transducer. This will enable acoustic angiography imaging through deeper tissue than previously reported with 4 MHz/30 MHz configurations. Extensive bubble tests with a tissue-mimicking phantom will be conducted for further research.

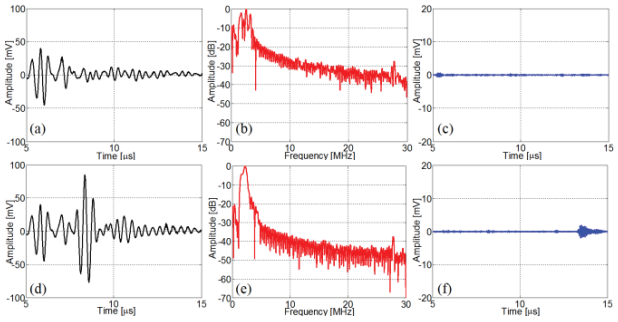

Fig. 7. Received signal from the micro-tube; (a) raw signal (water), (b) frequency spectrum (water), (c) filtered signal (water, 10 to 20 MHz), (d) raw signal (air), (e) frequency spectrum (air), (f) filtered signal (air, 10 to 20 MHz).

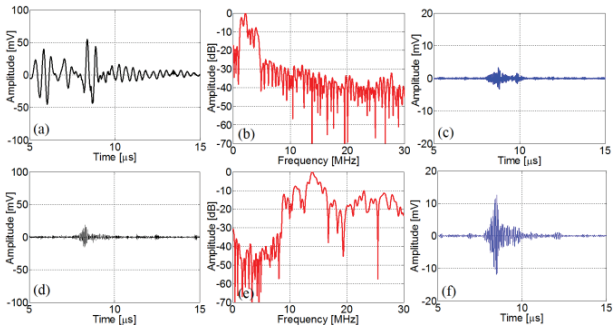

Fig. 8. Received signal from the micro-tube filled with bubbles; (a) raw signal, (b) frequency spectrum, (c) filtered signal (10 to 20 MHz), (d) raw signal (10 MHz analog HP filter), (e) frequency spectrum (10 MHz analog HP filter), (f) filtered signal (10 MHz analog HP filter).

Acknowledgment

The authors would like to acknowledge the financial support from U.S. Army Medical Research and Materiel Command under the contract PC111309.

References

[1] R. C. Gessner, C. B. Frederick, F. S. Foster, and P. A. Dayton, "Acoustic angiography: a new imaging modality for assessing microvasculature architecture," *Journal of Biomedical Imaging,* vol. 2013, p. 14, 2013.

[2] A. Bouakaz, S. Frigstad, F. J. Ten Cate, and N. de Jong, "Improved contrast to tissue ratio at higher harmonics," *Ultrasonics,* vol. 40, pp. 575-578, 2002.

[3] A. Bouakaz, S. Frigstad, F. J. Ten Cate, and N. de Jong, "Super harmonic imaging: a new imaging technique for improved contrast detection," *Ultrasound in medicine & biology,* vol. 28, pp. 59-68, 2002.

[4] R. Hansen and B. Angelsen, "Contrast imaging by non-overlapping dual frequency band transmit pulse complexes," *Ultrasonics, Ferroelectrics and Frequency Control, IEEE Transactions on,* vol. 58, pp. 290-297, 2011.

[5] R. Gessner, M. Lukacs, M. Lee, E. Cherin, F. Foster, and P. A. Dayton, "High-resolution, high-contrast ultrasound imaging using a prototype dual-frequency transducer: in vitro and in vivo studies," *Ultrasonics, Ferroelectrics and Frequency Control, IEEE Transactions on,* vol. 57, pp. 1772-1781, 2010.

[6] B. D. Lindsey, J. D. Rojas, K. H. Martin, S. E. Shelton, and P. A. Dayton, "Acoustic characterization of contrast-to-tissue ratio and axial resolution for dual-rrequency contrast-specific acoustic angiography imaging," *Ultrasonics, Ferroelectrics and Frequency Control, IEEE Transactions on,* in press.

[7] J. Ma, K. H. Martin, P. A. Dayton, and X. Jiang, "A preliminary engineering design of intravascular dual-frequency transducers for contrast-enhanced acoustic angiography and molecular imaging," *Ultrasonics, Ferroelectrics and Frequency Control, IEEE Transactions on,* vol. 61, pp. 870-880, 2014.

[8] J. Kim and Y. Roh, "Homogenization of PMN-PT/epoxy 1–3 piezocomposites by resonator measurements and finite element analysis," *Sensors and Actuators A: Physical,* vol. 206, pp. 97-106, 2014.

THE UNIVERSITY of NORTH CAROLINA at CHAPEL HILL

Department of Biomedical Engineering

NC STATE UNIVERSITY

152 MacNider Hall, Chapel Hill, NC 27599-7575
(919) 966-1175; (919) 966-2963 fax
http://www.bme.unc.edu

4130 Engineering Building III, Raleigh, NC 27695-7115
(919) 515-5252; (919) 513-3814 fax
http://www.bme.ncsu.edu

October 28, 2016

Equipment purchased on award W81XWH-12-1-0303:

1 Ultrasound Acquisition System
With: V-3 Chassis, PCI Express Cable, PCI Express Interface Card, Single Connector Scanhead Interface, Software including example scripts, HAL, VSX and firmware, Apple LED Cinema Display (27" flat panel)

Total: $60,000

Authorized Organizational Official
UNC Chapel Hill

on behalf of Terry Magnuson, PH.D.
Vice Chancellor for Research
University of North Carolina at Chapel Hill